AD-764 881

THE JOINT NOL/RAE/WRE RESEARCH PROGRAM ON BOMB DYNAMICS. PART III. A LOW-DRAG BOMB WITH FREELY SPINNING STABILIZERS

F. J. Regan, et al

Naval Ordnance Laboratory
White Oak, Maryland

4 May 1973

DISTRIBUTED BY:

NTIS

National Technical Information Service
U. S. DEPARTMENT OF COMMERCE
5285 Port Royal Road, Springfield Va. 22151

NOLTR 73-77

AD 764881

THE JOINT NOL/RAE/WRE RESEARCH PROGRAM ON BOMB DYNAMICS PART III A LOW-DRAG BOMB WITH FREELY SPINNING STABILIZERS

BY
F.J. Regan (NOL)
H.W. Shannon (WRE)
J.F. Tanner (RAE)

4 MAY 1973

NOL

NAVAL ORDNANCE LABORATORY, WHITE OAK, SILVER SPRING, MARYLAND

NOLTR 73-77

APPROVED FOR PUBLIC RELEASE;
DISTRIBUTION UNLIMITED

Best Available Copy

UNCLASSIFIED

Security Classification

DOCUMENT CONTROL DATA - R & D

(Security classification of title, body of abstract and indexing annotation must be entered when the overall report is classified)

1. ORIGINATING ACTIVITY (Corporate author)	2a. REPORT SECURITY CLASSIFICATION
Naval Ordnance Laboratory White Oak, Silver Spring, Maryland	UNCLASSIFIED
	2b. GROUP N/A

3. REPORT TITLE

The Joint NOL/RAE/WRE Research Program on Bomb Dynamics
Part II A Low-Drag Bomb with Freely Spinning Stabilizers

4. DESCRIPTIVE NOTES (Type of report and inclusive dates)

5. AUTHOR(S) (First name, middle initial, last name)

F. J. Regan (NOL), J. H. W. Shannon (WRE), J. F. Tanner (RAE)

6. REPORT DATE	7a. TOTAL NO. OF PAGES	7b. NO. OF REFS
4 May 1973	~~89~~ 92	24

8a. CONTRACT OR GRANT NO.	9a. ORIGINATOR'S REPORT NUMBER(S)
b. PROJECT NO.	NOLTR 73-77
c. AIRTASK No. A320-320C/WF-32-323-201	9b. OTHER REPORT NO(S) (Any other numbers that may be assigned this report) RAE-TR-73060 WRE-904

10. DISTRIBUTION STATEMENT

Approved for public release; distribution unlimited.

11. SUPPLEMENTARY NOTES	12. SPONSORING MILITARY ACTIVITY
	Naval Air Systems Command, Washington, D. C. 20360

13. ABSTRACT

The present document is the third in a series of reports on a tripartite bomb dynamics research program. It presents results relating to the study of free-fall stores having freely spinning cruciform and monoplane stabilizers. The freely spinning stabilizer is designed to minimize or eliminate the roll-induced forces and moments which have been shown to be a significant contribution to ballistic dispersion. Wind-tunnel measurements of the static and dynamic characteristics of these stabilizers are presented, along with computer simulations of actual trajectories of instrumented full-scale research vehicles. The mechanical feasibility of freely spinning stabilizers is also considered. Various stability criteria, based upon linear analysis, are developed for freely spinning stabilizers of various fin geometries. This report is being issued simultaneously by the Naval Ordnance Laboratory, the Royal Aircraft Establishment and the Weapons Research Establishment.

UNCLASSIFIED

Security Classification

14. KEY WORDS	LINK A		LINK B		LINK C	
	ROLE	WT	ROLE	WT	ROLE	WT
Bombs						
Free-Fall Store						
Freely Spinning Stabilizers						
Low Drag						

THE JOINT NOL/RAE/WRE RESEARCH PROGRAM ON BOMB DYNAMICS
PART III A LOW-DRAG BOMB WITH FREELY SPINNING STABILIZERS

Prepared by:
F. J. Regan (NOL)
J. H. W. Shannon (WRE)
F. J. Tanner (RAE)

ABSTRACT: Research on the free-fall dynamics of bombs has been conducted as a cooperative program supported by organizations in the United States, United Kingdom and Australia. In addition to full-scale flight trials of instrumented research stores carried out by the Australian Weapons Research Establishment (WRE), wind-tunnel tests have been made on mutually agreed upon models at the Aircraft Research Association and Royal Aircraft Establishment (RAE) in England; the Naval Ordnance Laboratory (NOL) in the United States; and at the Aeronautical Research Laboratory in Australia. RAE, NOL and WRE have separately prepared digital computer programs to simulate test vehicle trajectories using wind-tunnel measurements as inputs. Correlation between the predicted and observed flight results has provided considerable insight into problems associated with dynamic behavior during the critical release phase, as well as stability criteria needed for good ballistic consistency.

The present document is the third report on the research program. It presents results relating to the study of free-fall stores having freely spinning cruciform and monoplane stabilizers. The freely spinning stabilizer is designed to minimize or eliminate the roll-induced forces and moments which have been shown to be a significant contribution to ballistic dispersion. Wind-tunnel measurements of the static and dynamic characteristics of these stabilizers are presented, along with computer simulations of actual trajectories of instrumented full-scale research vehicles. The mechanical feasibility of freely spinning stabilizers is also considered. Various stability criteria, based upon linear analysis, are developed for freely spinning stabilizers of various fin geometries. This report is being issued simultaneously by the Naval Ordnance Laboratory, the Royal Aircraft Establishment and the Weapons Research Establishment.

NAVAL ORDNANCE LABORATORY
WHITE OAK, MARYLAND

NOLTR 73-77 4 May 1973

THE JOINT NOL/RAE/WRE RESEARCH PROGRAM ON BOMB DYNAMICS
PART III A LOW-DRAG BOMB WITH FREELY SPINNING STABILIZERS

The purpose of this report is to summarize the tripartite cooperative free-fall research effort among NOL, RAE and WRE. A study was made of the characteristics of various freely spinning stabilizers using wind tunnels, digital computer trajectory programs and instrumented free-fall weapons. This report is also being issued by the Royal Aircraft Establishment as RAE Technical Report 73060 and by the Weapons Research Establishment as WRE Report 904 (WR&D).

This project was sponsored by the Naval Air Systems Command under Airtask No. A320-320C/WF32-323-201.

ROBERT WILLIAMSON II
Captain, USN
Commander

Leon H. Schindel
LEON H. SCHINDEL
By direction

CONTENTS

TABLES

ILLUSTRATIONS

ILLUSTRATIONS (Cont'd)

ILLUSTRATIONS (Cont'd)

1.0 INTRODUCTION

The history of the Tripartite Bomb Stability Program has been described fully in Reference (1) and only a brief summary will be given here. The work began in 1960 as a cooperative program between the United Kingdom (U.K.) and Australia to study the dynamic behavior of free-fall weapons and to produce new design criteria for such weapons. Technical discussion between representatives of the two countries and the United States research establishments broadened the aims of the program and since 1964 it has been pursued on a tripartite, or cooperative, basis. As a tripartite effort, the scope of the research program was extended to the following three objectives:

1. To provide a more rigorous check on the validity of current stability theories by making correlations between the full-scale research vehicle's observed behavior and that predicted from its mathematical model using the most complete sets of wind-tunnel and free-flight data obtainable.

2. To investigate ideas, both experimentally and theoretically, which appear to provide solutions to some stability problems or to give weapons of greater tactical flexibility.

3. To develop new experimental methods for obtaining aerodynamic data.

Within the context of item 2 above, attention was given to the testing of novel stabilization devices, such as the split-skirt stabilizer (Ref. (2)). The results of the tripartite investigation of these stabilizers is documented in Reference (3).

A second innovative stabilizer is the freely spinning stabilizer. In the freely spinning stabilizer the panels are permitted to spin about the body's longitudinal axis. The forebody, on the other hand, has little or no spin rate. The ballistic advantages of this type of stabilizer are as follows:

1. The effects of the yaw-induced forces and moments associated with the fixed-cruciform stabilizers can be minimized or eliminated. Bomb-aircraft separation disturbances are therefore minimized.

2. The moment of inertia in roll of the tail cone is an order of magnitude less than that of the complete configuration. Since only the fins rotate, they rapidly accelerate after release to a roll rate above the bomb's pitch frequency, thereby avoiding roll-yaw resonance.

3. The freely spinning tail offers tactical advantages in that it can be used as an environmental sensor by replacing the commonly used air-arming vane.

4. The freely spinning monoplane stabilizer (in which two opposing panels are removed) has attractiveness in meeting space restrictions of underwing stowage.

The engineering aspects of freely spinning stabilizers have also been considered.

Following the general principles established earlier in the research program, careful attention has been given to wind-tunnel testing and to mathematical modeling, making use of the six-degree-of-freedom computer programs. Free-flight experiments were preceded by wind-tunnel tests. It should be emphasized that in addition to determining the aerodynamic performance of the freely spinning stabilizer, the important underlying principle is the evaluation of computer trajectory modeling as a tool in the prediction of bomb performance.

SYMBOLS

A_1	moment of inertia of forebody about X axis
A_2	moment of inertia of tail assembly about X axis
B	moment of inertia of complete vehicle about Y or Z axis
B'	$B/(1/8\rho Sd^3)$
C_D	drag coefficient, D/QS
C_ℓ	roll-moment coefficient, M_x/QSd
C_{ℓ_p}	damping-in-roll derivative, $\partial C_\ell/\partial(pd/2u)$
C_m	pitch-moment coefficient, M_y/QSd
C_{m_α}	pitch-moment derivative with respect to angle of attack, $\partial C_m/\partial\alpha$
$C_{m_q} + C_{m_{\dot\alpha}}$	damping-in-pitch derivative, $\partial C_m/\partial q + \partial C_m/\partial(\dot\alpha d/2u)$
C_n	yaw-moment coefficient, M_z/QSd

C_{n_p}	Magnus moment derivative, $\partial C_n/\partial(pd/2u)$
$C_{n_r} - C_{n_{\dot{\beta}}}$	damping-in-yaw derivative, $\partial C_n/\partial(rd/2u) - \partial C_n/\partial(\dot{\beta}d/2u)$
C_N	normal-force coefficient, $-C_z$
C_{N_α}	normal-force derivative with respect to angle of attack, $\partial C_N/\partial\alpha$
C_x	axial-force coefficient, F_x/QS
C_y	side-force coefficient, F_y/QS
C_{y_o}	side-force coefficient due to aerodynamic asymmetry
C_{y_p}	Magnus force derivative, $\partial C_y/\partial(pd/2u)$
C_z	force coefficient along Z axis, F_x/QS
C_{z_o}	force coefficient along Z axis due to aerodynamic asymmetry
d	reference length, maximum body diameter
D	drag force
F_x	component of aerodynamic force along the X axis
F_y	component of aerodynamic force along the Y axis
F_z	component of aerodynamic force along the Z axis
M	Mach number
M_x	roll moment, moment about the X axis
M_y	pitch moment, moment about the Y axis
M_z	yaw moment, moment about the Z axis
m	mass of complete missile
m'	$m/(1/4\rho Sd)$

p	spin rate of stabilizer, component of stabilizer angular velocity along X axis
pd/2u	reduced spin rate
P	spin rate of forebody, component of forebody angular velocity along X axis
P_o	total pressure
q	pitch rate, component of angular velocity along Y axis
Q	dynamic pressure, $1/2\rho u_\infty^2$
r	yaw rate, component of angular velocity along Z axis
S	reference area $\pi d^2/4$
s	Laplace transform variable
T	temperature
u	component of free-stream velocity along the X axis
v	component of free-stream velocity along the Y axis
V	free-stream velocity
w	component of free-stream velocity along Z axis
X	body axis colinear with the longitudinal axis of the store
x_o	location of aerodynamic asymmetric force from moment reference center
Y	body axis normal to the longitudinal axis and in a plane defined by two opposing fins
Z	body axis forming a right-handed triad with the X, Y axes
α	angle of attack, $\tan^{-1} \frac{w}{u}$
β	angle of sideslip, $\tan^{-1} \frac{v}{u}$
γ	orientation of body frame with respect to angle of attack, $\tan^{-1} \frac{v}{w}$

δ	fin-cant angle
ζ	complex angle of attack, $i\alpha + \beta$
ζ_α	damping ratio of the nonrolling missile in pitch
ζ_β	damping ratio of the nonrolling missile in yaw
λ	nondimensionalized pitch-damping factor, $\zeta_\alpha \omega_\alpha / p$
μ	nondimensionalized yaw-damping factor, $\zeta_\beta \omega_\beta / p$
ρ	air density
τ	inertia ratio, $\frac{A_2 + A_1 P/p}{B}$
ϕ	roll angle
$\Omega_{1,2}$	basic oscillatory frequencies in nonrolling axis system
$\omega_{1,2}$	basic oscillatory frequencies in rolling axis system
ω_α	natural frequency of nonrolling missile in pitch
ω_β	natural frequency of nonrolling missile in yaw

2.0 WIND-TUNNEL TESTS

In order to meet the goals of this research effort as set forth in the Introduction, it was necessary to provide the computer program with highly detailed aerodynamic measurements. Even from the beginning of this tripartite effort there existed strong convictions that static aerodynamic measurements alone would not be sufficient. Dynamic effects, that is, aerodynamic loads resulting from a changing flow field about the body, would also have to be measured.

In 1963 a critical examination was undertaken to determine if the requirements of a program with this scope could be adequately met by existing wind-tunnel measurement capabilities. Static wind-tunnel measurements, it was felt, did not pose any difficulties (Ref. (4)). Certainly, the determination of the normal force, pitch moment, side force, yaw moment and the roll moment would involve only well-established test techniques. However, drag, which is generally included under static measurements, is often of doubtful quality when obtained in a wind tunnel due to the sting support influencing the pressure at the model's base. Because of this pressure disturbance, drag measurements would not be considered part of this program. This was not thought to be a serious restriction for it was felt that drag would not be an important consideration since dispersion at impact would be

of little concern in this study. Rather, as motion during the first 20 seconds of flight was the focal point of the simulation work, drag variations would assume a relatively minor role. This position was amply substantiated by the results. Drag variations of the order of 20 percent had little effect on the resulting angular motion of the store. In the trajectory studies of the freely spinning stabilizer the drag data used was the zero lift drag coefficient, C_{D_o}, derived from the free-fall trial measurements of the M823 Research Store with a fixed-cruciform stabilizer.

When the need for highly detailed wind-tunnel measurements was first considered, it was recognized that the determination of dynamic effects in the wind tunnel involved techniques that were less well established than were the corresponding static techniques. For configurations with the freely spinning stabilizers there was no doubt that roll-damping, pitch-damping and Magnus measurements would be required. The stabilizers were large flat panels whose normals were perpendicular to the axis of rotation; the roll-damping moment, therefore, contributed by these surfaces would be influential in determining the steady-state spin rate of the stabilizer. The stabilizer spin rate, in turn, is influential in the yaw-pitch modal coupling, as well as in contributing an aerodynamic load through the Magnus effect. In addition, pitch-damping and Magnus measurements were also required.

The roll-damping data were provided by the Royal Aircraft Establishment (RAE) from roll-damping measurements made at the Aircraft Research Association on the M823 Research Store with the fixed-cruciform stabilizer. This approximation was felt to be justified on the grounds that the forebody's contribution to the damping-in-roll derivative would be negligible. Hence, roll-damping measurements on the fixed-cruciform weapon would be equally applicable to the case where the tail alone was allowed to spin.

NOL carried out both the pitch-damping measurements (using the free-oscillation support) and the Magnus measurements. In both of these tests only the stabilizer was permitted to freely spin, with spin torque being provided by the fin cant.

Static and pitch-damping measurements were carried out in the Naval Ordnance Laboratory's 16- x 16-inch Supersonic Tunnel No. 1. This is a one-atmosphere blowdown facility whose essential flow characteristics are given in Table 1. The Magnus measurements were conducted in the Naval Ship Research and Development Center's (NSRDC) 7- by 10-foot Transonic Wind Tunnel. Unlike the NOL facility, this tunnel has the capability of varying the total pressure head from one-half to one atmosphere. This facility's relevant flow characteristics under conditions of one atmosphere are also given in Table 1, together with corresponding data on the Aircraft Research Association's (ARA) 8- by 9-foot Tunnel.

The wind-tunnel models of the freely spinning cruciform and freely spinning monoplane configurations are shown in Figure 1. It will be noted in the upper figure that the freely spinning cruciform stabilizer is fabricated in four pieces: one piece for each panel. The monoplane stabilizer (lower illustration in Fig. 1) is then formed by removing two opposing fin panels and replacing these panels with blanks. The particular design of the model's stabilizer also permits rapid changes in cant angles.

The wind-tunnel sting and model base geometry for the NOL and ARA static wind-tunnel tests are shown in Figure 2. In the Magnus tests, conducted by NOL at the NSRDC facility, sting-body geometry closely approximated that indicated in the lower illustration of Figure 2.

A five-component strain-gage balance was used both by NOL and RAE in making static measurements. At NOL the sting was mounted into a rotating sector arm to provide the angle-of-attack traverse required by the test. After tunnel flow was established, the model was rotated through an angle-of-attack range. During this time the strain-gage signals were sampled and recorded on magnetic tape. The tape was then input into a digital computer data-reduction program. The output of the data-reduction program is a plotting tape from which a graphical record can be made of the various aerodynamic coefficients versus angle of attack. In addition, the data-reduction program also provides a printed record in tabular form.

When normal-force and pitching-moment measurements are made with the stabilizer freely spinning the roll angle dependency, usually evident in these coefficients, is "averaged." This is essentially true of the side force and yaw moment as well. This force and moment was virtually zero for all configurations with a freely spinning stabilizer (see Ref. (5)). Similar measurements on the same model with the stabilizer fixed indicated side-force and yaw-moment coefficients which varied periodically with four times the roll angle. The freely spinning stabilizer, in averaging these roll-induced effects, essentially eliminates their influence on bomb angular motion. Also, since the freely spinning stabilizer is uncoupled from the forebody, the induced rolling moment applied to the forebody may be neglected.

With the above information in hand, it was decided to simulate the first ten seconds or so of the flight of the store after release. The resulting poor agreement indicated that the assumption of steady-state spin conditions was invalid. Rather, it seemed more accurate that the stabilizer was in a condition of spin acceleration, and the roll averaging noted above was not entirely effective. Consequently, use was made of the static measurements of the fixed-cruciform stabilizer. These measurements were used to express the roll dependency of all the static coefficients.

Figures 3 and 4 present representative static pitching-moment and normal-force measurements used in the simulation of the freely spinning cruciform stabilizer. It will be noted in these figures that these normal-force and pitching-moment coefficients have strong roll angle dependencies. References (5), (6) and (7) present a detailed compilation of static wind-tunnel measurements used in the computer trajectory simulations of the freely spinning cruciform and monoplane stabilizers.

A bomb generally undergoes damped oscillatory motion in response to a disturbance. The damping-in-pitch derivative, $C_{m_q} + C_{m_{\dot{\alpha}}}$, is a measure of the influence of model shape on the rate at which these oscillations decay. One way of determining this quantity in a wind tunnel is through the method of free oscillation. In the free-oscillation technique the model has unrestricted freedom to rotate about the transverse support shaft. Prior to establishing tunnel flow, the model is constrained at an angle of attack relative to the eventual trim direction. After flow establishment, the model is released and allowed to oscillate freely about the transverse support. Except for a negligible amount of bearing friction, the torque acting on the model has an entirely aerodynamic origin. From the damped sinusoidal motion it is possible to use a variety of schemes to obtain the damping-in-pitch derivative. Regardless of the data-reduction program chosen, it is necessary to have raw data in the form of pitch angle versus time which is provided by a transducer internal to the model. Further details of the method of free-oscillation pitch damping are given in Reference (8). Reference (8) also contains extensive damping-in-pitch measurements. Additional pitch-damping data on the monoplane stabilizer are contained in Reference (9).

In considering the available wind-tunnel pitch-damping measurements, it was decided not to use the fixed-cruciform pitch-damping data for the freely spinning stabilizer studies. There were two main reasons for not making use of these data to introduce a roll effect: first, it was felt that the precision in measurement of the pitch-damping derivative would not adequately discern a roll angle effect; secondly, the trajectory simulations indicated that the store was lightly damped (about five percent critical) and that substantial changes in the damping-in-pitch derivative had a relatively minor effect on the overall bomb trajectory.

Representative damping-in-pitch measurements are shown in Figure 5. There are a number of schemes for obtaining and expressing the angle-of-attack dependency of the damping-in-pitch derivative. The quality of measurements obtained on this configuration did not seem to warrant this type of detail. Therefore, the damping-in-pitch derivative was input into the computer trajectory simulation program solely as a function of Mach number.

Another type of dynamic phenomenon that strongly influences bomb performance is commonly referred to as the Magnus effect. In its linear formulation this effect is commonly defined as that force and moment which are proportional to the product of angle of attack and the reduced spin rate, $pd/2u_\infty$, where d is a reference length and u_∞ is the free-stream velocity. Extensions of the basic linear relationship would account for nonlinear variations in the side force and yaw moment with angle of attack and spin rate, although it will be pointed out subsequently that nonlinearities with spin rate may be ignored under certain circumstances.

Magnus measurements were made with the model mounted on the balance through a ball-bearing support which enabled the model to spin about its longitudinal axis. The model was spun by means of fin cant. For tests involving the freely spinning stabilizer, the forebody was locked to the balance and only the stabilizing surfaces were spun. The first procedure in carrying out the test was the establishment and maintenance of the desired flow conditions. The model, or the fins alone if the freely spinning stabilizer was being tested, rapidly attained steady-state spin rate. Ideally all flow conditions should be constant during the period of data acquisition. However, it was necessary to make allowance for ramdom phenomena, such as balance vibration and flow perturbations. The approach taken here was to obtain about a 100-point sample of gage readings. This sample was then averaged to give one reading for each data point, defined by the number pair, angle of attack and Mach number. A comprehensive set of Magnus data on the M823 Research Store is available in References (10) and (11). It will be shown, subsequently, that the reduced spin rate is determined by angle of attack and Mach number.

In making Magnus measurements on bodies of revolution (usually spin stabilized) the normal procedure is to spin the body at discrete rates or permit spin decay of the body through a fairly wide range of rates. Side-loads and yawing-moment measurements are made continuously and presented as functions of reduced spin rate, $\hat{p}$. The reason for doing this is that the reduced spin rate experienced by a body of revolution depends upon the value of the initial spin rate (which, in the case of a shell, can be related to the barrel rifling twist). In addition, the reduced frequency depends upon the body's trajectory. One encounters, for example, the situation where the reduced spin rate often increases with down range distance, because although the spin rate decreases somewhat with range, the airspeed decreases more quickly so $\hat{p} = pd/2u_\infty$ usually increases.

For a finned body the situation is somewhat different. The steady-state reduced spin rate, p_{ss}, of a finned body may be related to the rolling-moment derivative due to fin cant, C_{ℓ_δ}, the fin cant, δ and the damping-in-roll derivative, C_{ℓ_p}, as,

$$\hat{p}_{ss} = -\frac{C_{\ell_\delta}\delta}{C_{\ell_p}} \qquad (1)$$

(See Eq. (A-8c) of Appendix A)

Equation (1) indicates that for a given shape, Mach number, Reynolds number and angle of attack, the reduced spin rate is fixed since C_{ℓ_δ}, δ and C_{ℓ_p} are determined by the similarity parameters mentioned. It might be reasoned further that the reduced spin rate, p, has little Mach number dependence because both C_{ℓ_δ} and C_{ℓ_p} are almost equally affected by changes in Mach number. Evidence of this effect may be seen in Reference (11) where direct measurements of reduced spin rate are recorded. Reference (11) also indicates how rapidly finned bodies reach the condition of steady-state spin. For most purposes it may be assumed that the stabilizer is at a steady spin rate and, hence, the Magnus effect is defined uniquely by Mach number, Reynolds number and angle of attack; the reduced spin rate being fixed by these quantities. This statement is equivalent to saying if Mach number, Reynolds number and angle of attack are matched between a full-scale weapon and sub-scale wind-tunnel model the reduced frequency and, hence, the Magnus load coefficients will be identical.

Figures 6 through 9 present typical Magnus measurements obtained in wind-tunnel tests on the research store fitted with a cruciform stabilizer. In Figures 6 and 7 the Magnus force and moment on the fixed and freely spinning stabilizer with a fin cant of two degrees are given at Mach numbers of 0.80 and 1.20. Figures 8 and 9 are a similar presentation for the configuration with a fin cant of four degrees.

An important aspect of these Magnus data is the opportunity given to evaluate the stabilizer-alone contribution to the Magnus effect. It will be noted upon examination of Figures 6 and 8 that both configurations at small angles of attack have a negative side force. In addition, this side force has nearly the same magnitude for both the fixed and freely spinning stabilizers. As angle of attack increases, the freely spinning stabilizer has a smaller side force than does the fixed stabilizer. For both configurations the side force becomes decreasingly negative; for the stabilizer with two-degree fin cant the side force of the freely spinning stabilizer becomes positive at seven degrees angle of attack, while the side force of the fixed stabilizer becomes positive at nine or ten degrees angle of attack.

The total side force may be assumed to have two components - one due to the forebody and another due to the stabilizer. It would be expected that the side force due to the forebody would be negative in keeping with extensive projectile Magnus measurements. However, the sign of the force on the stabilizer is less well established. It appears from Figures 6 and 8 that at small angles of attack the Magnus force on the stabilizer is also negative; however, as the angle of attack increases the stabilizer side force becomes positive. The exact value of the "cross over" angle of attack varies with fin-cant angle. According to a qualitative theory set forth, originally by Platou (Ref. (12)), the force on the stabilizer should be negative (for clockwise or positive spin direction). Thus, for subsonic Mach numbers and low angles of attack it appears that there is consistency in sign between the theory and measurements. A conflict between theory and measurement, of course, exists for angles of attack above seven degrees.

Referring to the Magnus moments, experience from projectile measurements would suggest that the center of pressure for the forebody would lie slightly aft of the body's midpoint. On the other hand, the center of pressure for the stabilizer is most likely to be in the vicinity of the fins and therefore well aft of the body's midpoint. Consequently, in the conventional aeroballistics axis system, the applied moment would be positive since both stabilizer and forebody forces are negative and both are longitudinally aft of the yaw axis. Figures 6 and 8 indicate that the Magnus moment is positive for small angles of attack. With increasing angle of attack the yaw moment becomes decreasingly positive as the side or Magnus force on the stabilizer first becomes less negative and then finally changes sign. From Figure 6 it is evident that the stabilizer's positive force contribution at high angles of attack is not sufficient to overcome the forebody's negative force and so the yaw moment remains positive. However, with four degrees of fin cant, as shown in Figure 8, the increasing contribution of the stabilizer to the Magnus effect results in a change in the sign of the Magnus moment.

For slightly supersonic Mach numbers the side force is entirely positive and the situation is somewhat the reverse of that at subsonic Mach numbers. If the forebody force is regarded as always being negative, then Figures 7 and 9 indicate that the side force on the stabilizer must always be positive - the exact opposite of that predicted by Platou's theory. It may be noted also in Figures 7 and 9 that when the forebody is spinning, i.e., the fixed-stabilizer configuration, the total Magnus force is diminished somewhat by the negative Magnus force contribution of the forebody.

A general conclusion that may be drawn from the Magnus measurements is that for subsonic Mach numbers the force contributed by the stabilizer is negative for small angles of attack and reverses sign for angles of attack above six or eight degrees. For supersonic Mach numbers the side or Magnus force is always positive.

Static measurements were made on the freely spinning stabilizers under conditions of steady-state spin of the tail (Ref. (3)). However, it was noted, in regard to the freely spinning cruciform stabilizer, that computer simulations were much improved when the static aerodynamic coefficients were entered as functions of panel roll angle. The RAE undertook to provide these roll-dependent static measurements for the monoplane stabilizer (see Ref. (6)). NOL carried out additional studies of the roll dependency for the monoplane static measurements (see Ref. (13)); also as a consequence of this simulation study, NOL conducted additional investigations of the induced-roll moment of the M823 (see Ref. (14)).

In the ARA's tests, five-component static measurements were made on a half-scale model in ARA's 9- x 8-foot Transonic Wind Tunnel. Measurements were made every 15 degrees through a roll angle range of from 0 to 180 degrees. Figure 10 presents the normal-force and pitching-moment data, while Figure 11 presents the three remaining static coefficients for side force, yaw force and roll moment.

No pitch-damping measurements were carried out on the M823 Research Store with freely spinning monoplane stabilizers. Estimates were based upon the pitch-damping measurements of the fixed and freely spinning cruciform stabilizers. As was pointed out earlier in this section, the weapon was lightly damped. Since the damping-in-pitch derivative had a relatively minor effect on the trajectories, it was felt that estimates based on other configurations would suffice (see Ref. (8)).

One of the objectives of the cooperative research program has been the evaluation of wind tunnels as a source of data for free-fall weapons. In Section 5 aerodynamic coefficients measured in the wind-tunnel are compared with those reduced from free-fall store angular measurements. A second way of establishing confidence in wind-tunnel data is to compare coefficients obtained in two different facilities. A comparison of NOL and RAE measurements, based upon normal force and pitch moment, is given in Figure 12. Agreement between measurements in the two facilities is considered satisfactory. The only disturbing aspect of the results is that, for low angles of attack, measurements at RAE indicate the center of pressure is further forward than do the comparable NOL measurements. It is believed that reasons for this disagreement stem from the differences in sting geometry and test Reynolds number. Since fin-cant angles for tests in both facilities were nominally four degrees, differences in spin rate between RAE and NOL models are unlikely to be significant. Reference (3) indicates that even for large differences in spin rate, the static characteristics are nearly the same.

3.0 FLIGHT TRIALS AND RESULTS

3.1 THE TEST VEHICLE

The trials program included three rounds with cruciform tails numbered 733, 734 and 735, the two rounds with monoplane tails numbered 737 and 738. These test vehicles were manufactured at WRE and the method of construction adopted is shown in Figure 13. Basically, the streamlined M823 body comprised six cast-aluminum alloy sections, four of which were flanged and fitted with studs to facilitate assembly of the overall center body. To maintain a "clean" external surface the body sections were bolted together by studs placed below the skin line making it necessary to assemble the store progressively from the aft end using a threaded nose cone to give final closure of the vehicle. The freely spinning tail cone and fin assembly was supported on a pair of ball bearings which were mounted on a tail shaft.

This shaft was anchored to a subsidiary conical casting held by studs within the adjacent body section. On release from the aircraft a simple lanyard-operated catch was removed allowing the tail to spin freely. Ready access to the telemetry sender was obtained by installing it as far forward as possible. The total weight of the complete streamlined body was kept somewhat below 400 pounds, leaving considerable freedom for the disposition of ballast needed to vary the center-of-gravity position and moments of inertia within the specified all-up weight of approximately 900 pounds. Body alignment was maintained by ensuring that the flanged ends of the cast sections were machined square with their individual axes of symmetry.

Because the experiments demanded control of fin cant to within ±0.1 degree, pressure molded plastic fins were designed with the required cant angle set on an integrally molded stock to ensure repeatability of the fin geometry. The fins were located in parallel-sided slots, accurately machined in the tail cone giving a range of cant angles from zero up to 3.5 degrees. Each fin was firmly wedged in position and its root leading and trailing edges and the complete tail assembly was balanced on its bearings and subjected to systematic measurements of the individual cant angles, chordwise chamber and spanwise twist. It was not practical to house telemetry aerials in the freely spinning stabilizer assembly and so flush-mounted quadra-loop aerials were mounted in the vicinity of the telemetry transmitter. Physical properties of the three cruciform and two monoplane stabilized rounds are given in Figures 14. Details of the trials release and impact conditions are given in Table 2 for the cruciform and Table 3 for the monoplane stabilizers.

Measurements required during the free-flight trials were as follows:

a. trajectory from ground-based instruments,

b. flight data telemetered from instruments carried in the test vehicles,

c. observation of the release disturbance from aircraft cameras,

d. meteorological measurements.

The methods used to obtain these data are outlined in Reference (1), together with an assessment of the accuracy achieved under the operating conditions at the Woomera Range.

3.2 RESULTS OF INSTRUMENTED BOMB TRIALS

Each test vehicle was released singly, in level flight, from the same station in the bomb bay of a Canberra aircraft. To assess the overall ballistic performance of individual rounds, the observed impact conditions were compared with those predicted on the IBM 7090 computer using the measured release conditions and meteorological data, together with the measured drag function for the bomb (see Ref. (1)). Particle trajectories were computed initially assuming a flat, nonrotating earth with constant gravitational attraction; corrections for the earth's rotation, the variation of gravity with height and the variable direction of gravity (spherical earth) were subsequently estimated and subtracted from the observed impact data to give the impact deviations in range, line and time of fall listed in Tables 2 and 3. These corrections were calculated for vacuum conditions because such an approximation was found to give results of sufficient accuracy.

In the following paragraphs a brief description of the flight behavior is given for the bomb test vehicles. Comparisons of free-flight and wind-tunnel measurements of the aerodynamic coefficients and theoretical studies of dynamic behavior are made subsequently in Sections 5 and 6.

3.2.1 ROUNDS 733, 734 and 735 WITH CRUCIFORM TAILS. Rounds 733, 734 and 735 with spinning cruciform tails, were each ballasted to have an all-up weight of nominally 680 pounds and center-of-gravity position at 52 percent of the body length from the nose. Ballasted in this way, the rounds closely resembled a series of fixed-cruciform tail stores previously tested under similar release conditions, namely, the bomb test vehicles of Group A in Reference (1). Consequently, the effectiveness of freely spinning cruciform tails may be assessed by comparing results from the two sets of trials. For convenient reference a description of the behavior of bombs from Group A is given below.

The overall ballistic performance of bombs in Group A was generally satisfactory with fin cants ranging from zero up to 1.0 degree. Response to the release disturbance was normal, with peak pitch amplitudes of about 20 degrees and initial yaw amplitudes increasing slightly with fin cant from approximately seven to ten

degrees. In general, the roll rate increased quite steadily during the fall but showed some influence of induced rolling moments, particularly during the release phase. However, with fin cants of nominally 1.5 and 3.0 degrees, the bombs performed large amplitude (30-degree maximum) circular yawing motions at release which were characteristic of roll lock-in and which persisted for up to six seconds after release. Under these conditions, the impact deviations were excessive (15 to 35 mils).

Spin histories of the stabilizers and forebodies for Round 733, 734 and 735 are shown in Figure 15. Except in the case of Round 735, which had the smallest fin cant of 0.24 degree, the effect of induced rolling moments appears to have been negligible. Furthermore, the very slow growth of forebody roll rate in each case indicated that the tail bearings performed satisfactorily and that rolling torques due to forebody asymmetries must have been quite small. Flight histories of angle of attack are given in Figures 16, 17 and 18 for Rounds 733, 734 and 735, respectively. The tail of Round 735, with 0.24-degree fin cant, momentarily locked-in during the release disturbance but quickly broke out again as indicated in Figure 18. Subsequently, from 28 seconds after release until impact, the tail spun at approximately the same rate as the pitch frequency, however, the incidence did not exceed about 1.0 degree over this period. The large dispersion in range (13.3 mils) for Round 735 was caused entirely by irregular disturbances experienced during the first four to five seconds of fall. In the case of Round 733 and 734, the release disturbance caused a slowly processing oscillation, as shown in Figures 16 and 17, which decayed smoothly and rapidly with no adverse Magnus effects. Consequently, these trials have clearly demonstrated the effectiveness of freely spinning cruciform tails in minimizing the influence of roll-yaw cross coupling and Magnus effects for streamlined bomb configurations.

3.2.2 ROUNDS 737 AND 738 WITH MONOPLANE TAILS. With only two research vehicles available for flight testing the monoplane tails, it was determined that Rounds 737 and 738 should be made as nearly as possible identical in all respects. This was done to provide some evidence of repeatability in the trials results and, as indicated in Table 3, quite close agreement in the physical properties of the stores was achieved. The monoplane tail units were obtained by simply removing one pair of fins from the otherwise cruciform assemblies and it was necessary to place the center of gravity well forward at nominally 35 percent of the body length to ensure an adequate degree of stability.

From Figure 15 it may be seen that the tail spin histories were closely alike and showed evidence of yaw-induced rolling moments for about the first ten seconds of fall. In general, response to the release disturbance for both rounds was similar to that exhibited by Round 733 which had a comparable amount of fin cant. In fact, all five spinning tails gave quite well-damped responses which decayed smoothly to amplitudes of five degrees or so at ten seconds after

release. Although the forebody spin histories for Rounds 737 and 738 differed quite considerably, the rates achieved were sufficiently low to indicate satisfactory tail bearing performance.

Flight records showing angles of attack are given in Figures 19 and 20 for Round 737 and in Figures 21 and 22 for Round 738. A significant feature of these records is the very low oscillation frequencies having periods of up to three seconds. Consequently, with virtually nonrolling forebodies, both rounds experienced prolonged periods of fall during which the lift vector changed its direction so slowly that excessive dispersion resulted even though the vehicles were dynamically stable. In the case of Round 737, Figure 20 clearly shows a condition of flight at trimmed incidence with a magnitude of about 2.5 degrees which provided an additional source of dispersion. The poor ballistic performance of the monoplane tail vehicles is indicated in Table 3 where impact deviations of 10 mils and 70 mils are recorded.

In Appendix A, a simple linear theory of flight dynamics is outlined to demonstrate the characteristic behavior of missiles stabilized by freely spinning tails which may have slight configurational asymmetries, both forebody and stabilizer associated. Based on this analysis, boundaries of dynamic stability are determined from which design criteria may be established for both cruciform and monoplane tails. Formulae are also derived for the prediction of basic oscillation frequencies permitting preliminary estimates of missile flight performance to be carried out with little effort.

It may be readily shown that the behavior of Rounds 737 and 738 would have been quite satisfactory with the addition of stub fins to the tail units in a plane normal to the existing monoplane fins and having a span no more than one caliber.

4.0 FREE-FLIGHT AERODYNAMIC ANALYSIS

Dependence of the measured aerodynamic forces and moments upon incidence, roll orientation and angular velocity is determined by using a least squares method to fit flight data to a mathematical model of the force and moment system developed by Maple and Synge (Ref. (15)). A detailed description of the methods which were used in analyzing the flight data may be found in References (16) and (17).

Basically, Maple and Synge represent the overall force and moment system by a complex Taylor series expansion, making use of the properties of rotational and reflectional symmetry to systematically eliminate particular terms. Two assumptions are made concerning the aerodynamic forces and moments acting on the body. These are:

a. that they depend only upon the instantaneous values of the linear and angular velocities of the body,

b. that they are analytic functions of the components of these velocities.

Applying the theory to the cruciform tail configuration, the representations used were as follows:

Static restoring moment and normal-force coefficients defined by similar expressions of the form:

$$a_1 \operatorname{Tan}|\gamma| + [a_2 + a_4 \operatorname{Cos} 4\phi] \operatorname{Tan}^3|\gamma| + [a_3 + (a_6 + a_8) \operatorname{Cos} 4\phi] \operatorname{Tan}^5|\gamma| \tag{2}$$

Static yawing moment and side-force coefficients defined by similar expressions of the form:

$$a_4 \operatorname{Sin}(4\phi) \operatorname{Tan}^3|\gamma| + (a_5 - a_6) \operatorname{Sin}(4\phi) \operatorname{Tan}^5|\gamma| \tag{3}$$

Magnus moment and force coefficients defined by similar expressions of the form:

$$b_1 \operatorname{Tan}|\gamma| \tag{4}$$

Corresponding expressions for the force and moment system on the monoplane tail were as follows:

Static restoring moment and normal-force coefficients defined by similar expressions of the form:

$$[C_1 + C_4 \operatorname{Cos} 2\phi] \operatorname{Tan}|\gamma| + [C_2 + (C_5 + C_6) \operatorname{Cos} 2\phi + C_9 \operatorname{Cos} 4\phi] \operatorname{Tan}^3|\gamma| + [C_3 + (C_7 + C_8) \operatorname{Cos} 2\phi + (C_{10} + C_{11}) \operatorname{Cos} 4\phi + C_{12} \operatorname{Cos} 6\phi] \operatorname{Tan}^5|\gamma| \tag{5}$$

Static yawing moment and side-force coefficients defined by similar expressions of the form:

$$C_4 \sin 2\phi \tan|\zeta| + [(C_5 - C_6)\sin 4\phi + C_9 \sin 4\phi]\tan^3|\zeta| + [(C_7 - C_8)\sin 2\phi + (C_{10} - C_{11})\sin 4\phi + C_{12}\sin 6\phi]\tan^5|\zeta| \quad (6)$$

Magnus moment and force coefficient defined by similar expressions of the form:

$$[d_1 + d_2 \cos 2\phi + d_3 \sin 2\phi]\tan|\zeta| \quad (7)$$

where the least square coefficients, a_1, a_2, ..., a_6, b_1, c_1, c_2, ..., c_{12} and d_1, d_2, d_3, depend upon Mach number and absolute stabilizer roll rate only. The magnitude of the angle-of-attack vector is $|\zeta|$ and ϕ is the angular orientation of a fin relative to the plane of the angle of attack (defined positive for a clockwise rotation viewed from the rear).

Only quantitative results for pitch and yaw damping could be obtained whatever representation was attempted. Consequently, constant values were derived using static wind-tunnel measurements in an empirical formula (Ref. (18)). These values are indicated below. The reference center for the moment derivatives is taken at the center of gravity (body midpoint).

	CRUCIFORM TAIL (M = 0.7)		MONOPLANE TAIL (M = 0.7)	
	MOMENT	FORCE	MOMENT	FORCE
Pitch	$C_{m_q} + C_{m_{\dot{\alpha}}} = -117$	$C_{z_{\dot{\alpha}}} = -10$	$C_{m_q} + C_{m_{\dot{\alpha}}} = -23$	$C_{z_{\dot{\alpha}}} = 25$
Yaw	$C_{n_r} - C_{n_{\dot{\beta}}} = -117$	$C_{y_{\dot{\beta}}} = 10$	$C_{n_r} - C_{n_{\dot{\beta}}} = -175$	$C_{y_{\dot{\beta}}} = 10$

By comparison with the wind-tunnel data shown in Figure 5, it appears that, on the basis of Robinson's method (Ref. (18)) for estimating the pitch-damping derivative, spin has relatively little effect at low angles of attack. This result is further confirmed by ARA wind-tunnel measurements on the M823 shape with fixed fins presented in Reference (1).

Since accurate values of roll acceleration could not be obtained, the rolling moments were not analyzed. However, some knowledge of the roll-exciting and roll-damping moments was required to simulate the free-flight histories of the instrumented rounds. Values of the roll-exciting moment were taken from the NOL static wind-tunnel

measurements for configurations with zero and four degrees fin cant. The roll-damping moment was determined for the cruciform stabilizer by varying the input to a six-degree-of-freedom trajectory program until a satisfactory fit of the measured stabilizer roll history was achieved for Round 733. A similar technique was adopted to estimate roll-exciting and damping moments for vehicles with a monoplane stabilizer.

The ranges of time from release, Mach number, tail roll rate and angle of incidence over which analyses were carried out are given in Table 4 for both the cruciform and monoplane stabilizer. The fin cant and Reynolds number (based on body diameter) are also given in this table.

5.0 COMPARISON OF FREE-FLIGHT AND WIND-TUNNEL MEASUREMENTS

5.1 CRUCIFORM STABILIZER

In this section, comparisons are made between aerodynamic coefficients measured in the wind tunnel and those reduced from free-fall tests. The wind-tunnel data were obtained from measurements made in the NOL Supersonic Tunnel No. 1 at a Mach number of 0.70 and a Reynolds number of 0.6 million (based on body diameter). Reference (5) is the principal source of the wind-tunnel data. These data comparisons are presented in Figures 23 and 24. In these figures the symbol A82, for example, refers to measurements obtained on the A, or fixed-cruciform configuration and is used to maintain consistency with data reports such as Reference (5). It was necessary to make use of the fixed-stabilizer data in order to obtain the roll dependency in the coefficients.

Comparisons of the free-flight and wind-tunnel measurements of the pitching-moment and normal-force coefficient are presented in Figure 23 for the zero fin-cant configuration at three stabilizer roll orientations. Of course the free-flight rounds 733, 734 and 735 had cant angles of 3.4, 1.4 and 0.24 degrees, respectively (see Fig. 14a). However, it was pointed out in Section 2 that fin cant had no discernable effect on the normal force and pitching moment. It may be seen that the agreement in the normal force is generally good; however, the pitching moment and, hence, center of pressure shows somewhat less satisfactory correlation.

Figure 24 presents a comparison between free-fall and wind-tunnel measurements of the side-force and yawing-moment coefficients at a roll angle of 22.5 degrees. Considering the small magnitude and often erratic behavior of the side force and yawing moment, it is felt that this figure indicates generally good agreement.

Data on Magnus effects have not been presented because they showed only qualitative agreement with the available wind-tunnel measurements.

5.2 MONOPLANE STABILIZER

For comparisons of the wind-tunnel and free-flight aerodynamic data in the case of the monoplane stabilizer, the source of the wind-tunnel data was measurements made at ARA and documented in Reference (6). Normal-force and pitching-moment and side-force and yawing-moment data are presented in Figures 25 and 26 for a Mach number of 0.70 and a Reynolds number of 2.5 million (based on body diameter).

The results covered a range of roll orientations beteeen 0 and 180 degrees, but the mathematical model used to fit the flight data assumed reflectional symmetry (see Eqs. (5), (6) and (7), Sec. 4). Therefore, the effect of fin cant could not be represented. Consequently, the mathematical model averaged the effect of fin cant; for comparison, the appropriate wind-tunnel results were averaged to produce a range of values for roll orientations between 0 and 90 degrees. The wind-tunnel results were available at fin cants of two and four degrees; since both Rounds 737 and 738 had the same nominal fin cant of 3.5 degrees, a set of wind-tunnel values were obtained for a 3.5-degree fin cant by linear interpolation.

It may be seen in Figures 25 and 26 that good agreement was obtained between rounds but that agreement between rounds and wind-tunnel data was only fair. Free-flight measurements for both the restoring moment and normal-force coefficients were roughly 25 percent less than the corresponding wind-tunnel values. A similar reduction of between 10 and 15 percent was observed with the side-force and yawing-moment coefficients at a roll angle of 45 degrees. As may be expected with the limitations of the mathematical model, the free-flight measurements of the side-force and yawing-moment coefficients at roll angles of 30 and 60 degrees do not differ by very much. It is more appropriate to compare the free-flight measurements with the average of the wind-tunnel values for the two roll orientations.

Data on the Magnus effects have not been presented because they showed only qualitative agreement with the available NOL wind-tunnel measurements.

A possible explanation for the differences observed between free-flight and wind-tunnel measurements is that the wind-tunnel tests were performed on a model with the stabilizer fixed in various roll positions, whereas the free-flight tests had a rapidly spinning tail from which measurements were recorded as a function of stabilizer orientation.

6.0 FLIGHT SIMULATION

With quite modest airborne instrumentation and the aid of digital computing facilities, it has proved feasible to apply curve fitting techniques to very large quantities of flight data, making it possible to obtain detailed information on the aerodynamic force and moment system of the test vehicles. Such results, when taken

from the full-scale trials, have shown highly favorable agreement with measurements which were carried out in a variety of wind tunnels. Furthermore, by programming the six-degree-of-freedom equations of motion (Refs. (19) and (20)) for solution by digital computer and using wind-tunnel data as an input, it was possible to predict the missile behavior and this showed good correlation with the observed trials data.

Typical predictions for the freely spinning cruciform and monoplane tail vehicles are given in Figures 16 and 19, respectively, where simulations of response to the release disturbance are compared with the recorded flight histories for the angle of attack. From these figures it is evident that such oscillation parameters as frequency, amplitude, damping, phase and precession are all quite precisely reproduced for the critical flight period during response to the release disturbance. However, the dispersion of Rounds 737 and 738 proved very difficult to predict. For these vehicles it was found necessary to program the measured forebody roll history into the process of trajectory simulation and, by trial and error, determine the magnitude and initial orientation of a tail axis misalignment which yielded a satisfactory match with the observed impact point. In Figure 27 the result of this matching technique is clearly indicated for the case of Round 737. With a tail axis misalignment set at 0.4 degree, excellent correlation between the predicted and observed trajectories is shown throughout the entire period of fall. Similar results were obtained for Round 738 using the same tail misalignment of 0.4 degree. From considerations of the test vehicle construction it was believed unlikely that such a large asymmetry would arise from the tail unit alone and it was thought that errors had probably accumulated in alignment of the multi-jointed forebody.

Performance of the monoplane tail was critically influenced by body misalignments because this unit provided a very low stability factor as exhibited by the low natural pitching frequencies of Rounds 737 and 738. When trajectory simulations were carried out for the cruciform spinning tails with the same axis misalignment of 0.4 degree, the variations in predicted impact point were less than 0.1 percent of a nominal trajectory with zero misalignment.

Because of the observed flight characteristics of all three freely spinning cruciform rounds, as well as the excellent agreement between Round 733 predictions and measurements, it was decided to investigate the ballistics of freely spinning stabilizers in more detail. The principal advantage of the freely spinning stabilizer, as indicated in the static tests (Ref. (5)), was the virtual elimination of the roll-induced forces and moments. The implication was that if these effects could be eliminated, or at least greatly reduced, instabilities, such as roll resonance and catastrophic yaw, could be virtually eliminated. To carry out this investigation it was decided to make computer investigations of a number of flight regimes. Under identical initial and environmental conditions, the trajectories of rounds with fixed and freely spinning stabilizers

would be compared. Such a comparison should permit an adequate assessment of the advantages of the freely spinning stabilizer concept.

The first conditions selected concerned a bomb release at an altitude of 45,000 feet, an initial pitch rate (in the vertical plane) of one radian per second and an initial yaw rate of 0.08 radian per second. In this simulated drop the fin-cant angle was set at 0.007 radian (0.401 degree). The spin rate histories corresponding to the fixed and freely spinning cruciform stabilizers are given in Figure 28. Quite obviously the fixed stabilizer had a much slower spin acceleration than did the freely spinning stabilizer, equaling three radians per second at about the time that the freely spinning stabilizer reached its steady-state value of nearly 14 radians per second. The spin rate of three radians per second is approximately the weapon's pitch frequency. The result of this near equality of pitch and spin rates is evident in the right-hand graph of Figure 28. The fixed-stabilizer configuration develops a large total angle of attack. This allows the weapon to lock-in and to remain in this locked-in condition for a sufficient time for the induced yaw moment to cause excessive angle of attack. By the way of contrast, the freely spinning stabilizer, in virtually eliminating these induced effects, allowed the motion to damp. The only force perpendicular to the angle-of-attack plane was that attributed to the Magnus effect and this force is not large enough to alter significantly the decay of the pitch oscillations. Clearly, in this case, the freely spinning stabilizer prevented catastrophic yaw.

For the next set of trajectories, a release at a lower altitude of 10,000 feet was studied. In this case the initial weapon speed was set at 800 feet per second and initial pitch and yaw rates of 1.8 and 0.2 radians per second, respectively. The fin-cant angle was set at 3.44 degrees. Because of the rather large angle of fin cant, it is not too surprising to find large spin rates and spin accelerations. Figure 29 shows that the freely spinning stabilizer under these conditions reaches a nearly steady-state value of spin rate of 130 radians per second in less than two seconds after release. The angular history shown to the right in Figure 29 indicates that the fixed stabilizer again performs unsatisfactorily. The angular amplitude continues to grow for the fixed stabilizer and to decrease for the freely spinning stabilizer.

Earlier it was mentioned that while the freely spinning stabilizer largely eliminated roll-induced effects, the Magnus force is still present as a load normal to the angle-of-attack plane. The question arose as to what effect the Magnus force and moment would have at large angles of attack and large spin rates. This problem was addressed by carrying out a dual trajectory simulation (fixed and freely spinning) at an altitude of 4000 feet and a speed at launch of 793 feet per second. The launch aircraft was assumed to be diving at an angle of 60 degrees (bomb's initial flight path angle). The store, at release, was at an effective angle of attack of five degrees, an initial pitch rate of three radians per second and an initial yaw

rate of 0.5 radian per second. The angle of fin cant was set at 3.44 degrees. This simulation represents a severe release condition. The resulting large amplitude response is shown in Figure 30. Under these circumstances the Magnus effect has a strong influence on both the freely spinning and fixed-stabilized stores alike. Each configuration rapidly develops a circular coning motion with an amplitude of approximately eight degrees which would be quite unacceptable for weapon delivery. However, performance of the store with the freely spinning stabilizer could be substantially improved over that of the fixed stabilizer by reducing fin cant to about 1.0 degree.

From the foregoing cases it is apparent that the freely spinning stabilizer offers significant advantage by comparison with the conventional fixed stabilizer in overcoming the adverse effects of roll lock-in and catastrophic yaw. Furthermore, by careful choice of fin cant it should be possible to design a freely spinning tail capable of operating satisfactorily over a wide range of release conditions, including situations where a fixed-tail design would give an unacceptable performance due to Magnus effects.

7.0 DESIGN FEASIBILITY

A further advantage of the freely spinning stabilizer, in addition to those listed in the Introduction, became apparent as the program developed. It was suggested in Reference (1), for a conventional fixed-cruciform free-fall store, that the adoption of accurately produced fins can control the effect of accidental occurrence of spin to such an extent that most problems of flight instability are avoided. However, with modern trends placing greater emphasis upon multiple carriage of aircraft weapons, the need for smaller fins and, hence, lower static stability demands stricter fin manufacturing tolerances. Consequently, as these tolerances become more stringent the overall stabilizer production costs are increased due to additional expenses in tooling and inspection. In the case of a freely spinning tail, the tolerances can be relaxed; perhaps the extra costs caused by mechanical complexity can be partly, if not wholly, offset by the saving in tooling and inspection costs.

Clearly, bearing friction in the tail mounting must be kept to a minimum to allow full advantage of the low-roll inertia of the freely spinning stabilizer. Otherwise the body will experience some roll acceleration transmitted through the bearings. Since virtually no aerodynamic roll damping is present in the forebody, its spin rate would, in time, be equal to that of the stabilizer. Therefore, the successful operation of any such stabilizer will depend very critically upon minimizing torque transfer from stabilizer to forebody. This design goal can be reached only by assuring good bearing design, long bearing life during weapon storage and correct alignment of body and spin axes.

Results obtained from the full-scale flight trials at Woomera have demonstrated that the concept of freely spinning stabilizers is technically feasible. Tail units for the test vehicle were fitted with commercially available deep-groove ball bearings which performed quite satisfactorily. However, it is unlikely that this type of bearing would be acceptable in a free-fall bomb context. Weapons have to be stored before use, hopefully for many years. The life of commercially available lubricants for the type of ball bearing used is inadequate to guarantee successful operation of the tail even after a relatively short storage period. This would mean that either the lubricant should be replaced at regular intervals, say annually, or that the tail be relubricated prior to use. Either of these alternatives is unacceptable to military use of a free-fall bomb. There is, therefore, a necessity to explore the use of dry bearings in this context.

Another advantage of the freely spinning stabilizer lies in its use as an environmental sensor. In conventional free-fall weapons a nose-mounted vane is often used in this role in the fuzing and arming functions. Although an evaluation of this concept was not carried out during this computer wind-tunnel free-fall study, such a concept seems to warrant further consideration.

8.0 CONCLUSIONS

Summarizing the results obtained from the research program on freely spinning stabilizers, the following conclusions have been established:

1. Rapid spin acceleration of the tail after store release to spin rates well above the bomb's natural pitch frequency eliminates the problems of roll-yaw resonance and catastrophic yaw.

2. Fin cant should be chosen so that the stabilizer reaches steady-state spin rate quickly and yet does not spin too rapidly for Magnus effects to predominate.

3. The Magnus force and moment are nearly identical for the fixed and freely spinning stabilizer for small angles of attack. For higher angles of attack the Magnus moment is less for the freely spinning stabilizer.

4. The freely spinning stabilizer has little effect on the normal force, pitching moment and drag; it does eliminate the induced roll and yaw moments.

5. The monoplane stabilizer offers an attractive advantage in underwing carriage, but it does require larger fins than a cruciform configuration for the same restoring moment.

6. Experience obtained from the flight trials indicates that it should be feasible to fit freely spinning tails with conventional ball bearings. However, it is considered that a specific weapon design and development study would be required to fully explore the various aspects of production, storage life and reliability to match the military requirement.

7. The freely spinning stabilizer has a possible advantage as an environmental sensor in the fuzing and arming operation.

8. Correlations between the predicted and observed flight results based on wind-tunnel measurements and computer studies have provided considerable insight into weapon dynamic behavior both during the critical release phase and the subsequent flight to impact.

REFERENCES

(1) Rhodes, C. W. and Shannon, J. H. W., "Results and Conclusions of the Joint RAE/WRE Reseach Programme on the Flight Dynamics and Ballistics Consistency of Freely Falling Missiles. Part 1 Bombs Stabilized by Fixed Cruciform Fins," Report HSA 20, Department of Supply, Australian Defence Scientific Service, Weapons Research Establishment, Salisbury, South Australia, 1965 (Also issued as Report RAE TRG 5200, Royal Aircraft Establishment, Farnsborough, Hants, U. K.)

(2) Regan, F. J., Falusi, M. E. and Holmes, J. E., "The Aerodynamic Characteristics of an Ogive Cylinder with Split-Skirt Stabilizer at Subsonic, Transonic and Supersonic Speeds," NOLTR 63-86, 1965

(3) Regan, F. J., Shannon, J. H. W. and Tanner, F. J., "The Joint NOL/RAE/WRE Research Program on Bomb Dynamics. Part II A Low-Drag Bomb with Split-Skirt Stabilizers," NOLTR 69-232, 1969 (Also issued as RAE Technical Report 70038, Royal Aircraft Establishment, Farnsborough, Hants, U. K. and WRE Report HSA26)

(4) Secomb, D. A., "Comparisons of Bomb Stability Data at Transonic Speeds from Several Wind Tunnels and Free Flight," ARL Report A 132 Sep 1969, Aeronautical Research Laboratories, Melbourne, Victoria

(5) Regan, F. J., Falusi, M. E. and Holmes, J. E., "Static Wind Tunnel Tests of the M823 Research Store with Fixed and Freely Spinning Tails," NOLTR 65-14, 1967

(6) Marsden, P., "Results of Wind Tunnel Tests on the M823 Research Store with Fixed Monoplane Fins (ARA Model M23)," ARA Model Test Note M25/1, Aircraft Research Association, Bedford, U. K. 1967

(7) Wingfield, J. G., "Results of Further Wind Tunnel Tests on the M823 Research Store with Fixed Monoplane Fins (ARA Model M25)," ARA Model Test Note M25/2 Dec 1968. Aircraft Research Association, Bedford, U. K.

(8) Regan, F. J., Holmes, J. E. and Falusi, M. E., "Pitch Damping Tests of the M823 Research Store with Cruciform and Split-Skirt Stabilizers," NOLTR 65-68, 1966

(9) Regan, F. J., "Pitch-Damping Wind-Tunnel Measurements on the M823 Research Store with a Monoplane Stabilizer," NOL Wind-Tunnel Report No. 55, 1971

(10) Regan, F. J., Holmes, J. E. and Falusi, M. E., "Magnus Measurements on the M823 Research Store with Fixed and Freely Spinning Cruciform Stabilizers, Freely Spinning Monoplane Stabilizers and Split-Skirt Stabilizers," NOLTR 69-214, 1969

(11) Regan, F. J. and Falusi, M. E., "The Static and Magnus Aerodynamic Characteristics of the M823 Research Store Equipped with Fixed and Freely Spinning Stabilizers," NOLTR 72-291, 1972

(12) Platou, A. S., "Magnus Force on a Fixed Body," Ballistics Research Laboratories Report No. 1193, Mar 1963

(13) Regan, F. J., "Preliminary Static Wind-Tunnel Measurements on the M823 Research Store with a Monoplane Stabilizer," NOL Wind-Tunnel Report No. 49, 1971

(14) Regan, F. J., Schermerhorn, V. L. and Falusi, M. E., "Roll-Induced Force and Moment Measurements of the M823 Research Store," NOLTR 68-195, 1968

(15) Maple, C. G. and Synge, J. L., "Aerodynamic Symmetry of Projectiles," Quarterly Applied Mathematics, Vol. 6, No. 4, 1949

(16) Gilbert, N. E., "A Method for Deriving Aerodynamic Force and Moment Coefficients from Free Flight Data Using a Computer Programme," WRE Tech Note HSA157, Oct 1969

(17) Gilbert, N. E., "Free Flight Measurement of Aerodynamic Forces and Moments on Bombs with Freely Spinning Cruciform and Monoplane Tails with Fixed Split-Skirt Configurations," WRE Tech Note HSA162, 1969

(18) Robinson, M. L., "The Estimation of Pitch Damping Derivatives of Missile Configurations at Subsonic Speeds," WRE Tech Note HSA144, Jan 1969

(19) Holmes, J. E., "A Powered Six-Degree-of-Freedom Trajectory Program for Vehicles with Freely Spinning Tail Stabilizers," NOLTR 69-155, Oct 1969

(20) Goodale, P. L., "An IBM 7090 Six-Degree-of-Freedom Rigid Body Trajectory Programme," WRE Tech Note HSA118, Weapons Research Establishment, Salisbury, South Australia, Jun 1966 (Programme IG2.6.2/G2 adapted for freely spinning tails by Merchant, D. G. and Hunter, J. S. on basis of Goodale's original Programme IG2.6.2)

(21) Shannon, J. H. W., "An Analysis of the Effect of Fin Attachments Upon the Ballistic Performance of 500 lb MC Mk 13 and 1000 lb GP Mk 4 Bombs," WRE Tech Note HSA90, Weapons Research Establishment, Salisbury, South Australia, 1962

(22) Phillips, W. H., "Effects of Steady Rolling on Longitudinal and Directional Stability," NACA Technical Note 1627, National Advisory Committee of Aeronautics, 1948

(23) Regan, F. J., "Static and Dynamic Stability of Free-Fall Stores with Freely Spinning Stabilizers," NOLTR 73-19, 1973

(24) Wylie, C. R., Advanced Engineering Mathematics, Third Edition, McGraw-Hill Book Co., 1966

Table 1

TEST CONDITIONS FOR NAVAL ORDNANCE LABORATORY
SUPERSONIC TUNNEL NO. 1

Mach Number	Dynamic Pressure(lbs/in^2)	Reynolds No/ft x 10^{-6}
0.50	2.10	3.00
0.60	2.80	3.40
0.70	3.48	3.75
0.80	4.13	4.00
0.85	4.42	4.15
0.90	4.70	4.25
0.95	4.90	4.35
1.50	6.13	4.40
1.75	5.80	4.12

TEST CONDITIONS FOR NAVAL SHIP RESEARCH AND DEVELOPMENT
CENTER 7-BY 10-FOOT TRANSONIC TUNNEL

Mach Number	Dynamic Pressure(lbs/in^2)	Reynolds No/ft x 10^{-6}
0.5	2.10	2.90
0.6	2.80	3.20
0.7	3.48	3.65
0.8	4.13	3.95
0.9	4.70	4.20
1.0	5.34	4.45

Table 1 (Cont'd)

TEST CONDITIONS FOR AIRCRAFT RESEARCH ASSOCIATION
TRANSONIC WIND TUNNEL

Mach Number	Dynamic Pressure (lbs/in^2)	Reynolds No/ft $\times 10^{-6}$
0.5	2.16	2.9
0.7	3.63	3.6
0.8	4.31	3.9
0.9	4.91	4.1
0.98	5.33	4.3
1.05	5.64	4.3

Table 2

PHYSICAL PROPERTIES OF CRUCIFORM SPINNING TAIL INSTRUMENTED BOMB TEST VEHICLES AND IMPACT DEVIATIONS FROM PARTICLE TRAJECTORIES

Round Number			733	734	735
Body Shape			M823	M823	M823
Center of Gravity (percent of body length from nose)			52.0	51.9	52.4
Average Fin Cant Measured (degrees)			3.39	1.39	0.24
All-up Weight (lb)			878.75	885.0	878.5
Transverse Moment of Inertia (B, slug ft^2)			178.0	177.8	173.9
Polar Moment of Inertia (A_1, slug ft^2)			5.6	6.5	5.3
Rotating Assembly Moment of Inertia (A_2, slug ft^2)			0.48	0.48	0.48
Release Height			45,176	45,346	45,676
Release Mach Number			0.74	0.71	0.69
Impact Deviation from Particle Trajectory	Range	feet mils	157 short 3.5	354 short 5.6	607 short 13.3
	Line	feet mils	176 left 3.9	28 left 0.6	122 left 2.7
	Time	secs.	0.76	0.51	0.42

Table 3

PHYSICAL PROPERTIES OF MONOPLANE SPINNING TAIL INSTRUMENTED BOMB TEST VEHICLES AND IMPACT DEVIATIONS FROM PARTICLE TRAJECTORIES

Round Number			737	738
Body Shape			M823	M823
Center of Gravity (percent of body length from nose)			34.8	35.0
Average Fin Cant Measured (degrees)			3.34	3.46
All-up Weight (lb)			917.25	901.2
Transverse Moment of Inertia (B, slug ft^2)			262.5	265.8
Polar Moment of Inertia (A_1, slug ft^2)			8.4	9.0
Rotating Assembly Moment of Inertia (A_2, slug ft^2)			0.38	0.38
Release Height			46,289	45,994
Release Mach Number			0.73	0.73
Impact Deviation from Particle Trajectory	Range	feet mils	28 over 0.6	3255 short 70.8
	Line	feet mils	736 left 16.3	132 right 2.9
	Time	secs.	+0.39	-0.02

Table 4

FLIGHT CONDITIONS FOR AERODYNAMIC ANALYSIS

CRUCIFORM TAIL

Round Number	Fin Cant degrees	Time seconds	Mach Number	Tail roll rate radians/sec.	Angle of Attack degrees	Reynolds Number x 10^{-6}
733	3.30	1.885-5.001	0.737-0.744	40-46	3.3-16.1	1.3
734	1.39	1.843-5.174	0.713-0.721	13-19	0.3-17.9	1.2
735	0.24	4.187-7.764	0.697-0.725	1.3-2.3	2.1-17.1	1.2

MONOPLANE TAIL

Round Number	Fin Cant degrees	Time seconds	Mach Number	Tail roll rate radians/sec.	Angle of Attack degrees	Reynolds Number x 10^{-6}
737	3.34	2.251-5.163	0.725-0.738	40-50	1.8-14.0	1.1
738	3.46	2.271-5.101	0.728-0.737	40-50	3.0-15.7	1.2

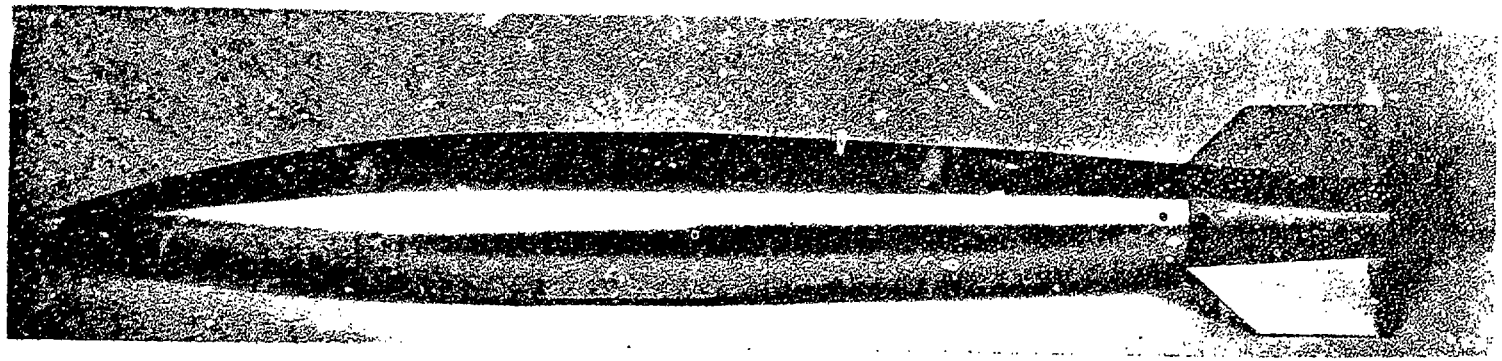

CRUCIFORM TAIL

MONOPLANE TAIL

FIG. 1 RESEARCH STORE WITH FREELY SPINNING MONOPLANE AND CRUCIFORM STABILIZERS

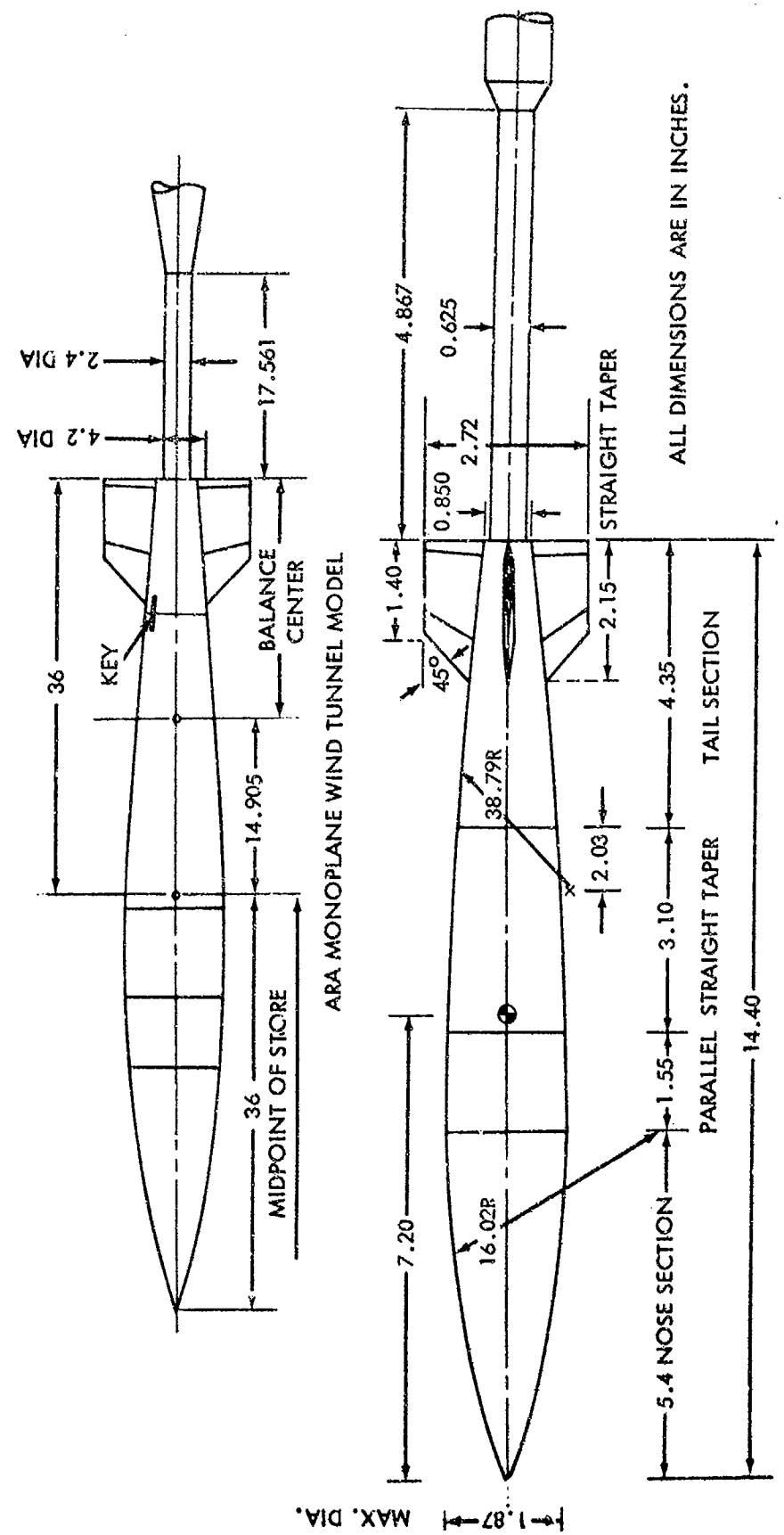

FIG.2 STING GEOMETRY FOR ARA AND NOL WIND-TUNNEL MODELS OF THE M823 RESEARCH STORE

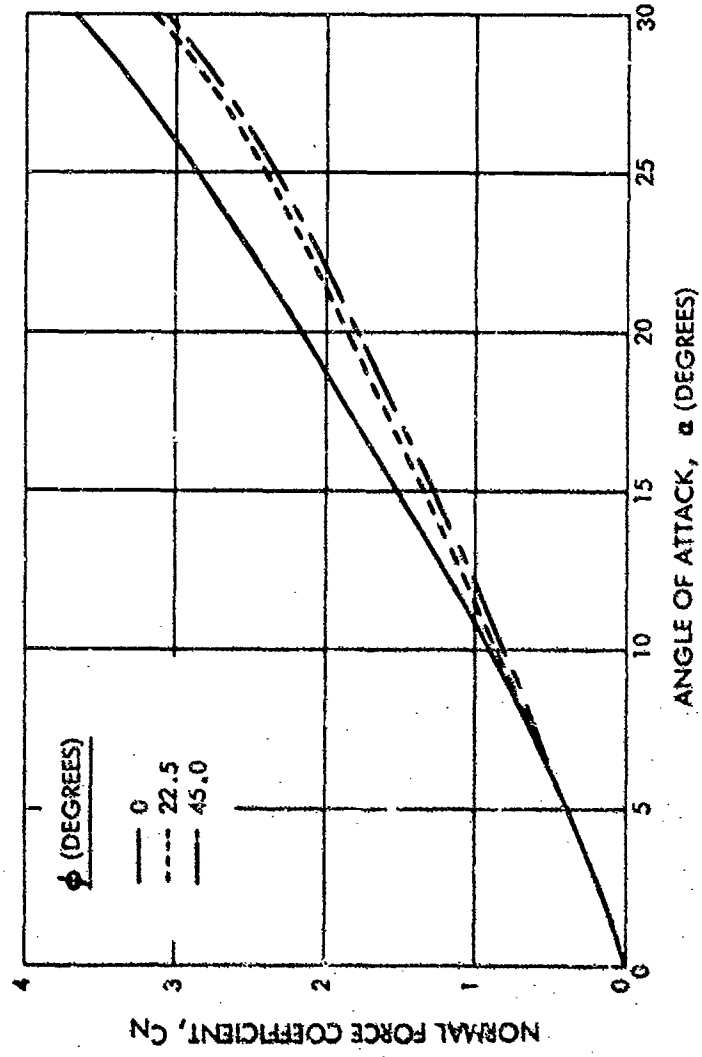

FIG. 3 NORMAL-FORCE COEFFICIENT VERSUS ANGLE OF ATTACK FOR THE M823 RESEARCH STORE WITH A FIXED CRUCIFORM STABILIZER AT A MACH NUMBER OF 0.85

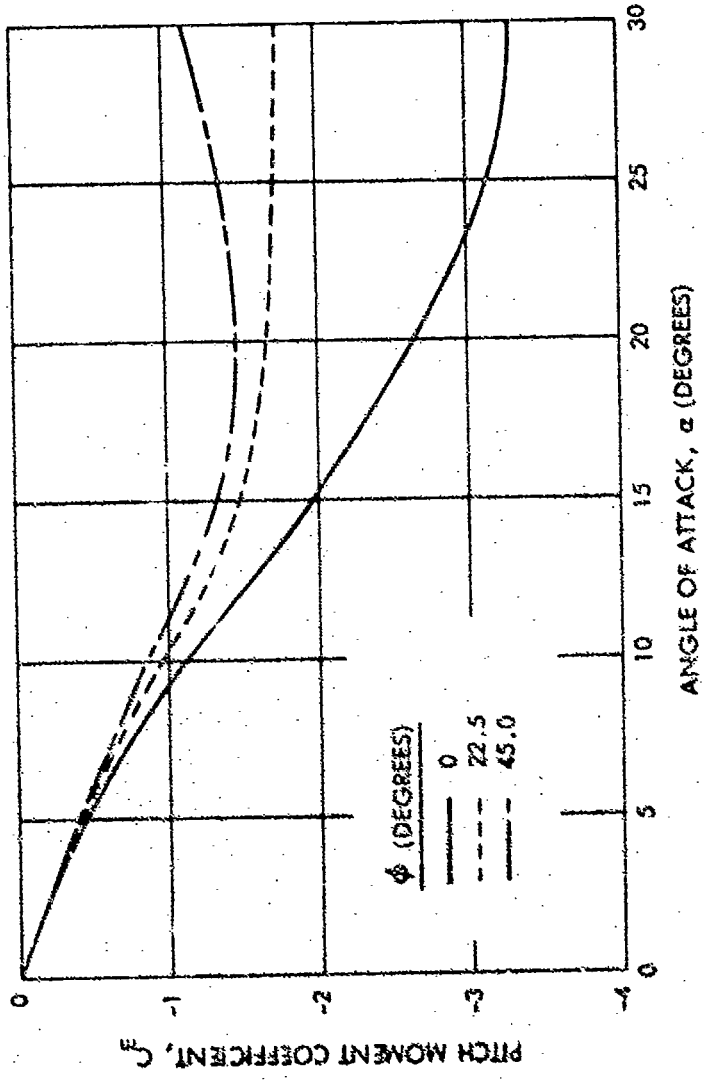

FIG. 4 PITCH-MOMENT COEFFICIENT VERSUS ANGLE OF ATTACK FOR THE M823 RESEARCH STORE WITH A FIXED CRUCIFORM STABILIZER AT A MACH NUMBER OF 0.85

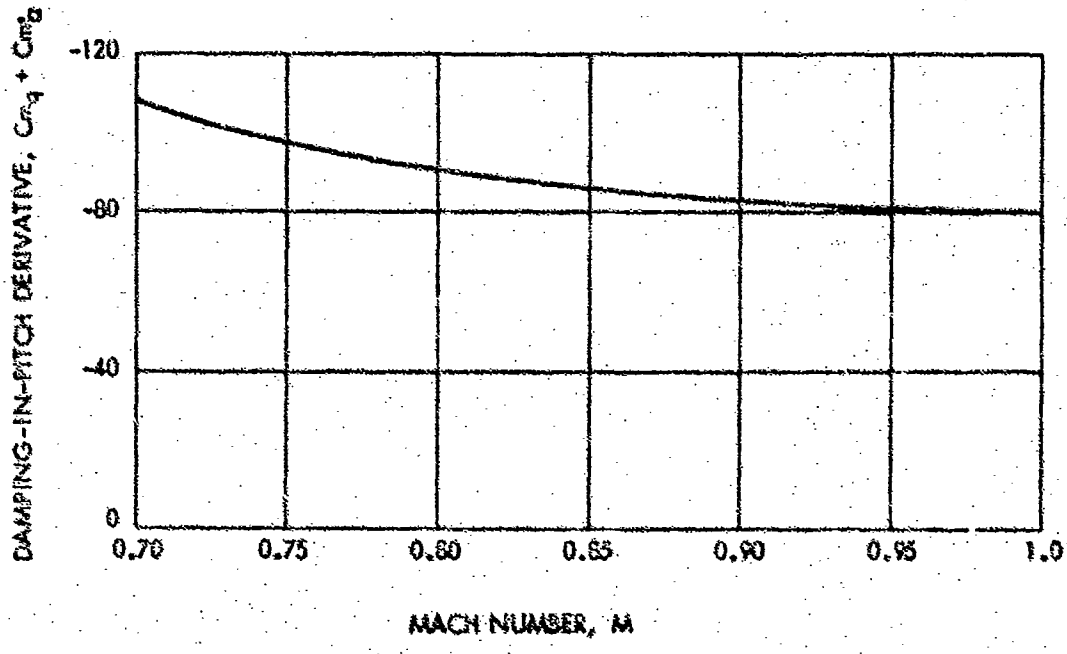

FIG. 5 DAMPING-IN-PITCH DERIVATIVE VERSUS MACH NUMBER FOR THE M823 RESEARCH STORE WITH A FREELY SPINNING CRUCIFORM STABILIZER WITH A FIN CANT OF 4 DEGREES

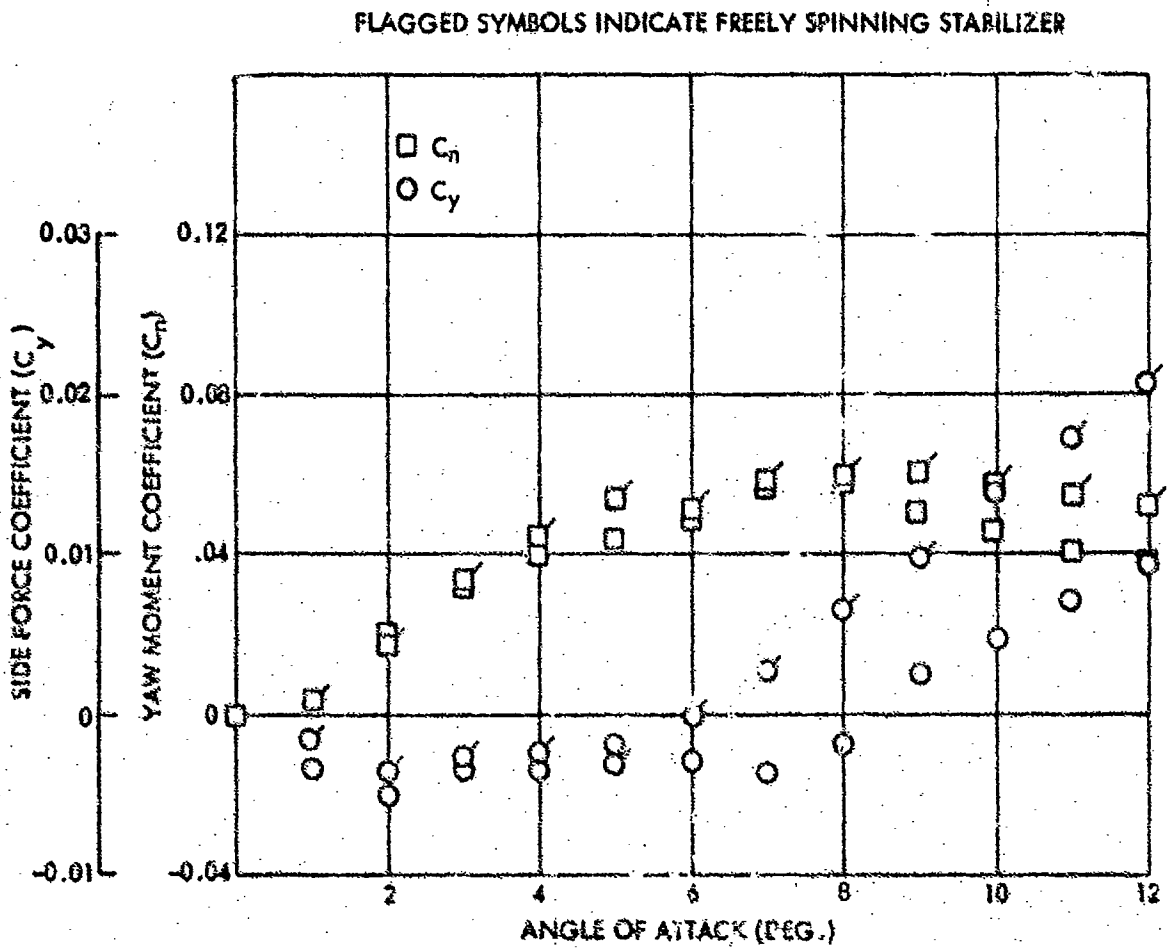

FIG. 6 SIDE-FORCE AND YAWING-MOMENT COEFFICIENTS VERSUS ANGLE OF ATTACK AT A FIN CANT OF 2 DEGREES AND AT A MACH NUMBER OF 0.60

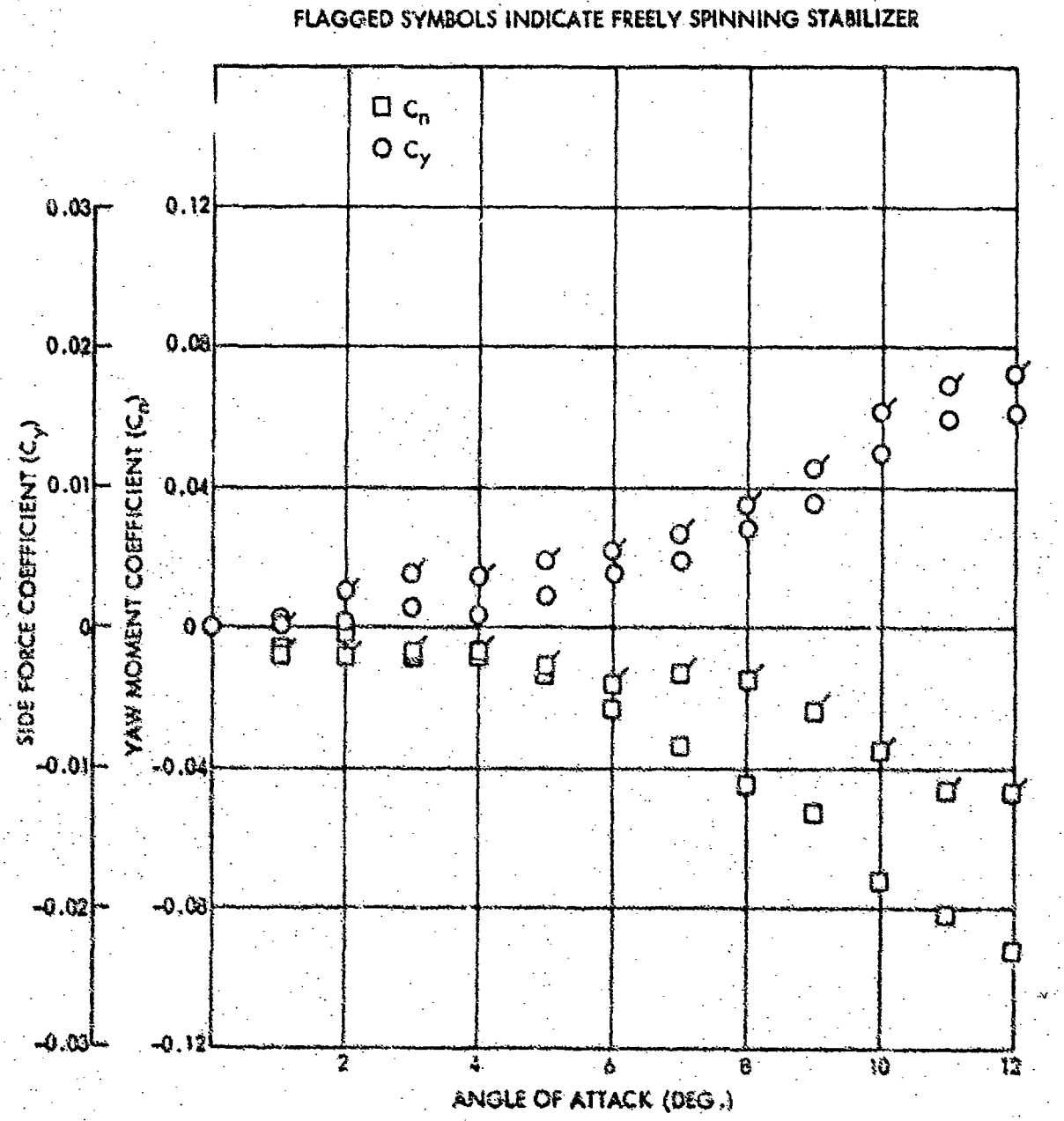

FIG. 7 SIDE-FORCE AND YAW-MOMENT COEFFICIENTS VERSUS ANGLE OF ATTACK AT A FIN CANT OF 2 DEGREES AND AT A MACH NUMBER OF 1.20

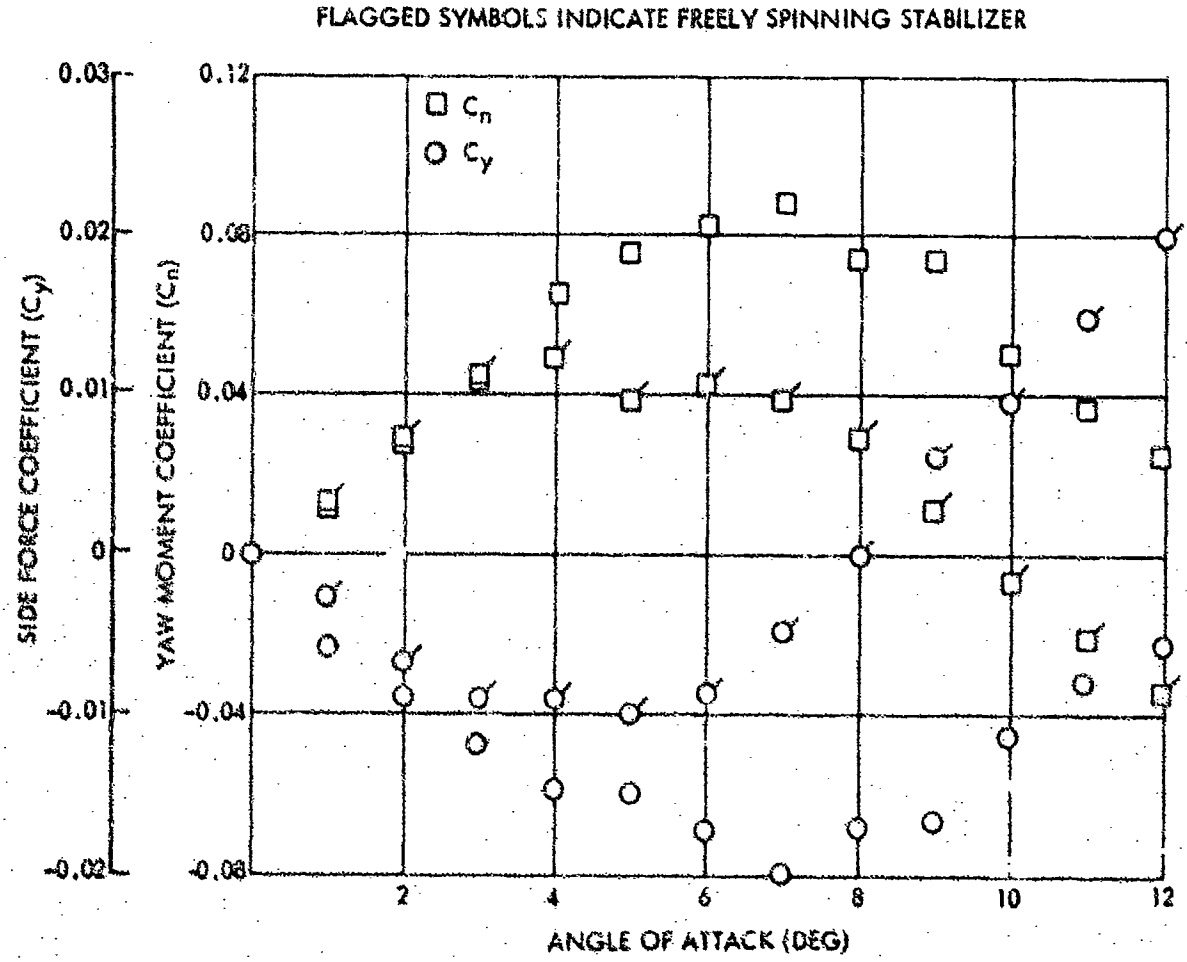

FIG. 8 SIDE-FORCE AND YAW-MOMENT COEFFICIENT VERSUS ANGLE OF ATTACK AT A FIN CANT OF 4 DEGREES AND AT A MACH NUMBER OF 0.80

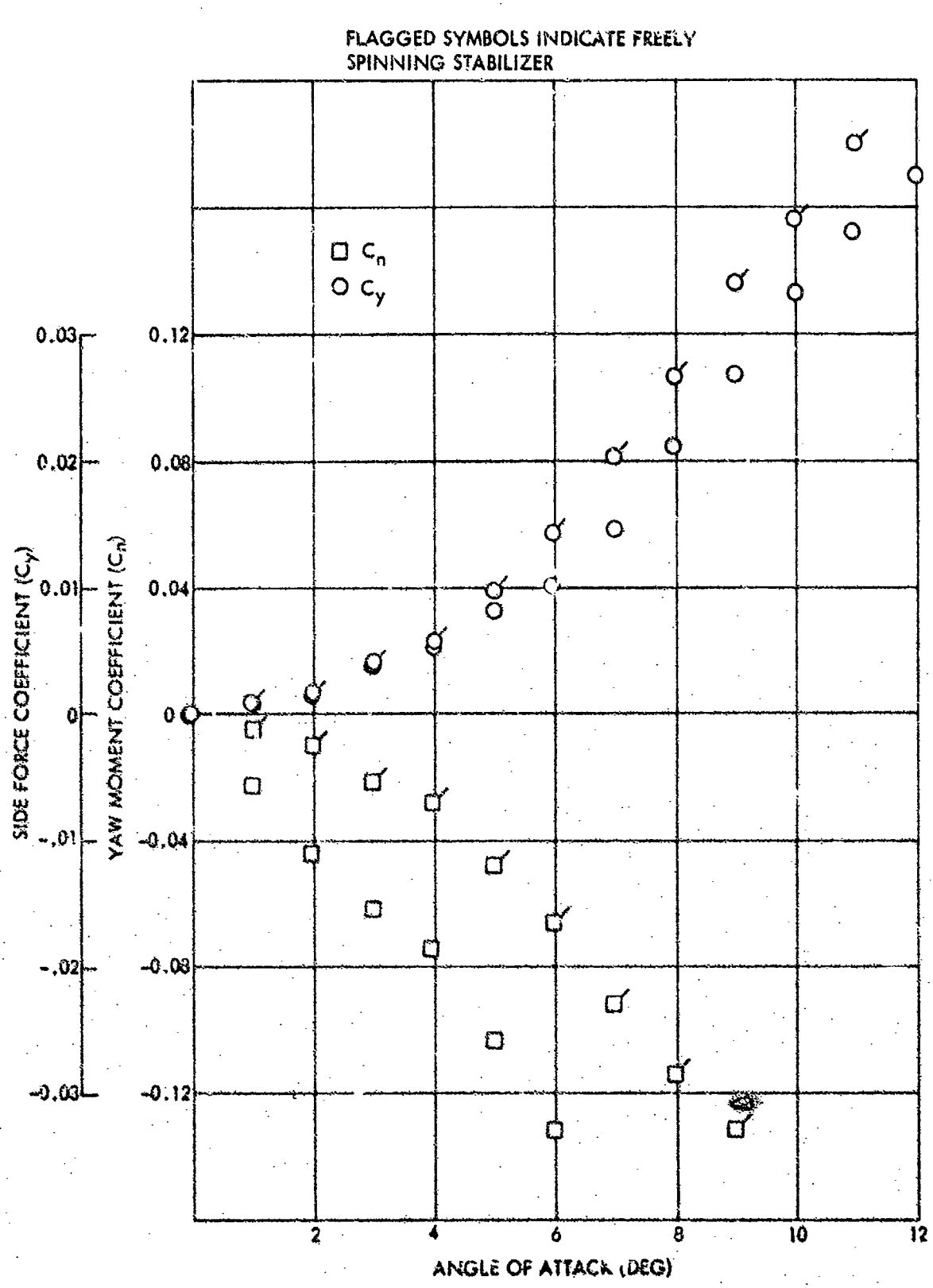

FIG. 9 SIDE-FORCE AND YAW-MOMENT COEFFICIENT VERSUS ANGLE OF ATTACK AT A FIN CANT OF 4 DEGREES AND AT A MACH NUMBER OF 1.20

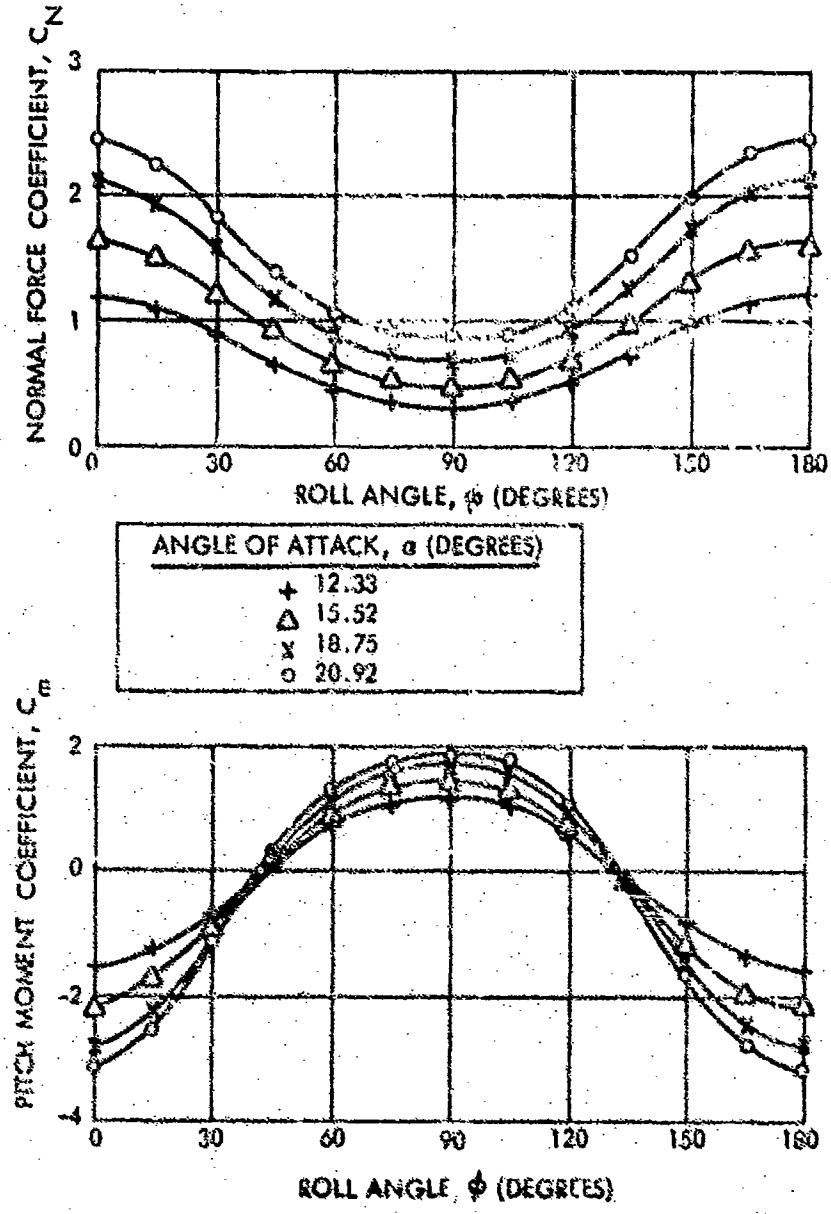

FIG. 10 WIND-TUNNEL NORMAL-FORCE AND PITCH-MOMENT COEFFICIENTS VERSUS ROLL ANGLE FOR THE MONOPLANE STABILIZER WITH A FIN CANT OF 4 DEGREES AND AT A MACH NUMBER OF 0.81

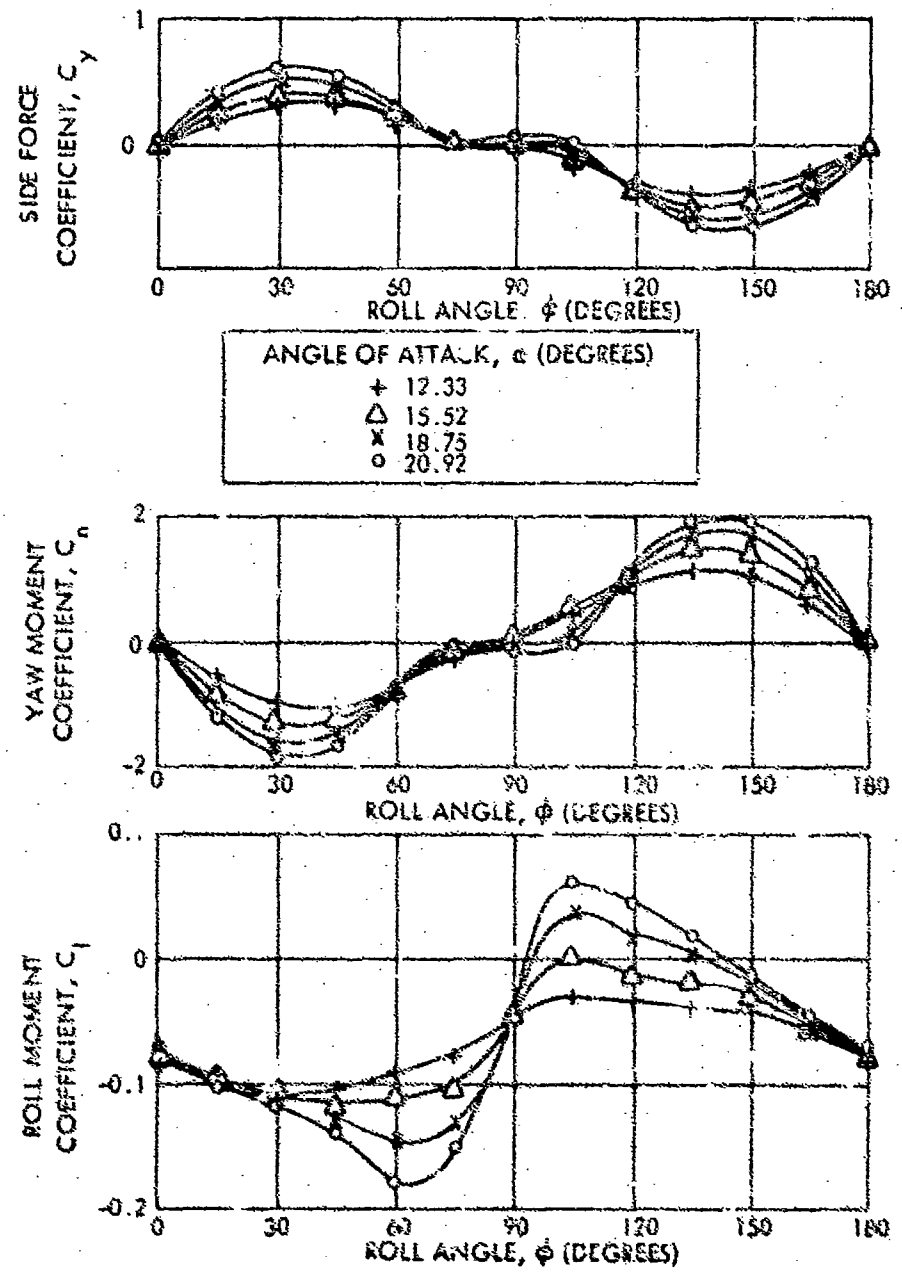

FIG. 11 WIND-TUNNEL SIDE-FORCE, YAW-MOMENT AND ROLL-MOMENT COEFFICIENTS VERSUS ROLL ANGLE FOR THE MONOPLANE STABILIZER WITH A FIN CANT OF 4 DEGREES AND AT MACH NUMBER OF 0.81

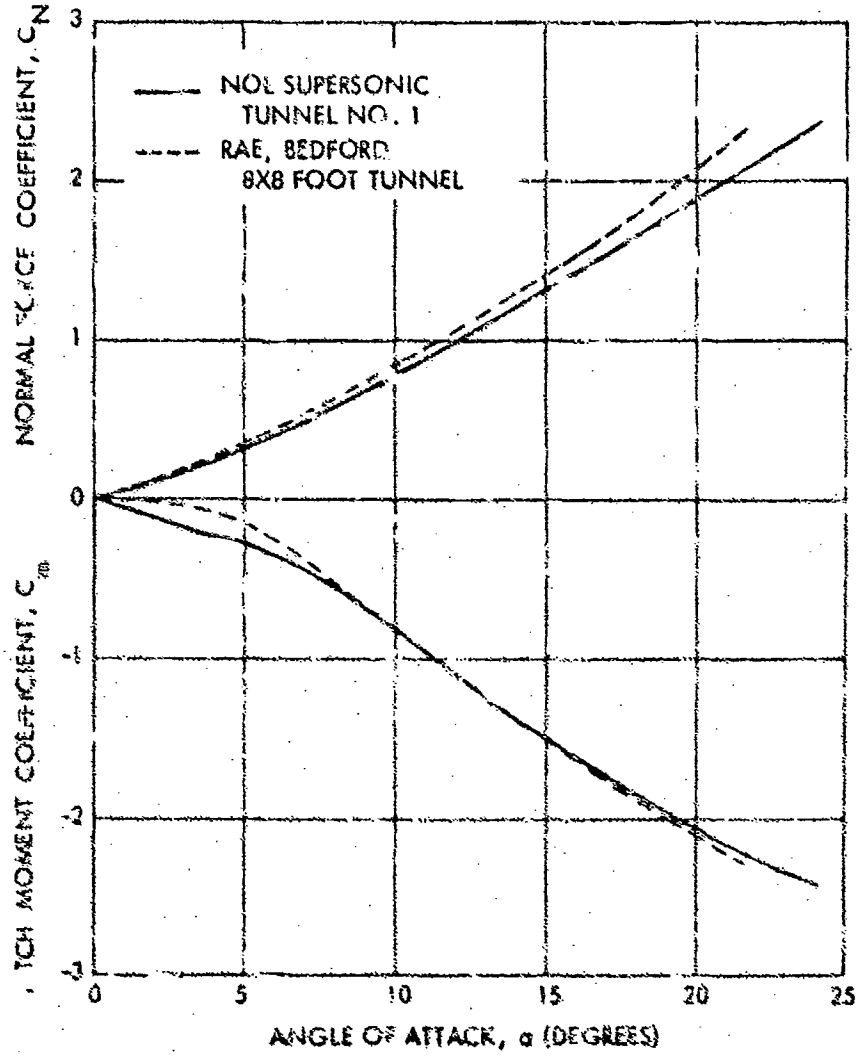

FIG. 12 COMPARISON OF WIND-TUNNEL DATA BETWEEN NOL SUPERSONIC TUNNEL NO. 1 AND RAE, BEDFORD 8X8-FOOT TUNNEL FOR A CONFIGURATION WITH A FREELY SPINNING CRUCIFORM STABILIZER OF 4-DEGREE FIN CANT AT A MACH NUMBER OF 0.70

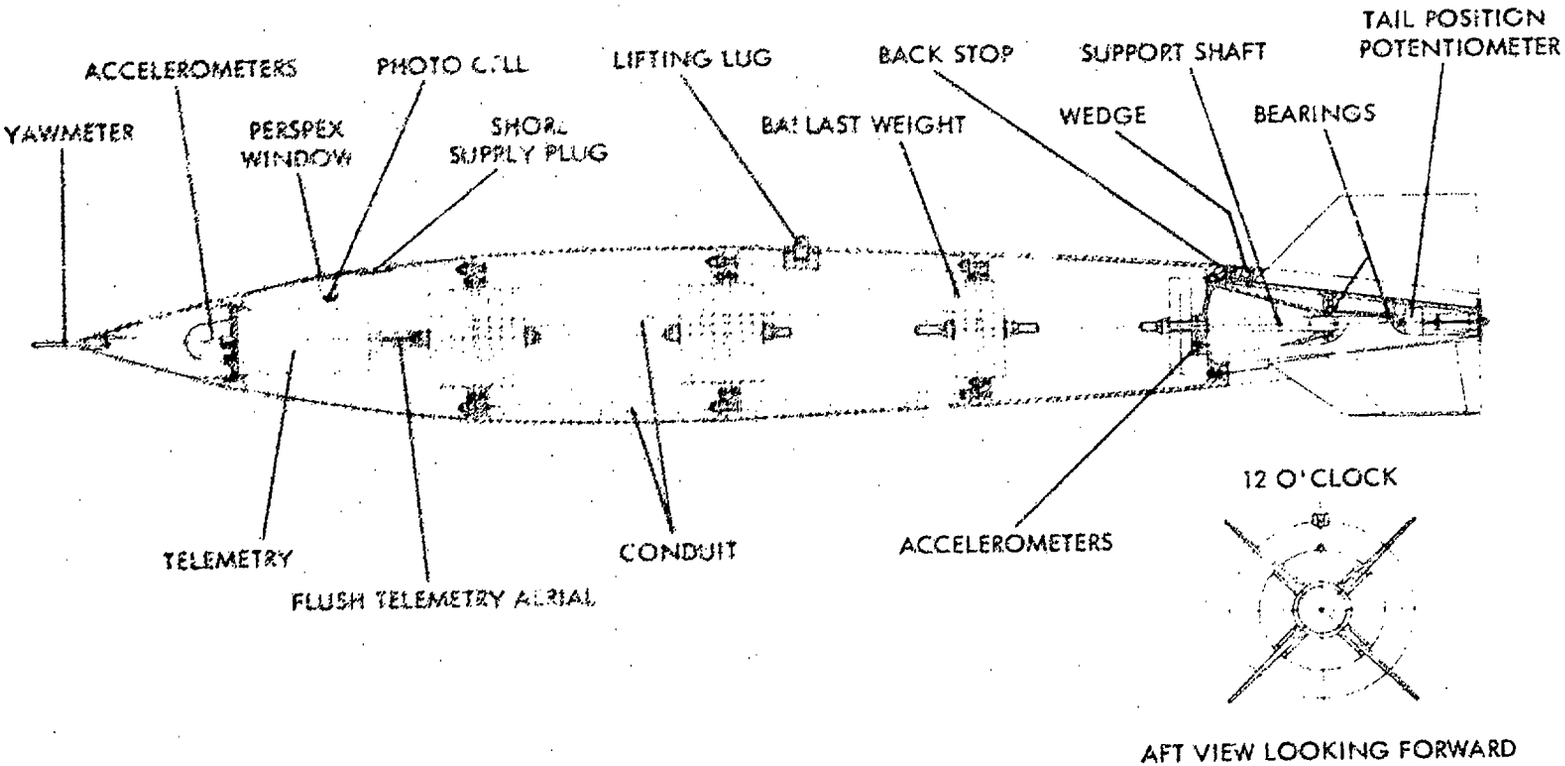

FIG. 13 INTERNAL DETAILS OF M823 TEST VEHICLE WITH SPINNING CRUCIFORM TAIL

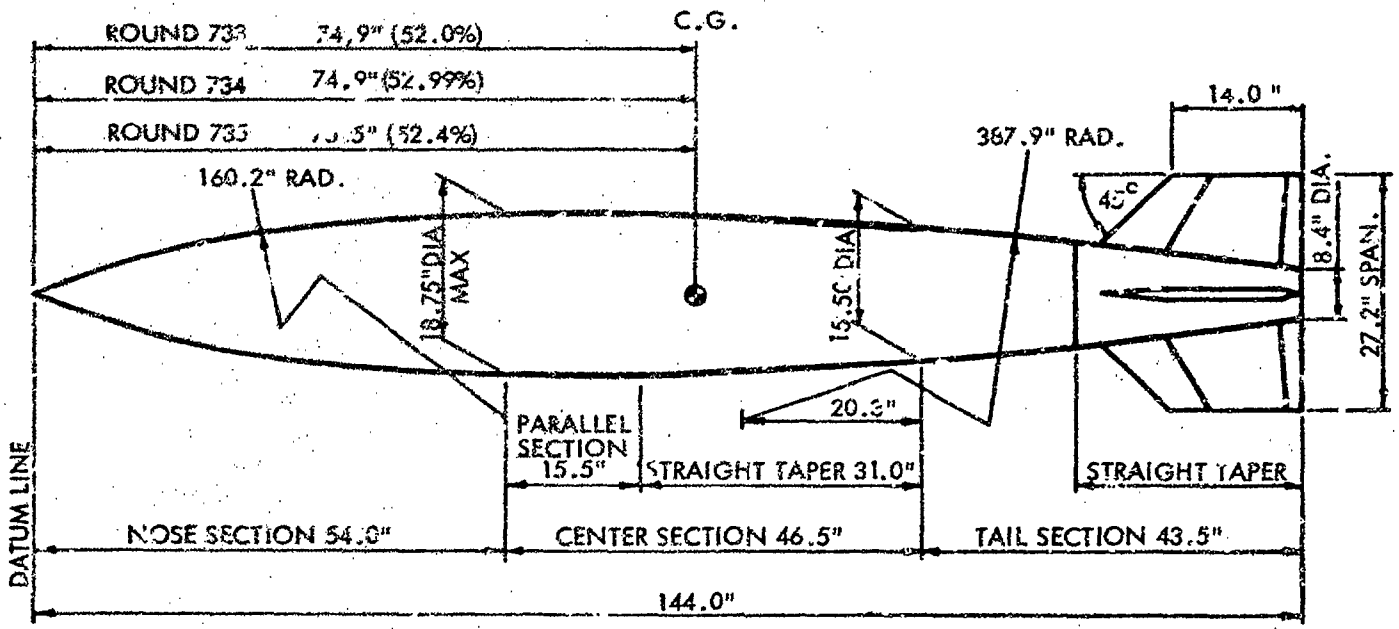

NOTES.

1. ROUND NUMBER	733	734	735	
VEHICLE WEIGHT	878.75	885.0	878.5	lb
MOMENT OF INERTIA IN PITCH OF COMPLETE ROUND	178.0	177.8	173.9	SLUG FT.^{2}
MOMENT OF INERTIA IN ROLL OF COMPLETE ROUND	5.6	6.5	5.3	SLUG FT.^{2}
MOMENT OF INERTIA IN ROLL OF TAIL SECTION	0.48	0.48	0.48	SLUG FT.^{2}
2. FIN CANT ANGLE	3.39	1.39	0.24	DEGREES.

3. FIN SECTION IS AN EXTENDED DOUBLE WEDGE. MAX. THICKNESS $(\frac{t}{c})$ = 3%
PARALLEL SECTION BETWEEN 30% and 90% CHORD.

FIG. 14a M823 ROUNDS WITH FREELY SPINNING CRUCIFORM STABILIZERS

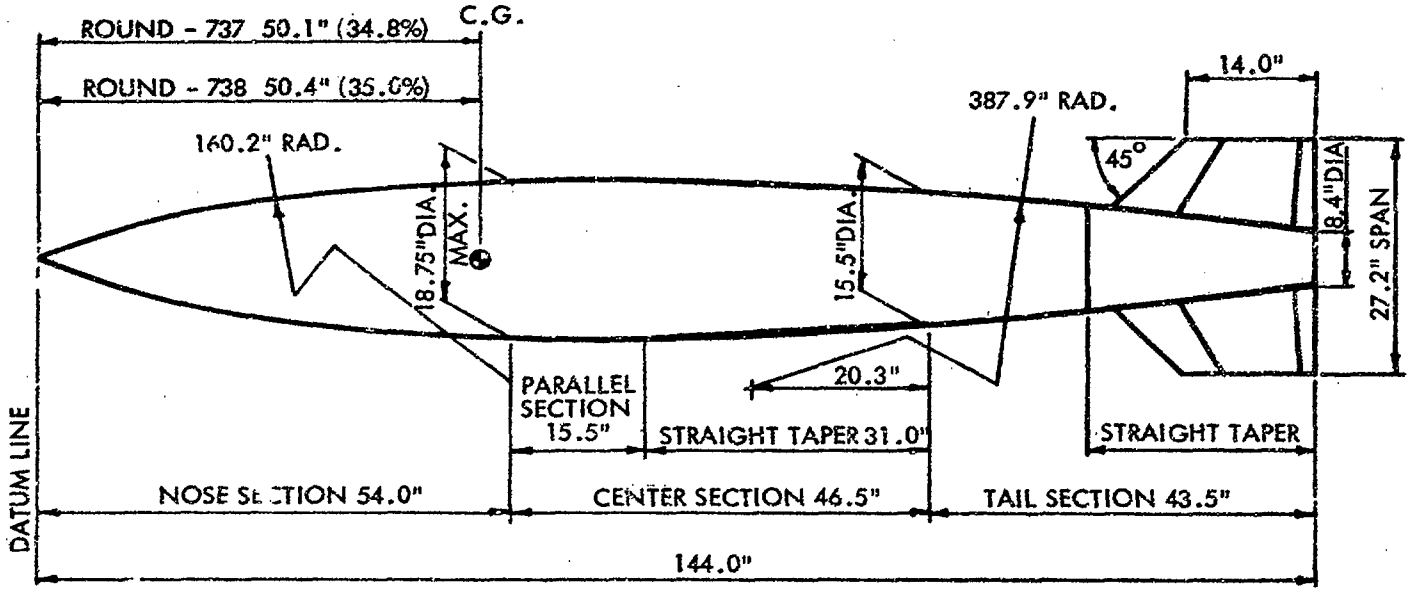

NOTES.

1. ROUND NUMBER 737 738

VEHICLE WEIGHT	917.25	901.2	lb.
MOMENT OF INERTIA IN PITCH OF COMPLETE ROUND	262.5	265.8	SLUG FT.^{2}
MOMENT OF INERTIA IN ROLL OF COMPLETE ROUND	8.4	9.0	SLUG FT.^{2}
MOMENT OF INERTIA IN ROLL OF TAIL SECTION	0.38	0.38	SLUG FT.^{2}

2. FIN CANT ANGLE 3.34 3.34 DEGREES.

3. FIN SECTION IS AN EXTENDED DOUBLE WEDGE. MAS. THICKNESS ($\frac{t}{c}$) = 3% PARALLEL SECTION BETWEEN 30% and 90% CHORD

FIG. 14b M823 ROUNDS WITH FREELY SPINNING MONOPLANE STABILIZERS

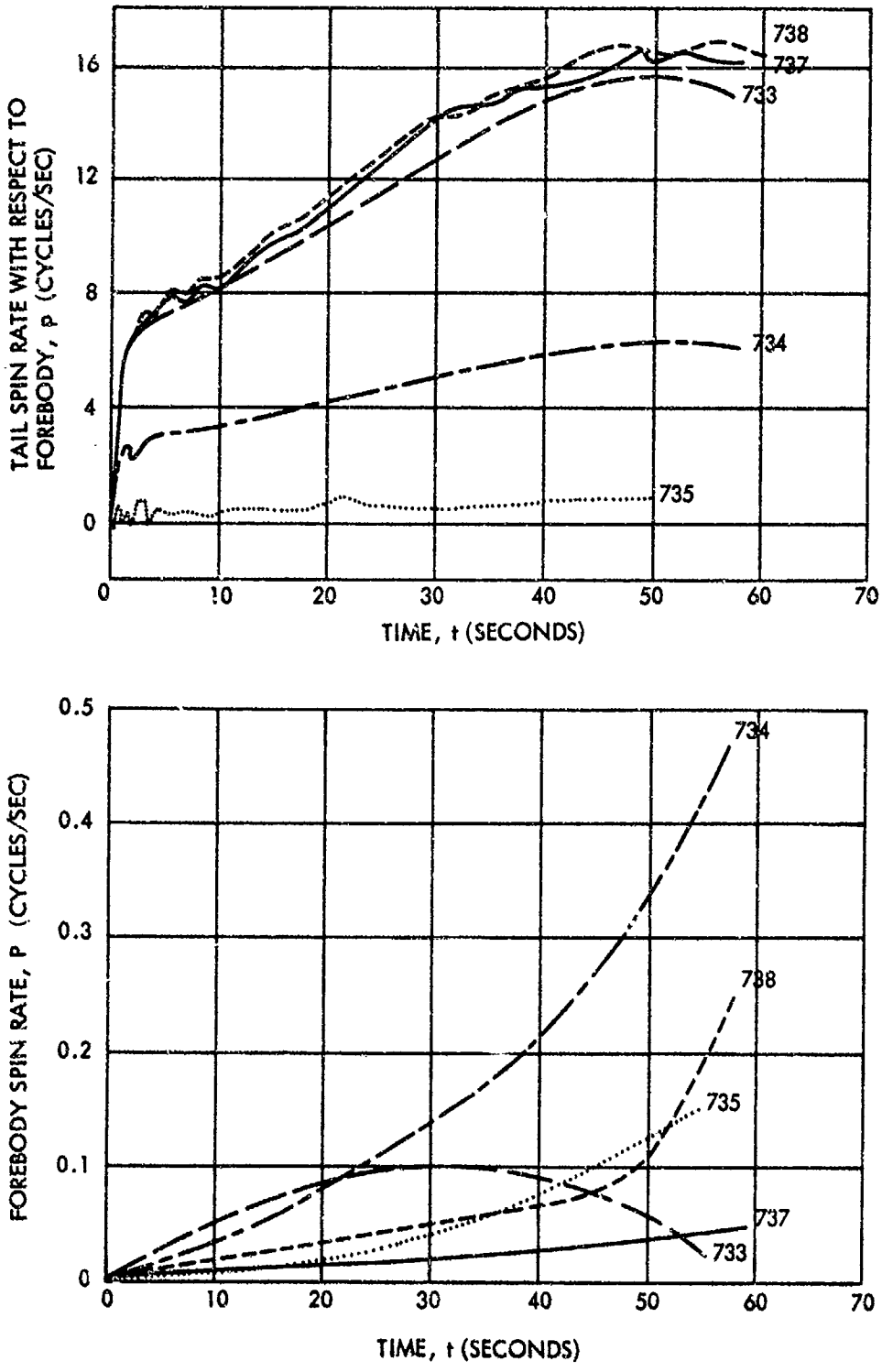

FIG. 15 ROLL RATE HISTORIES OF TAIL AND FOREBODY FOR ROUNDS 733, 734, 735, 737 AND 738

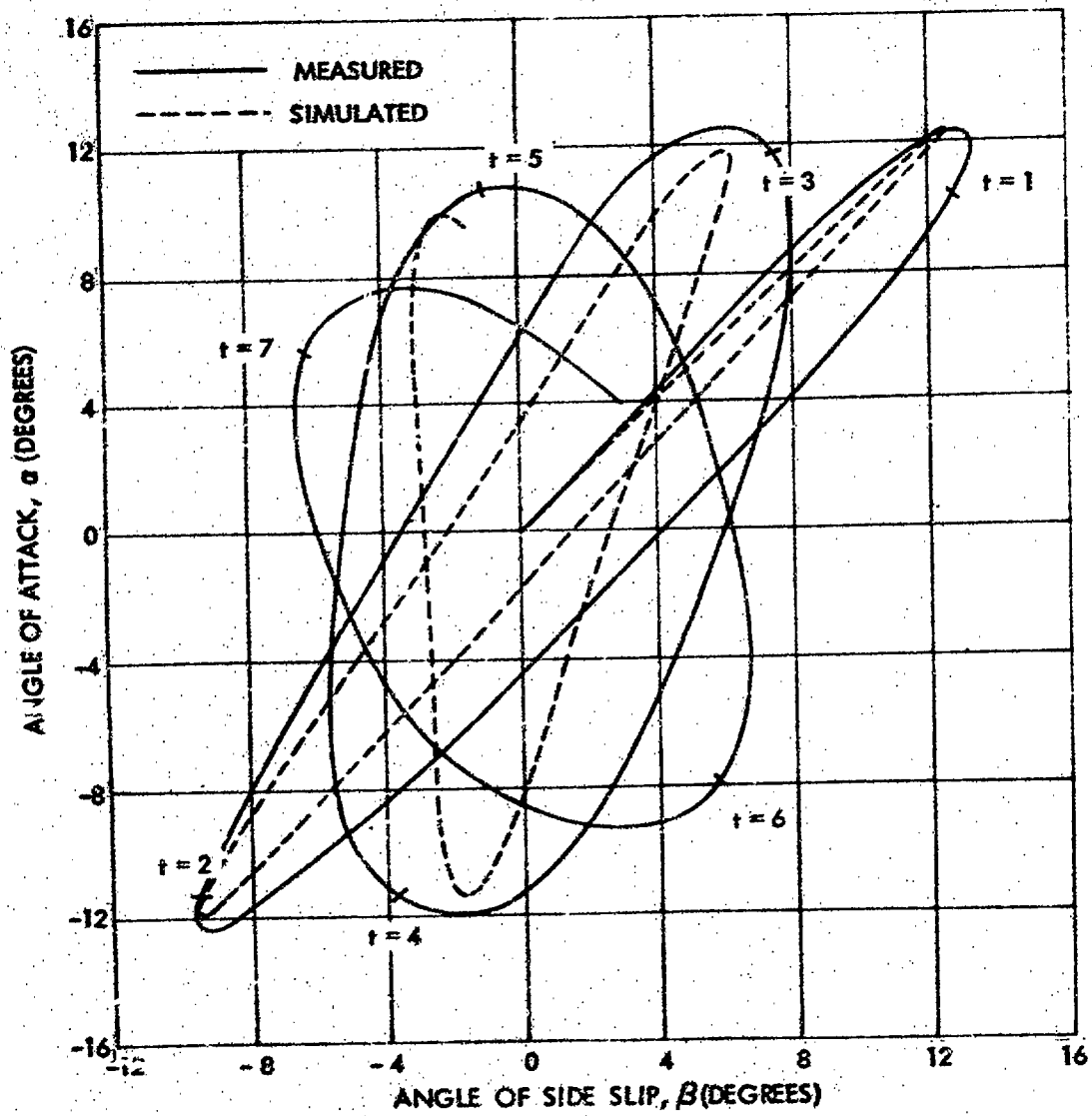

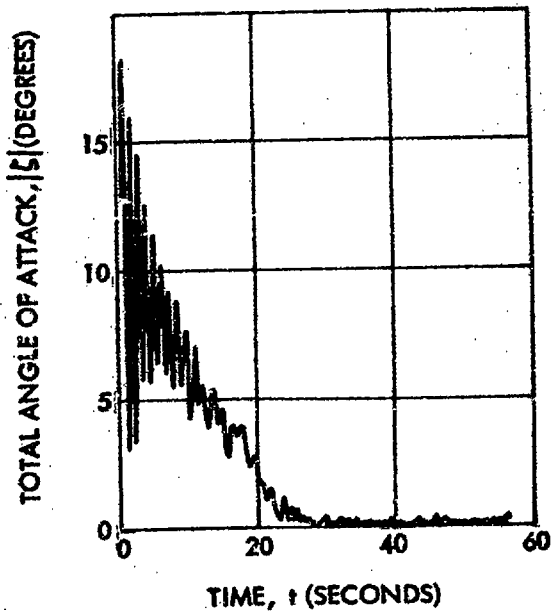

FIG. 16 COMPARISON OF SIMULATED AND MEASURED FLIGHT HISTORY OF ANGLE OF ATTACK AND ANGLE OF SIDE SLIP REFERRED TO FOREBODY AXES FOR ROUND 733

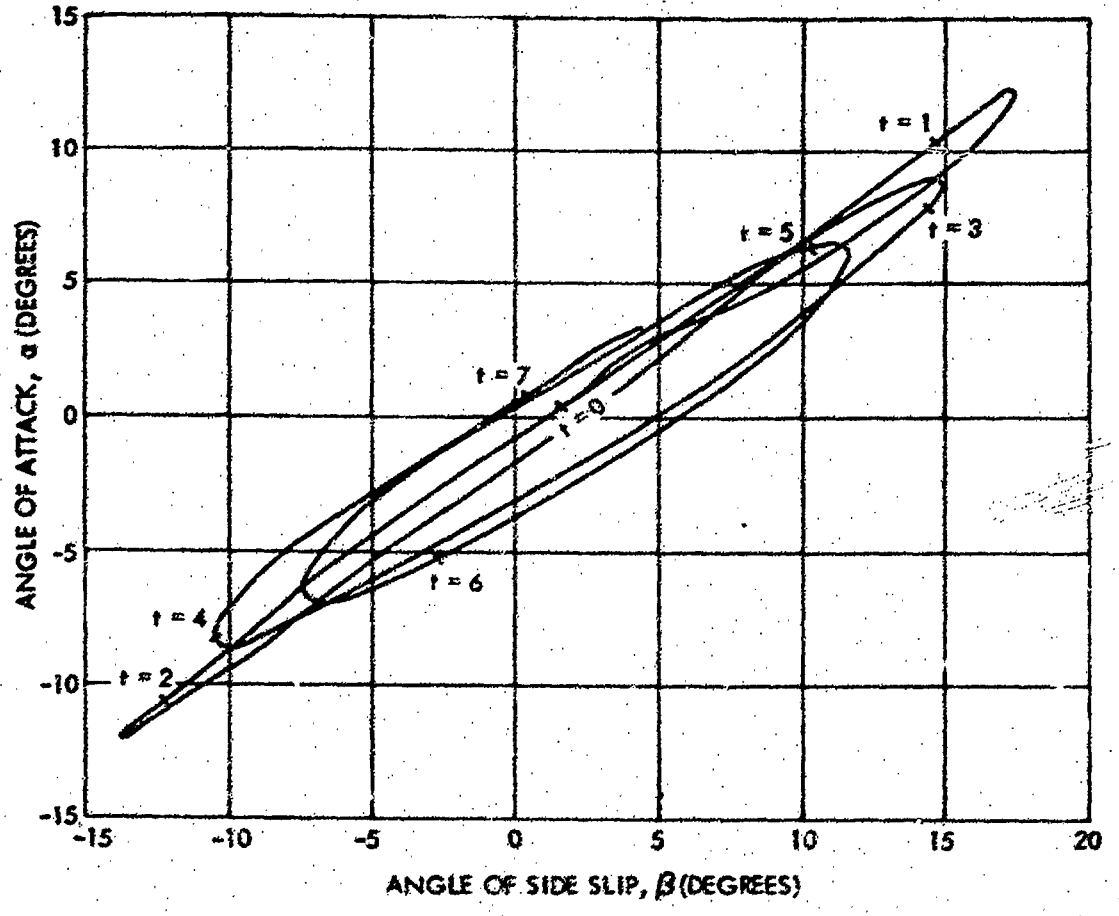

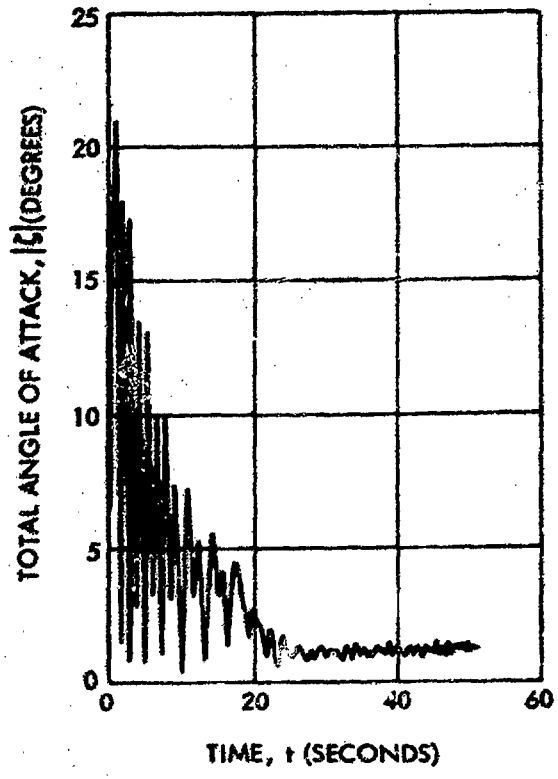

NOLTR 73-77

FIG. 17 MEASURED FLIGHT HISTORY OF ANGLE OF ATTACK AND SIDE SLIP REFERRED TO FOREBODY AXES FOR ROUND 734.

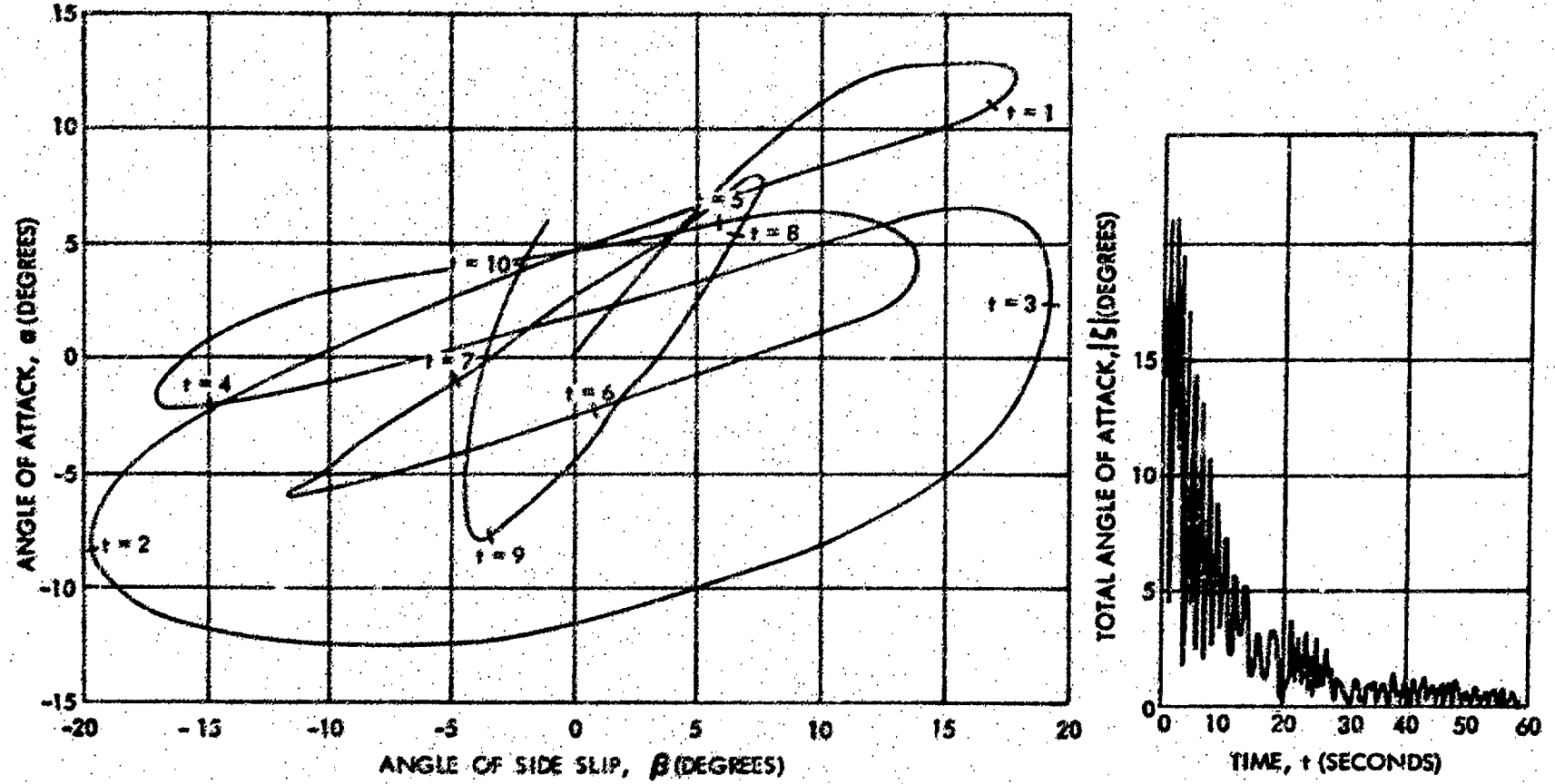

FIG. 18 MEASURED FLIGHT HISTORY OF ANGLE OF ATTACK AND SIDE SLIP REFERRED TO FOREBODY AXES FOR ROUND 735

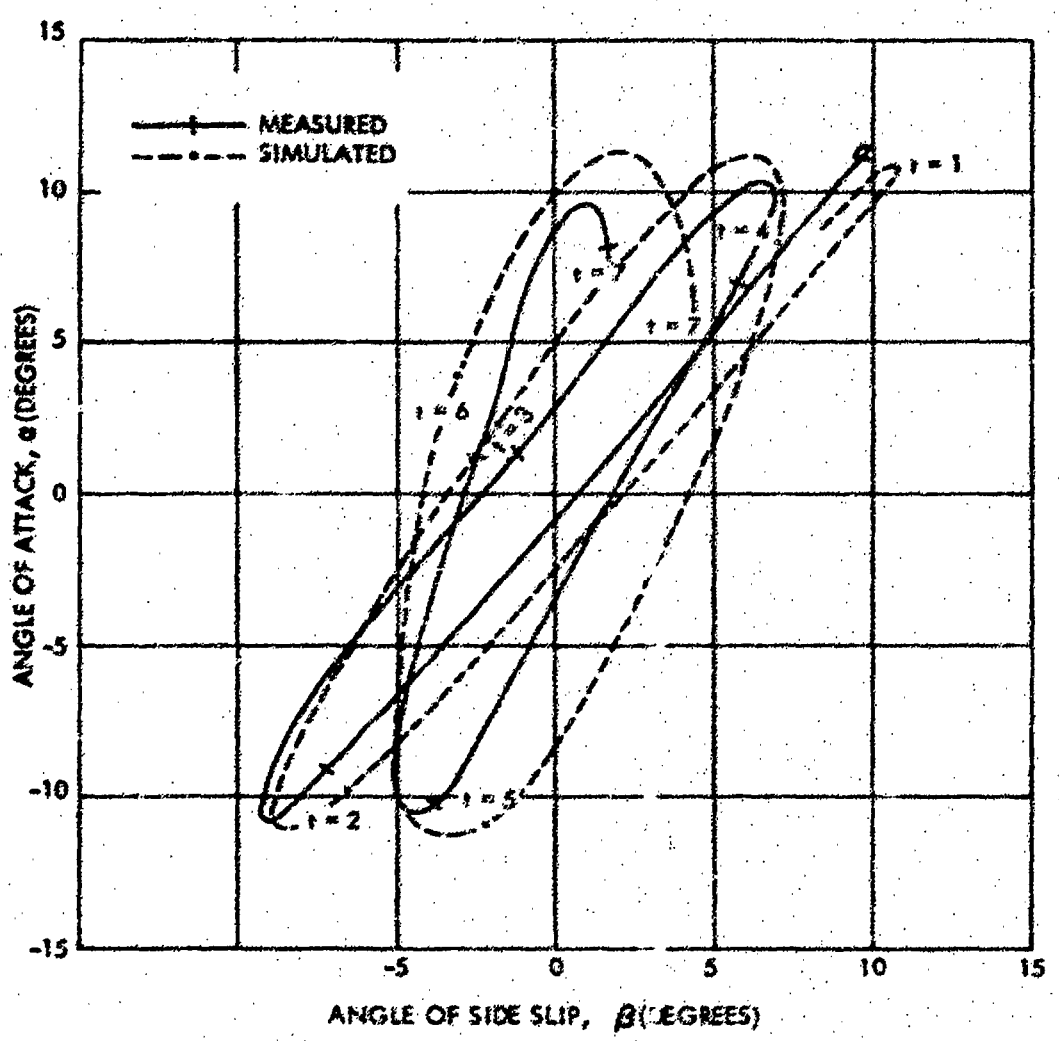

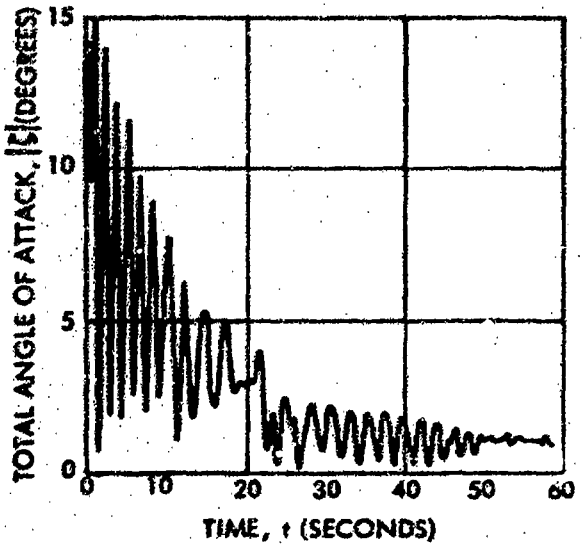

FIG. 19 COMPARISON OF SIMULATED AND MEASURED FLIGHT HISTORY OF ANGLE OF ATTACK AND ANGLE OF SIDE SLIP REFERRED TO FOREBODY AXES FOR ROUND 737

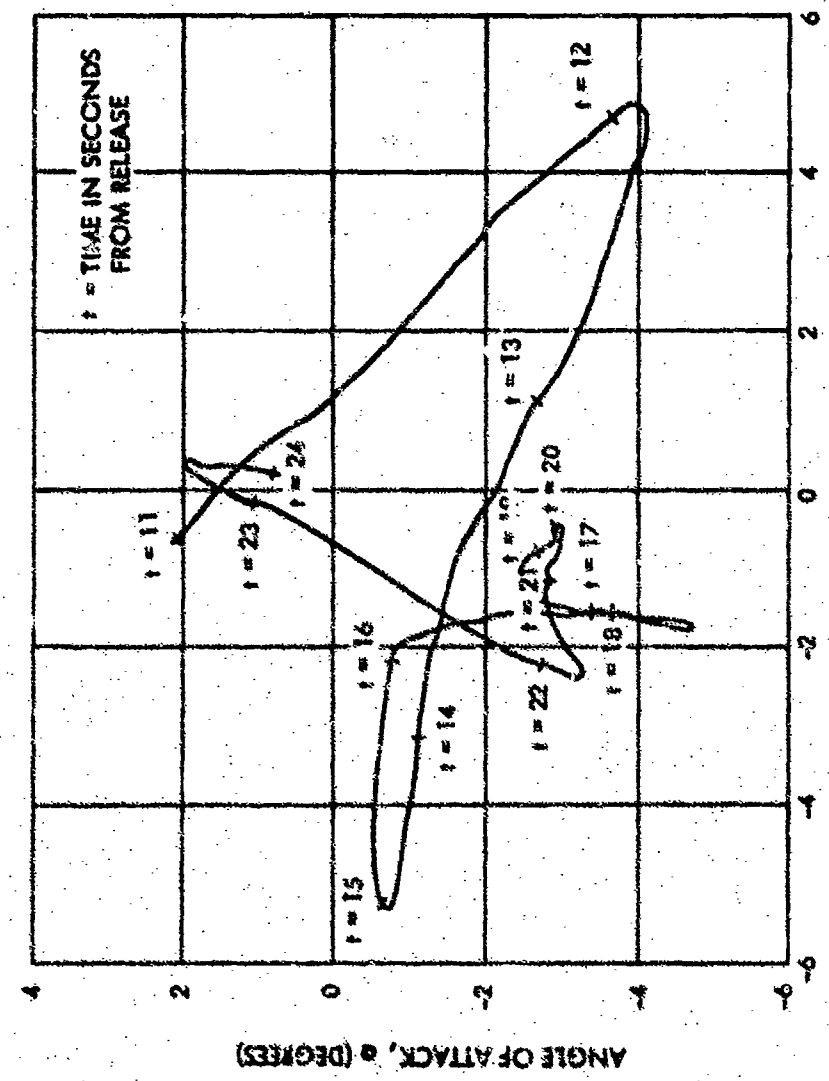

FIG. 20 MEASURED FLIGHT HISTORY OF ANGLE OF ATTACK AND ANGLE OF SIDE SLIP REFERRED TO FOREBODY AXES FOR ROUND 737

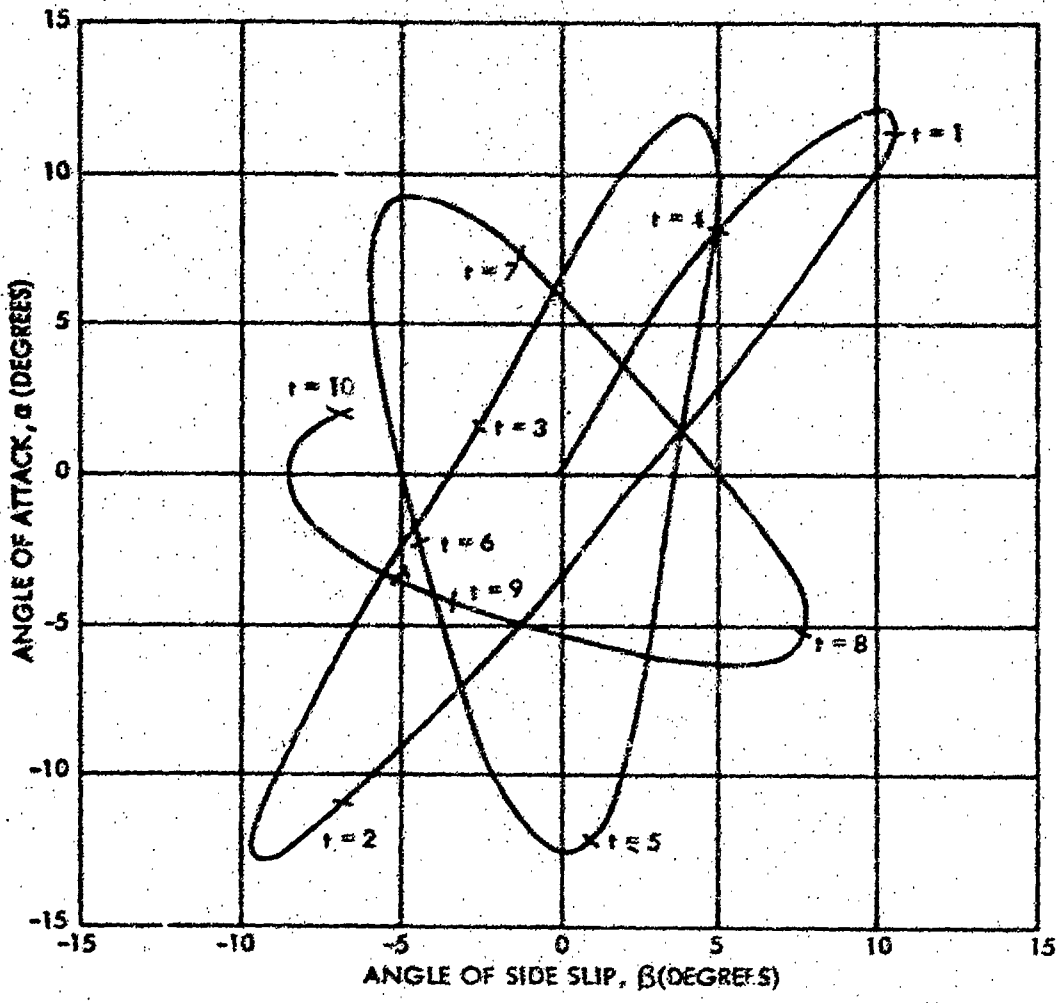

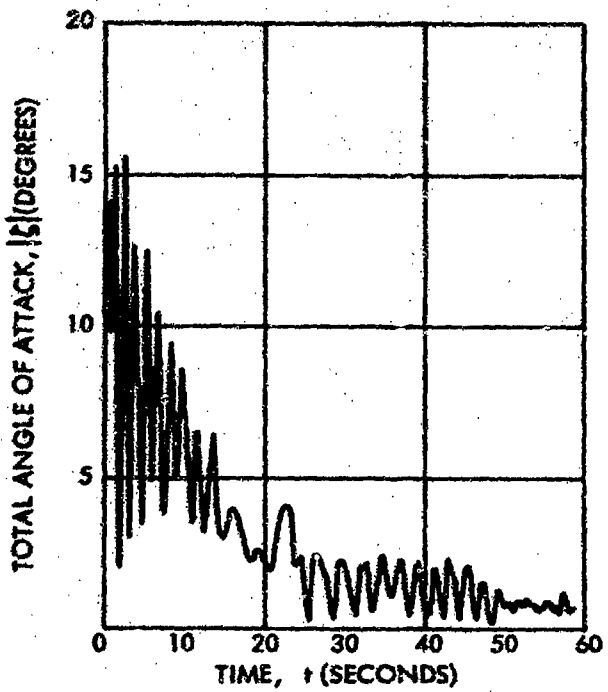

FIG. 21 MEASURED FLIGHT HISTORY OF ANGLE OF ATTACK AND ANGLE OF SIDE SLIP REFERRED TO FOREBODY AXES FOR ROUND 738 FROM ZERO TO TEN SECONDS

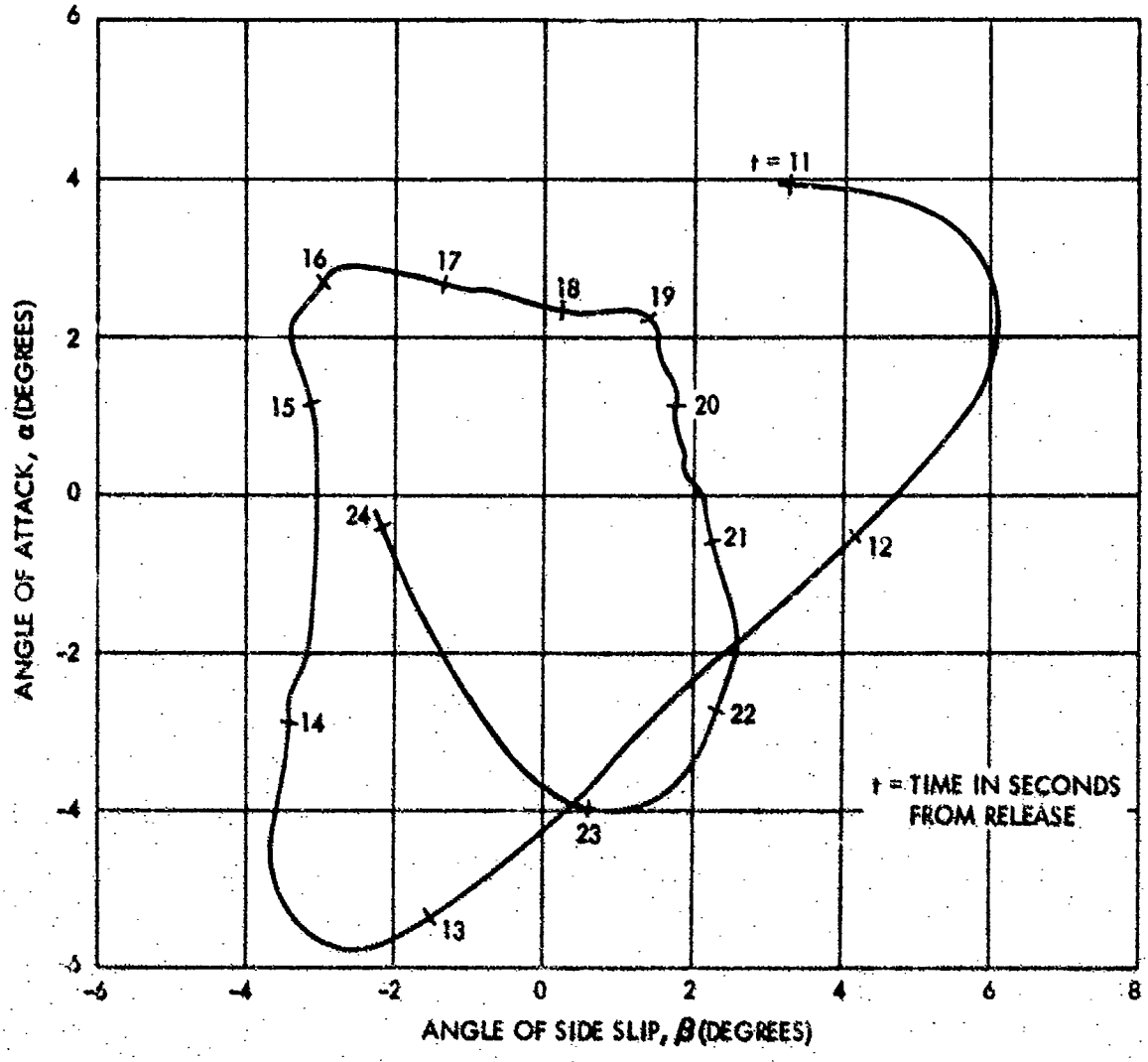

FIG. 22 MEASURED FLIGHT HISTORY OF ANGLE OF ATTACK AND ANGLE OF SIDE SLIP REFERRED TO FOREBODY AXES FOR ROUND 738 FROM ELEVEN TO TWENTY-FOUR SECONDS

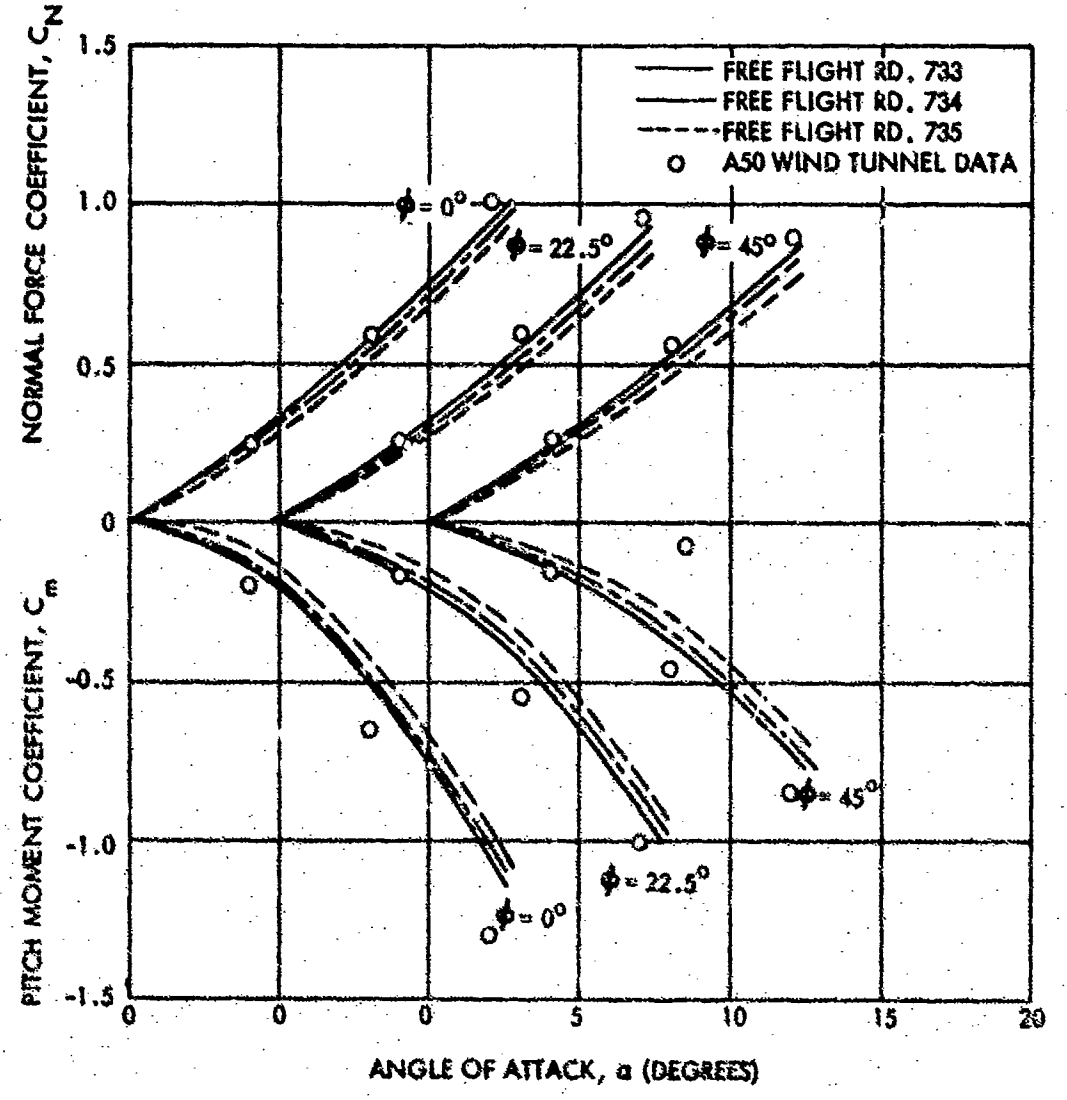

FIG. 23 COMPARISON OF FREE-FLIGHT AND WIND-TUNNEL MEASUREMENTS ON A CRUCIFORM TAIL: VARIATION OF NORMAL-FORCE AND PITCH-MOMENT COEFFICIENTS WITH ANGLE OF ATTACK

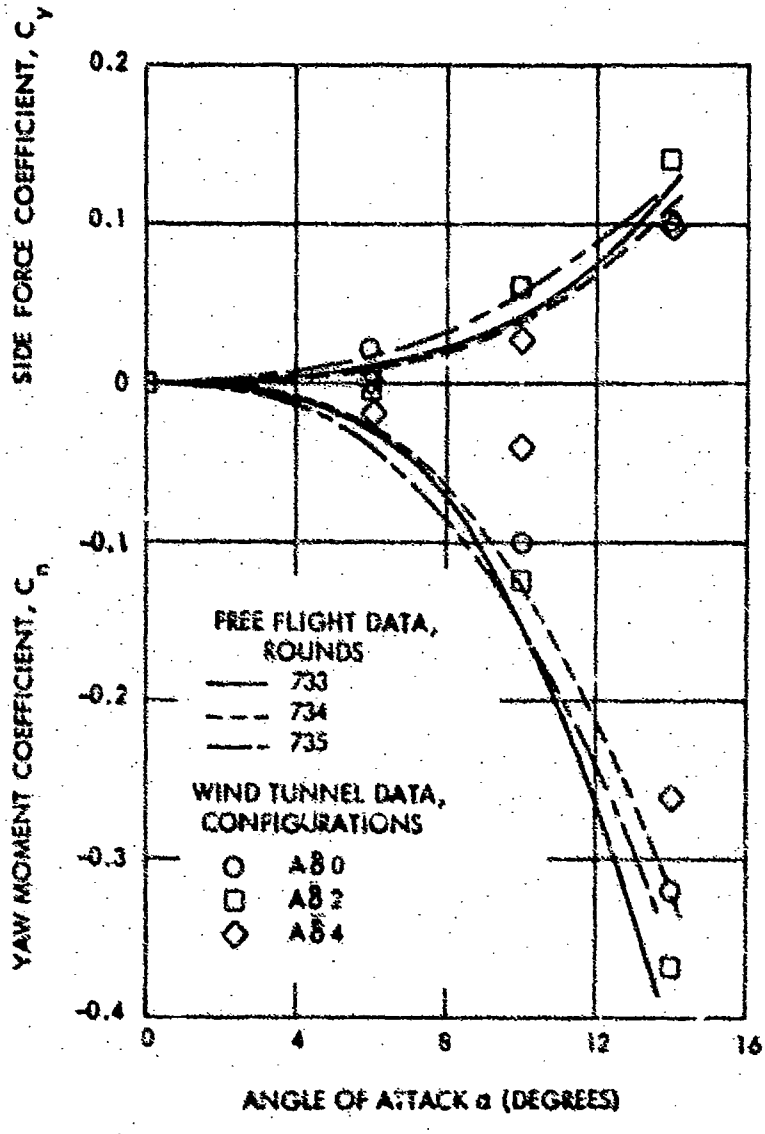

FIG. 24 COMPARISON OF FREE-FLIGHT AND WIND-TUNNEL MEASUREMENTS ON A CRUCIFORM TAIL: VARIATION OF SIDE-FORCE AND YAW-MOMENT COEFFICIENTS WITH ANGLE OF ATTACK FOR A MACH NUMBER OF 0.70 AND A ROLL ANGLE OF 22.5 DEGREES

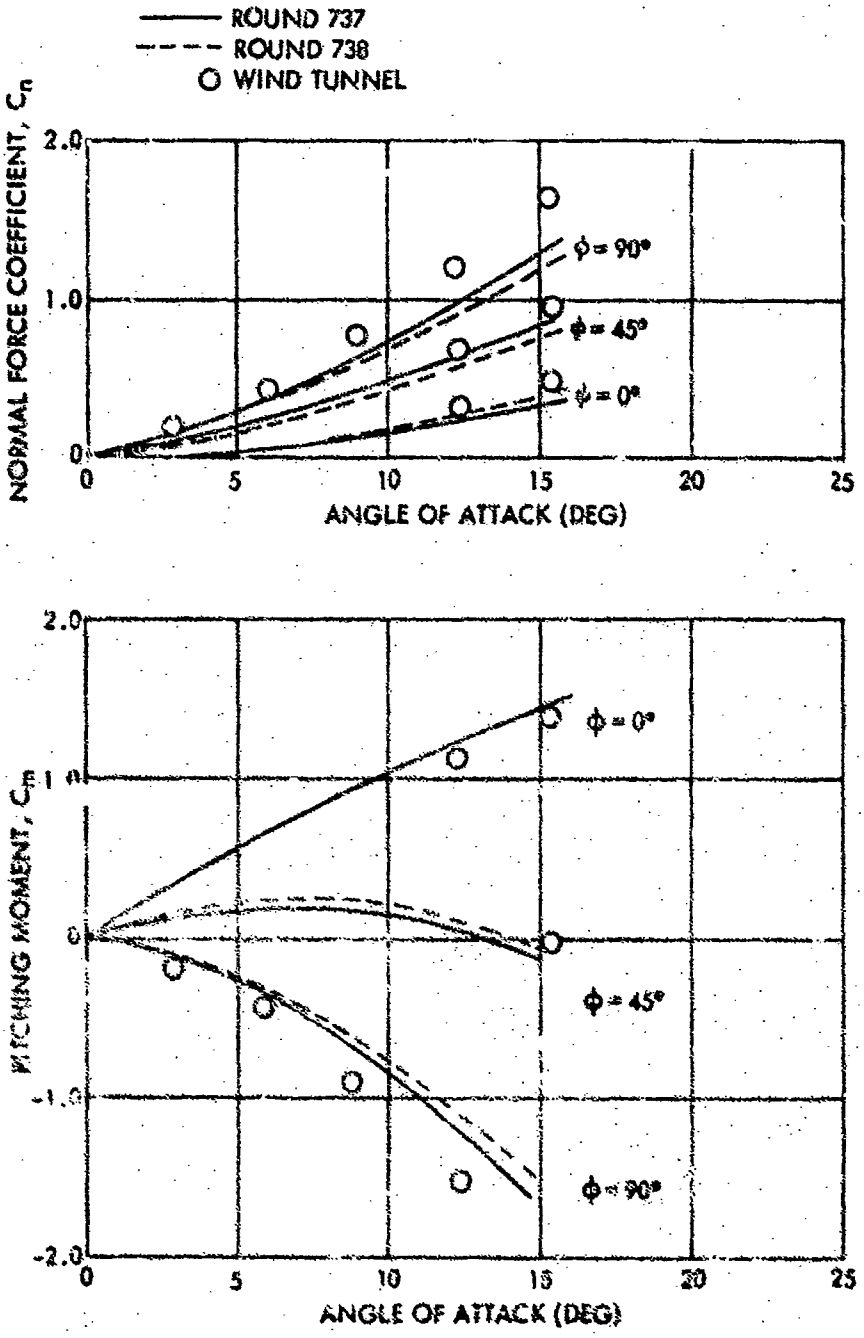

FIG. 25 COMPARISON OF FREE-FLIGHT AND WIND-TUNNEL MEASUREMENTS ON A MONOPLANE STABILIZER: VARIATION OF NORMAL-FORCE AND PITCHING-MOMENT COEFFICIENTS WITH ANGLE OF ATTACK FOR A MACH NUMBER OF 0.70

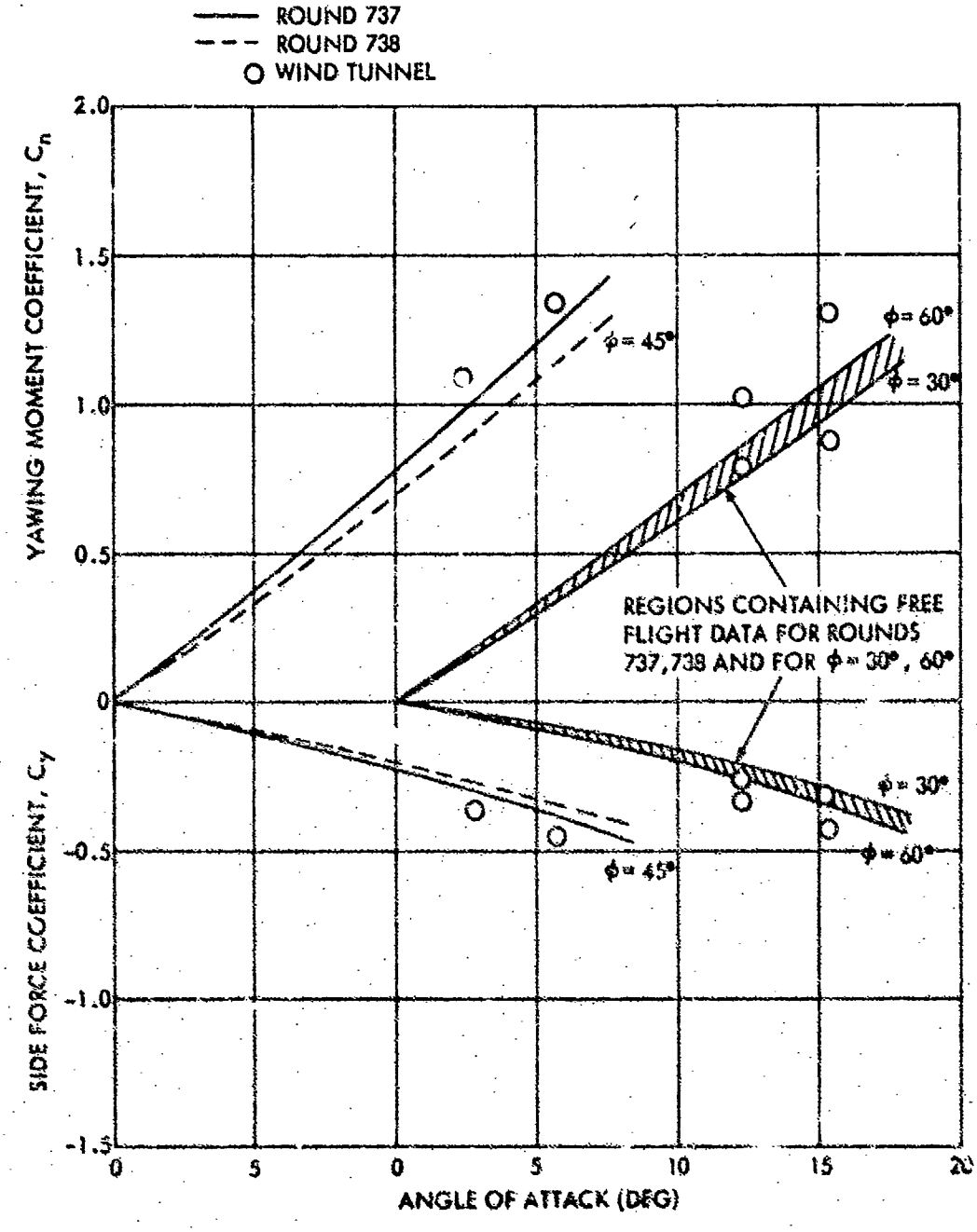

FIG. 26 COMPARISON OF FREE-FLIGHT AND WIND-TUNNEL MEASUREMENTS ON A MONOPLANE STABILIZER: VARIATION OF SIDE-FORCE AND YAWING-MOMENT COEFFICIENTS WITH ANGLE OF ATTACK FOR A MACH NUMBER OF 0.70

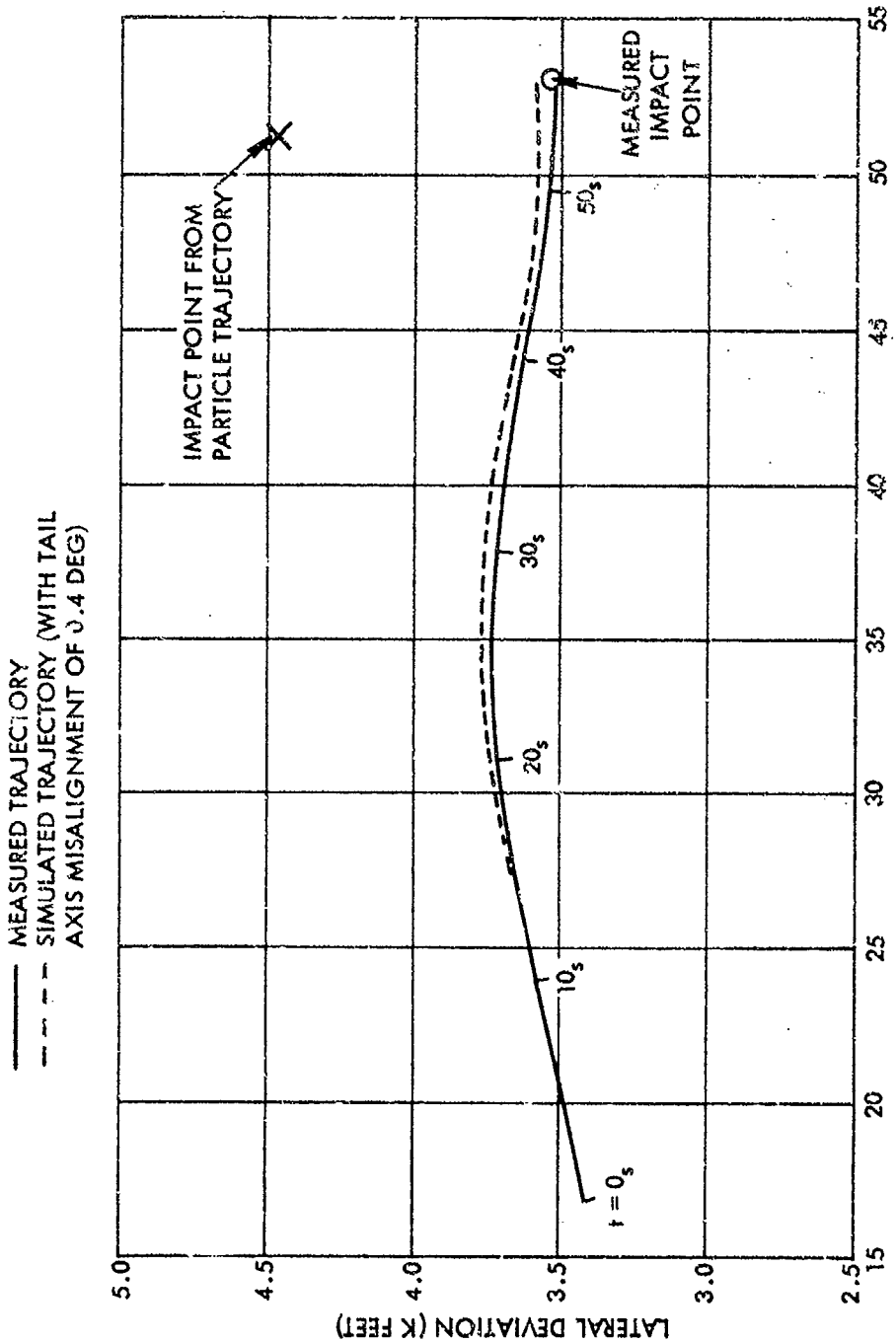

FIG. 27 COMPARISON OF MEASURED AND SIMULATED TRAJECTORIES FOR ROUND 737

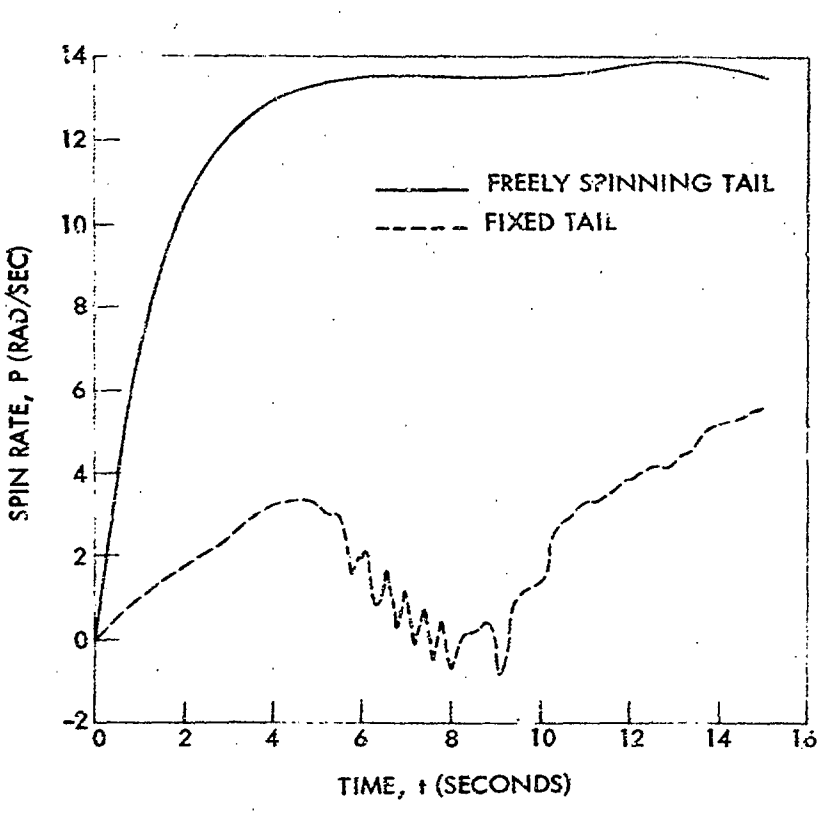

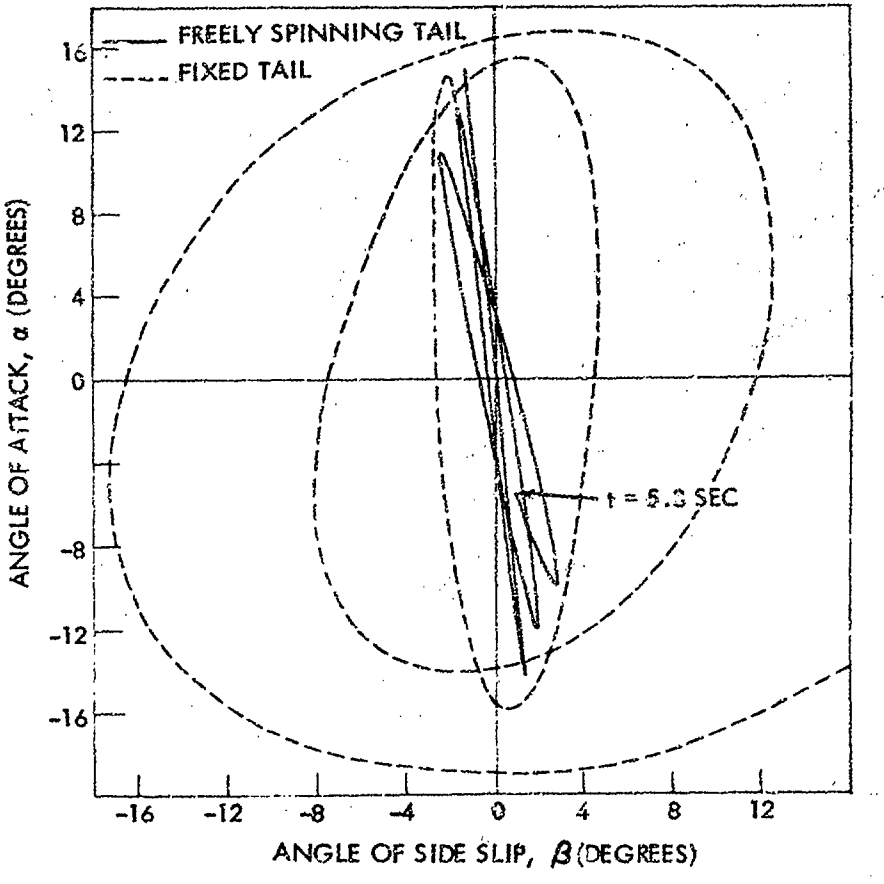

NOLTR 73-77

FIG. 28 SIMULATED RELEASE AT 45,000 FT. ALTITUDE WITH A FIN-CANT ANGLE OF 0.401 DEGREE

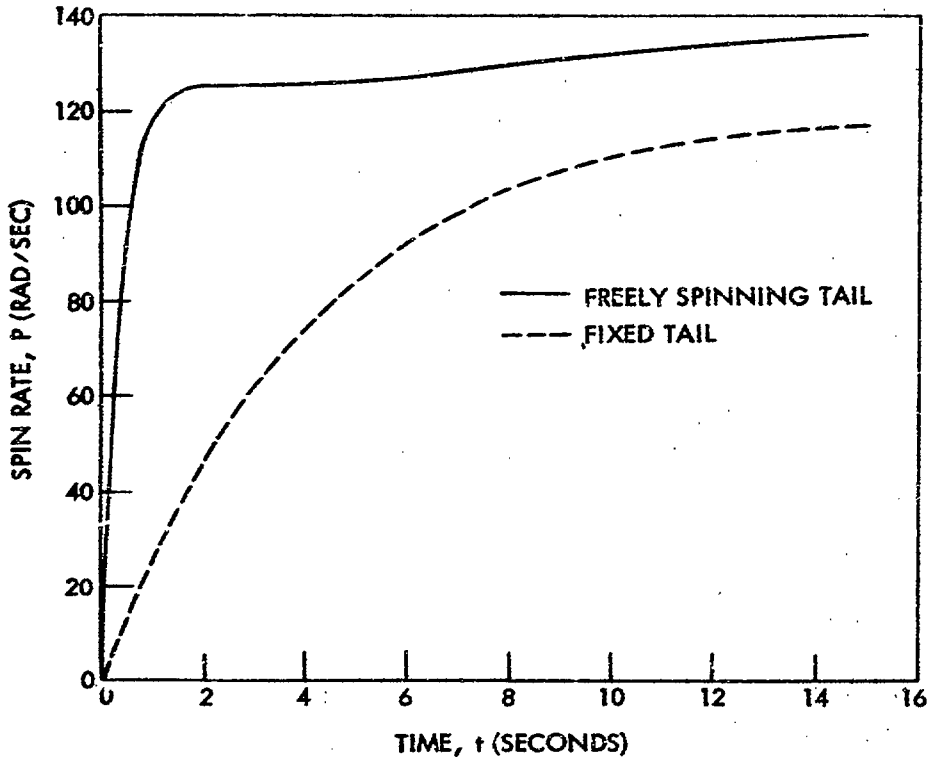

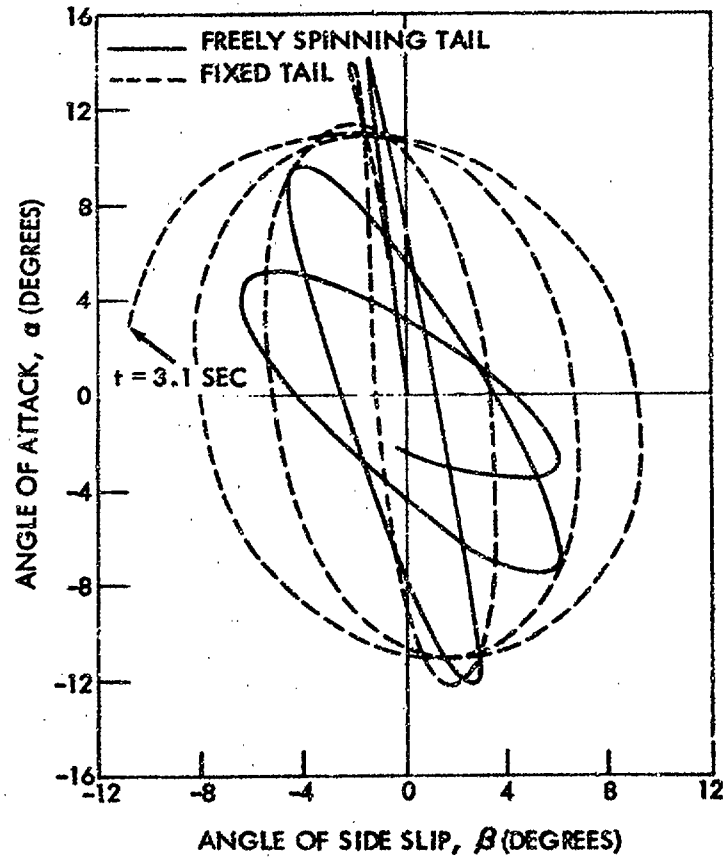

FIG. 29 SIMULATED RELEASE AT 10,000 FT. ALTITUDE WITH A FIN-CANT ANGLE OF 3.44 DEGREES

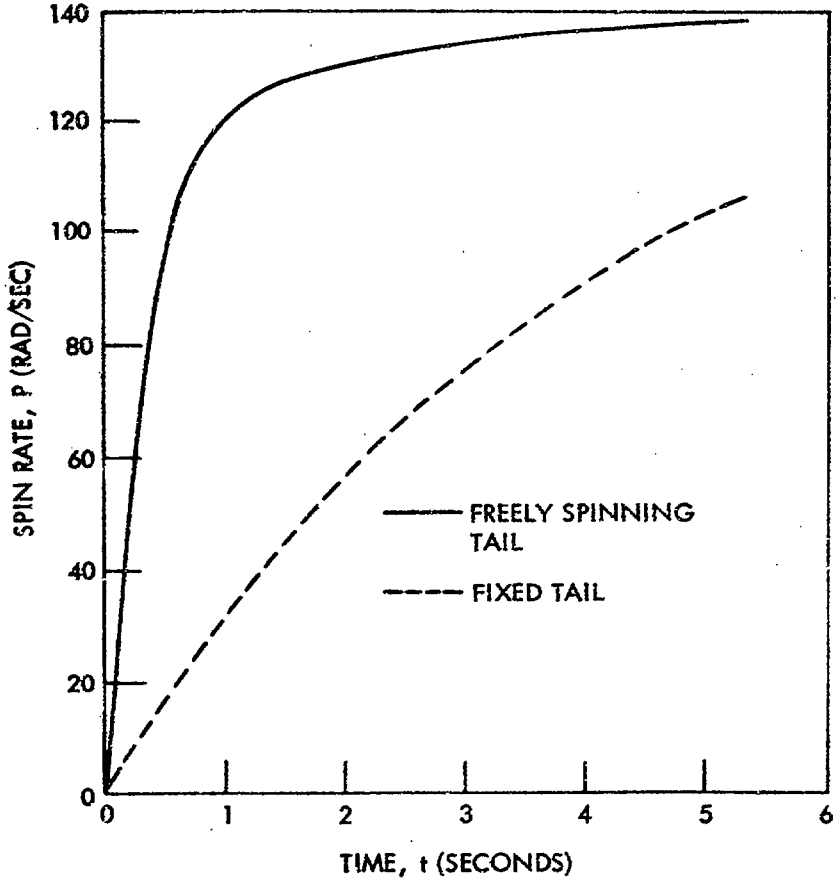

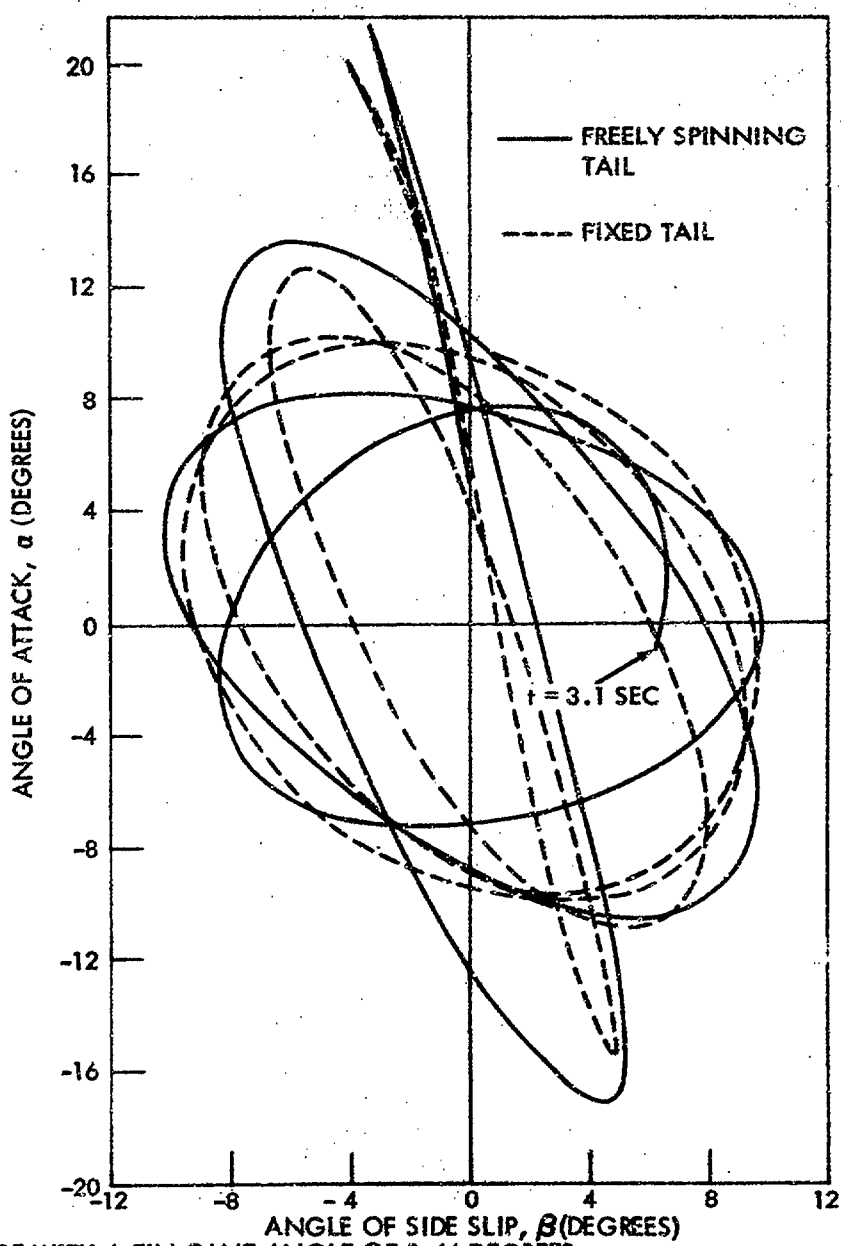

FIG. 30 SIMULATED RELEASE AT 4,000 FT. ALTITUDE WITH A FIN-CANT ANGLE OF 3.44 DEGREES

APPENDIX A

DYNAMIC ANALYSIS

Not too surprisingly, the uncoupling of the stabilizer from the forebody introduces certain complexities in the stabilization of the overall weapon. Extending the freely spinning stabilizer concept to bistable configurations complicates stability even further. This appendix contains a linear analysis of the freely spinning stabilizer which is an application and extension of a dynamic analysis carried out earlier by WRE (see Ref. (21)) which, in turn, was an application of an aircraft dynamic analysis carried out by Phillips (Ref. (22)). The material contained in this appendix is treated in a highly detailed form in Reference (23).

In considering the stability of bistable free-fall weapons, the essential parameters are the pitch and yaw restoring moment derivatives, C_{m_α} and C_{n_β}, respectively; the forebody and stabilizer spin rates, P and p, respectively; the pitch- and yaw-damping derivatives, $C_{m_q} + C_{m_{\dot\alpha}}$ and $C_{n_r} - C_{n_{\dot\beta}}$, respectively; and the ratio of the longitudinal to the transverse moment of inertia indicated by the parameter, τ. The analysis in this appendix, as is that in Reference (23), is confined to configurations having 180-degree rotational symmetry. Included are the effects of stabilizer and forebody asymmetries.

If a free-fall weapon is stabilized with a panel stabilizer that is free to rotate about the longitudinal axis of the store, the total aerodynamic moment, $\vec{G}$, may be written in vectoral form as:

$$\vec{G} = \frac{d\vec{H}}{dt} + \vec{\Omega}\times\vec{H} + \frac{d\vec{h}}{dt} + \vec{\Omega}\times\vec{h} \qquad \text{(A-1)}$$

where $\vec{H}$ and $\vec{h}$ are the angular momentum of the forebody and stabilizer, respectively. Similarly, the applied aerodynamic force is written as,

$$\vec{F} = m\left[\frac{d\vec{V}}{dt} + \vec{\Omega}\times\vec{V}\right] \qquad \text{(A-2)}$$

Equations (A-1) and (A-2) represent, in component form, a total of six equations, three force and three moment equations. These equations may be expressed in nondimensional form by writing the linear velocities as,

$$\hat{u} = \frac{u}{u_o} \qquad \alpha = \frac{w}{u_o} \qquad \beta = \frac{v}{u_o} \qquad \text{(A-3)}$$

where u_o is the magnitude of the total air velocity and $\{u,v,w\}$ are the components of this velocity about the $\{X_s,Y_s,Z_s\}$ stabilizer-fixed axis system. For the freely spinning stabilizer the $\{X_s,Y_s,Z_s\}$ frame rotates relative to the $\{X_B,Y_B,Z_B\}$ body associated frame at a relative angular rate $(p - P)$. The relationship between these two frames is shown for the case of the monoplane stabilizer in Figure A-1.

Time may be nondimensionalized by $t^* = d/2u_o$ to give $\hat{t} = t/t^*$. This normalization results in the angular rates being written as,

$$\hat{P} = Pt^* \qquad \hat{p} = pt^* \qquad \hat{q} = qt^* \qquad \hat{r} = rt^* \tag{A-4}$$

and time derivatives as,

$$\frac{d}{d\hat{t}}\{\ \} = t^* \frac{d}{dt}\{\ \} \tag{A-5}$$

The moments of inertia ratio may be nondimensionalized as,

$$\tilde{\iota} = \frac{A_2 + A_1\left(\frac{\hat{P}}{\hat{p}}\right)}{B} \tag{A-6}$$

where A_1 and A_2 are the axial moments of inertia of the forebody and stabilizer, respectively. The moments of inertia $A = A_1 + A_2$ and B and the mass, m, may be nondimensionalized as,

$$A' = \frac{A}{\left(\frac{1}{8}\rho S d^3\right)} \; ; \; B = \frac{B}{\left(\frac{1}{8}\rho S d^3\right)} \; ; \; m' = \frac{m}{\left(\frac{1}{4}\rho S d\right)} \tag{A-7}$$

If in Equations (A-1) and (A-2) the applied moment, $\bar{G}$, and force, $\bar{F}$, are written in terms of the aerodynamic derivatives, the moment and force equations become:

$$\dot{\hat{q}} - \hat{r}\hat{p}(1-\tilde{\iota}) = \frac{1}{B'}\left[C_{m_\alpha}\alpha + C_{m_q}\hat{q} - \frac{X_o}{d}C_{z_o}\right] \tag{A-8a}$$

$$\dot{\hat{r}} + \hat{q}\hat{p}(1-\tilde{\iota}) = \frac{1}{B'}\left[C_{n_\beta}\beta + C_{n_r}\hat{r} + \frac{X_o}{d}C_{y_o}\right] \tag{A-8b}$$

$$\hat{p} = -\frac{C_{\ell_\delta}\delta}{C_{\ell_p}} \tag{A-8c}$$

$$\dot{\beta} - \hat{p}\alpha + \hat{r} = \frac{1}{m'}\left[C_{Y_\beta}\beta + C_{Y_0}\right] \tag{A-8d}$$

$$\dot{\alpha} + \hat{p}\beta - \hat{q} = \frac{1}{m'}\left[C_{Z_\alpha}\alpha + C_{Z_0}\right] \tag{A-8e}$$

$$\dot{\hat{u}} = 0 \tag{A-8f}$$

For the present purposes the important equations are (A 8a,b,d,e). It will be noted that the pairs (A-8a,b) and (A-8d,e) are coupled in by spin rate, $\hat{p}$. Between these two pairs of equations the {r,q} variables may be eliminated to give:

$$\ddot{\beta} + k_1\dot{\beta} + k_2\beta + k_3\dot{\alpha} + k_4\alpha = k_5 \tag{A-9a}$$

and

$$\ddot{\alpha} + k_6\dot{\alpha} + k_7\alpha + k_8\dot{\beta} + k_9\beta = k_{10} \tag{A-9b}$$

where the k's are constituted of sums and products of the inertia ratios and aerodynamic derivatives. A systematic method for solving Equations (A-9) is to rewrite the equations in terms of the Laplace transform variables, S (Ref. (22)). Carrying out this operation gives,

$$\bar{\beta}(s)\left\{s^2 + k_1 s + k_2\right\} + \bar{\alpha}(s)\left\{k_3 s + k_4\right\} = \frac{k_5}{s} + \dot{\beta}(o)^+ + \beta(o)^+(s + k_1) + \alpha(o)^+ k_3 \tag{A-10a}$$

and

$$\bar{\beta}(s)\left\{s k_8 + k_9\right\} + \bar{\alpha}(s)\left\{s^2 + k_6 s + k_7\right\} = \frac{k_{10}}{s} + \dot{\alpha}(o)^+ + \alpha(o)^+(s + k_6) + \beta(o)^+ k_8 \tag{A-10b}$$

where $\alpha(o)^+$, $\dot{\alpha}(o)^+$, $\beta(o)^+$, $\dot{\beta}(o)^+$ are the initial displacement and initial rates of the $\{\alpha,\beta\}$ variables and $\bar{\beta}(S)$ and $\bar{\alpha}(S)$ are the Laplace transform of $\beta(t)$ and $\alpha(t)$.

A relatively straightforward way of assessing the stability of the system is to examine the characteristic equations of the homogeneous equation (right side of Eqs. (A-10)). The requirements for a unique solution of Equations (A-9) is that the characteristic

equations be set equal to zero, thus:

$$(s^2 + k_1 s + k_2)(s^2 + k_6 s + k_7) - (k_3 s + k_4)(k_8 s + k_9) = 0$$

or

$$\Delta(s) = s^4 + \bar{K}_1 s^3 + \bar{K}_2 s^2 + \bar{K}_3 s + \bar{K}_4 = 0 \qquad \text{(A-11)}$$

where the $\bar{K}$'s are obviously related to the k's which are, in turn, composed of the inertia ratio and stability derivatives as pointed out earlier.

The stability of the solution of Equations (A-9) depends upon the characteristic equation (Eq. (A-11) above) having no positive and real roots and no complex roots with positive real parts. The presence of real roots indicates exponential divergence or subsidence depending upon whether the sign of the root is positive or negative; the complex roots indicate divergent or convergent oscillatory motion depending upon whether the sign of the real part of the root is positive or negative. In the subsequent discussion motion associated with a real root will be termed static, while motion associated with a complex root will be considered dynamic. In using such terminology a distinction should be made between static and dynamic stability as measured in the wind tunnel and that deduced from the roots of the characteristic equation: wind-tunnel static stability would be indicated by negative C_{m_α} (and positive C_{n_β}) and wind-tunnel dynamic stability by negative $C_{m_q} + C_{m_{\dot{\alpha}}}$ (and negative $C_{n_r} - C_{n_{\dot{\beta}}}$).

The boundary between stability and instability occurs when the real root or the real part of a complex root is zero. The condition for any real root to be negative is

$$\bar{K}_4 = 0 \qquad \text{(A-12a)}$$

and the condition for any complex root to have a zero real part is that Routh's discriminant be zero or,

$$R = \bar{K}_1 \bar{K}_2 \bar{K}_3 - \bar{K}_3^2 - \bar{K}_1^2 \bar{K}_4 = 0 \qquad \text{(A-12b)}$$

Equations (A-12) may be used to describe the boundaries of static and dynamic stability, respectively.

As pointed out above, the $\bar{K}$'s are constituted of the stability derivatives, mass and moment of inertia ratio. The stability derivatives may be rewritten in a more convenient form in terms of the pitch and yaw frequencies and the pitch- and yaw-damping ratios as,

$$\omega_\alpha^2 = -C_{m_\alpha}/B' \tag{A-13a}$$

$$\omega_\beta^2 = C_{n_\beta}/B' \tag{A-13b}$$

$$2\zeta_\alpha\omega_\alpha = -\left[\frac{C_{m_q}}{B'} + \frac{C_{Z_w}}{m'}\right] \tag{A-13c}$$

$$2\zeta_\beta\omega_\beta = -\left[\frac{C_{n_r}}{B'} + \frac{C_{Y_\beta}}{m'}\right] \tag{A-13d}$$

$$\lambda = \zeta_\alpha\omega_\alpha/\hat{p} \tag{A-13e}$$

$$\mu = \zeta_\beta\omega_\beta/\hat{p} \tag{A-13f}$$

Equations (A-12) may be rewritten as follows using the definitions of Equations (A-13)

$$\bar{K}_4 = \hat{p}\left\{\left(\frac{\omega_\beta}{\hat{p}}\right)^2\left(\frac{\omega_\alpha}{\hat{p}}\right)^2 - \left[\left(\frac{\omega_\alpha}{\hat{p}}\right)^2 + \left(\frac{\omega_\beta}{\hat{p}}\right)^2\right](1-\gamma) + (1-\gamma)^2 + 4\mu\lambda\right\} \tag{A-14a}$$

and

$$\begin{aligned} R = 4\hat{p}^6\Bigg\{&\lambda\gamma\left(\frac{\omega_\alpha}{\hat{p}}\right)^4 + \lambda\mu\left(\frac{\omega_\beta}{\hat{p}}\right)^2 - 2\lambda\mu\left(\frac{\omega_\alpha}{\hat{p}}\right)^2\left(\frac{\omega_\beta}{\hat{p}}\right)^2 \\ &+ \left(\frac{\omega_\alpha}{\hat{p}}\right)^2(\lambda+\mu)\left[\mu(2-2\gamma+\gamma^2) + 4\lambda\mu^2 + \lambda - \gamma + (1-\gamma)(\lambda+\mu)\right] \\ &+ \left(\frac{\omega_\beta}{\hat{p}}\right)^2(\lambda+\mu)\left[\lambda(2-2\gamma+\gamma^2) + 4\lambda^2\mu + \mu - \lambda + (1-\gamma)(\lambda+\mu)\right]\Bigg\} \end{aligned} \tag{A-14b}$$

Obviously, various simplifications can be made to Equations (A-10) by allowing damping terms to be equal to zero, $\lambda = \mu = 0$, limiting the inertia ratio, τ, to small values or even zero and/or restricting attention to the case where yaw and pitch frequencies are equal, i.e., $\omega_\beta^2 = \omega_\alpha^2$. These various special cases will not be examined here. However, it should be mentioned that free-fall weapons are generally lightly damped so $\lambda = \mu = 0$ might be an acceptable first approximation; also, for most practical free-fall weapons, τ is usually less than 0.1 and a value of 0.01 is not uncommon.

Equations (A-14) have been plotted in Figure A-2 as $(\omega_\beta/\hat{p})^2$ versus $(\omega_\alpha/\hat{p})^2$ and for the case where τ equals zero and $\lambda = \mu = 0.1$. The boundary in the first quadrant comes from Equation (A-14a) and that in the second and fourth quadrant from Equation (A-14b). If both $(\omega_\beta/\hat{p})^2$ and $(\omega_\alpha/\hat{p})^2$ are positive, then the configuration will not experience dynamic instability (oscillatory divergence). For the case of the freely spinning monoplane $(\omega_\beta/\hat{p})^2$, say, will be negative. One such case might place a restriction on $(\omega_\alpha/\hat{p})^2$ as

$$.6 < \left(\frac{\omega_\alpha}{\hat{p}}\right)^2 < 1.0 \quad \text{FOR} \quad \left(\frac{\omega_\beta}{\hat{p}}\right)^2 = -1 \qquad \text{(A-15)}$$

The essential point of Figure A-2 is that it is possible under some circumstances to statically and dynamically stabilize a weapon which is unstable in one plane, i.e., $(\omega_\beta/\hat{p})^2 < 0$.

The first quadrant of Figure A-2 is enlarged in Figure A-3 and attention is confined to considerations of static stability alone. From Equation (A-14a) the stability boundaries may be written as,

$$\left[\left(\frac{\omega_\beta}{\hat{p}}\right)^2 - (1-\tau)\right]\left[\left(\frac{\omega_\alpha}{\hat{p}}\right)^2 - (1-\tau)\right] = -4\lambda\mu \qquad \text{(A-16)}$$

In the no-damping case,

$$\frac{\omega_\alpha}{(1-\tau)^{1/2}} = \hat{p} \qquad \text{(A-17)}$$

which is the familiar condition for yaw-roll resonance. With damping present, the boundaries form the hyperbolic shape indicated in Figure A-3. Clearly, increasing the damping increases the region of static stability. The effect of increasing τ opens a "corridor of static stability" where the vehicle is statically stable for a given damping level regardless of the magnitude of τ.

An alternate form of the presentation in Figures A-2 and A-3 is given in Figure A-4. This figure presents no new information, but introduces the relative yaw-pitch stiffness ratio as the dependent variable, i.e., $(\omega_\beta/\omega_\alpha)^2$. The dynamic-stability boundary in this figure may be written for the limiting case where $\lambda, \mu, \tau \ll 1$ as

$$\left(\frac{\omega_\beta}{\omega_\alpha}\right)^2 = -3\left(\frac{\hat{p}}{\omega_\alpha}\right)^2 + \sqrt{\left[9\left(\frac{\hat{p}}{\omega_\alpha}\right)^2+1\right]\left[\left(\frac{\hat{p}}{\omega_\alpha}\right)^2-1\right]} \qquad \text{(A-18)}$$

Under the same conditions the static-stability boundaries are easily shown to be:

$$\left(\frac{\omega_\beta}{\omega_\alpha}\right)^2 = (1-\hat{\tau})\left(\frac{\hat{p}}{\omega_\alpha}\right)^2 \qquad \text{(A-19a)}$$

or

$$\left(\frac{\hat{p}}{\omega_\alpha}\right)^2 = \frac{1}{(1-\hat{\tau})} \qquad \left(\frac{\hat{p}}{\omega_\beta}\right)^2 = \frac{1}{(1-\hat{\tau})} \qquad \text{(A-19b)}$$

From Equation (A-18) it is possible to show that the horizontal asymptote to the dynamic stability curve is -4/3. Thus, if $(\omega_\beta/\omega_\alpha)^2 > -4/3$, the configuration will always be dynamically stable (i.e., give no evidence of oscillatory divergence).

ASYMMETRIES

Another point that must be considered is the effect of asymmetries associated with the stabilizer and the forebody. Both types of asymmetries are treated at length in Reference (23); some of the more interesting results are presented below. First, considerations will be confined to asymmetries associated with the stabilizer alone. Aerodynamic asymmetries are contained in the k_5 and k_{10} terms of Equations (A-9). If Equations (A-10) are solved by $\bar{\beta}(S)$ and $\bar{\alpha}(S)$ and the final value theorem of the Laplace transform applied, one obtains for $\beta(\infty)$ (see p. 242, Ref. (24)):

$$\lim_{\hat{t}\to\infty} \beta(\hat{t}) = \beta(\infty) = \frac{k_7 k_5 - k_{10} k_7}{K_1} \qquad \text{(A-20)}$$

and a similar expression for $\alpha(\infty)$. Using the definitions of Equations (A-13), the above expression may be written as,

$$\beta(\infty) = \frac{\left[\left(\frac{\omega_\alpha}{\hat{p}}\right)^2 - (1-\hat{\tau})\right]\left(\frac{\omega_\beta}{\hat{p}}\right)\beta(\infty)_0}{D} - \frac{\left[2\mu\left(\frac{\omega_\alpha}{\hat{p}}\right)^2\alpha(\infty)_0\right]}{D} \qquad \text{(A-21)}$$

where

$$D = \left[\left(\frac{\omega_\beta}{\hat{p}}\right)^2 - (1-\nu)\right]\left[\left(\frac{\omega_\alpha}{\hat{p}}\right)^2 - (1-\nu)\right] + 4\lambda\mu$$

The expression for $\alpha(\infty)$ would have the symbols for α and β on the right of Equation (A-21) interchanged. The terms $\alpha(\infty)_o$ and $\beta(\infty)_o$ refer to the no-spin values of these quantities and may be shown to be equal to

$$\beta(\infty)_o = M_\beta/\omega_\beta^2 \qquad \alpha(\infty)_o = -M_\alpha/\omega_\alpha^2 \tag{A-22}$$

An amplitude ratio, $\bar{\zeta}$, may be defined as follows:

$$\bar{\zeta} = \sqrt{\frac{\overline{\alpha(\infty)}^2 + \overline{\beta(\infty)}^2}{\alpha(\infty)_o^2 + \beta(\infty)_o^2}} \tag{A-23a}$$

The nonrolling trim angle, γ_o, and the rolling trim angle, γ, are given as follows,

$$\gamma_o = \tan^{-1}\left\{\frac{\alpha(\infty)_o}{\beta(\infty)_o}\right\}$$

$$\gamma = \tan^{-1}\left\{\frac{\alpha(\infty)}{\beta(\infty)}\right\} - \gamma_o \tag{A-23b}$$

The amplitude ratio of the rolling to the nonrolling trim arm is given in Figure A-5. The configuration for which this figure was prepared is bistable, having a yaw-to-pitch ratio, $(\omega_\beta/\omega_\alpha)^2$ of 0.5. It will be noted that a bistable configuration has two resonant frequencies, one when the pitch frequency equals the spin rate and a second when the yaw frequency equals the spin rate. Therefore, care must be taken in design that these frequencies are avoided.

Obviously, plots similar to that given in Figure A-5 could be made for other values of the yaw-to-pitch ratio, $(\omega_\beta/\omega_\alpha)^2$. For the special case of the freely spinning cruciform stabilizer, $(\omega_\beta/\omega_\alpha)^2$

could be unity and there would be only one resonant frequency, i.e., $(\hat{p}/\omega_\alpha)^2 = 1/(1 - \tau)$.

The above analysis has been concerned with the effect of asymmetries on the trim amplitude. For a nonrolling vehicle this trim moment is represented by $\alpha(\infty)_o$ and $\beta(\infty)_o$ which result, in turn, from the trim forces C_{y_o} and C_{z_o} acting at a center-of-pressure location, X_o, from the center of gravity (see Eqs. (A-8a,b,d,e). The presence of spin rate, $\hat{p}$, alters the amplitude of the trim arm and the plane in which it acts. Although not shown in Figure 5-A, the effect of spin rate is to cause a change in γ, as indicated by Equation (A-23b). It is important to remember that the asymmetries under discussion are fixed in the rolling frame. Thus, for the freely spinning stabilizer the asymmetries must be confined to the stabilizer. The effect of forebody asymmetries must be treated separately.

Since the forebody is not spinning with the stabilizer, the asymmetries associated with the forebody will enter the moment equations as a periodic forcing function. The magnitude of this asymmetric moment at zero spin rate is designated as $C^B_{m_o}$. Although the forebody does not spin with the stabilizer, the forebody may acquire a spin rate, $\hat{p}$, of its own as a result of bearing drag. While in a practical weapon the forebody spin will probably not be constant during the flight (see Fig. 18) it will be assumed to be constant for the subsequent analysis. The yaw and pitch moments imparted by a forebody asymmetry may be expressed in the stabilizer-fixed frame, (X_s, Y_s, Z_s) as

$$C^B_{m_y} = C_{m_o} Re\langle exp\{-jbt\}\rangle \qquad \text{(A-24a)}$$

and

$$C^B_{m_z} = C_{m_o} Im\langle exp\{-jbt\}\rangle \qquad \text{(A-24b)}$$

where $b = \hat{p} - \hat{P}$, or the difference between the spin rates of the stabilizer and the forebody. For the present purposes the stabilizer associated asymmetries may be ignored in Equations (A-8), while the forebody asymmetries are included to give,

$$\hat{q}_\sigma - \hat{r}\hat{p}(1-\hat{\tau}) = \frac{1}{B}\left[C_{m_\alpha}\alpha + C_{m_q}\hat{q}_\sigma + C^B_{m_o} Re\langle exp\{-jbt\}\rangle\right] \qquad \text{(A-25a)}$$

and

$$\hat{r} + \hat{q}_\sigma\hat{p}(1-\hat{\tau}) = \frac{1}{B}\left[C_{n_\beta}\beta + C_{n_r}\hat{r} + C^B_{m_o} Im\langle exp\{-jbt\}\rangle\right] \qquad \text{(A-25b)}$$

If Equations (A-25) are solved simultaneously with Equations (A-8d,e) the result is identical to Equations (A-9) except that

$$\mathcal{R}_5 = -\frac{C_{m_\alpha}^B}{B'} J_m \langle \exp\{-jb\hat{t}\} \rangle \tag{A-26a}$$

and

$$\mathcal{R}_{10} = \frac{C_{m_\alpha}^B}{B'} Re\langle \exp\{-jb\hat{t}\} \rangle \tag{A-26b}$$

If the Laplace transform is taken of both of these equations, a solution may be obtained for $\bar{\alpha}(S)$ and $\bar{\beta}(S)$. The $\bar{\alpha}(S)$ solution may be written as,

$$\bar{\alpha}(s) = H_1(s) + H_2(s) \tag{A-27}$$

where

$$H_1(s) = \frac{S^2 + \mathcal{R}_1 S + \mathcal{R}_2}{\Delta(s)} \left[\dot{\alpha}(0^+) + \alpha(0^+)(S + \mathcal{R}_6) + \mathcal{R}_8 \beta(0^+) \right]$$

$$- \frac{\mathcal{R}_3 S + \mathcal{R}_4}{\Delta(s)} \left[\dot{\beta}(0^+) + \beta(0^+)(S + \mathcal{R}_7) \right] \tag{A-28a}$$

and

$$H_2(s) = \frac{S^2 + \mathcal{R}_1 S + \mathcal{R}_2}{\Delta(s)} \mathcal{L}\{\mathcal{R}_{10}\} - \frac{\mathcal{R}_3 S + \mathcal{R}_4}{\Delta(s)} \mathcal{L}\{\mathcal{R}_5\} \tag{A-28b}$$

where $\Delta(S)$ is the characteristic equation as expressed in Equation (A-11). An expression for the $\bar{\beta}(S)$ solution may be obtained in a similar fashion to that of the $\bar{\alpha}(S)$ solution.

If the final value theorem of the Laplace transform were applied to the $H_1(S)$ term of Equation (A-28a), the result would indicate that the inverse transform vanishes, i.e., this term represents only a system transient. Thus, the $H_1(S)$ term in Equation (A-27) may be ignored in making a contribution to steady-state conditions. The steady-state motion must be associated with the $H_2(S)$ term.

The steady-state condition might be expressed as

$$\alpha(\infty) = \lim_{\hat{t}\to\infty} \alpha(\hat{t}) = \lim_{\hat{t}\to\infty} h_2(\hat{t}) \tag{A-29}$$

where

$$h_2(\hat{t}) = \frac{C_{m_\delta}^B}{B'} \mathrm{Re} \int^{-1}\left\{ \frac{s^2 + k_1 s + k_2}{\Delta(s)(s+jb)} \right\} + \frac{C_{m_\delta}^B}{B'} \mathrm{Im} \int^{-1}\left\{ \frac{k_8 s + k_9}{\Delta(s)(s+jb)} \right\} \tag{A-30}$$

It may be shown that Equation (A-29) cannot be solved by applying the final value theorem of the Laplace transform to Equation (A-28b) (Ref. (24), p. 242). An alternate approach will be taken. Assume that a typical fraction in Equation (A-30) may be written as

$$X(s) = \frac{C_{m_\delta}^B}{B'} \frac{q(s)}{\Delta(s)(s+jb)} \tag{A-31a}$$

where q(S) is one of two numerators in Equation (A-30). The inverse transform of X(S) of $\int^{-1} X(S)$ may be written as follows,

$$x(\hat{t}) = \frac{C_{m_\delta}^B}{B'} \sum_{r=1}^{r=n} \left. \frac{(s-a_r)q(s)}{(s+jb)\Delta(s)} \right|_{s=a_r} e^{a_r \hat{t}} + \frac{C_{m_\delta}^B}{B'} \left. \frac{(s+jb)q(s)}{(s+jb)\Delta(s)} \right|_{s=-jb} e^{-jb\hat{t}} \tag{A-31b}$$

where a_r are the roots of the characteristic equation $\Delta(S)$ (or Eq. (A-11)). If a_r is negative, if real or has a negative part, if complex, then it may be shown that the first term on the right of Equation (A-31) vanishes. Thus, Equation (A-29) may be written as

$$\lim_{\hat{t}\to\infty}\alpha(\hat{t}) = \frac{C_{m_\delta}^{B}}{B'}\,\mathrm{Re}\left\{\frac{(s^2+k_1 s+k_2)e^{-jb\hat{t}}}{\Delta(s)}\right\}\Bigg|_{s=-jb} + \frac{C_{m_\delta}^{B}}{B'}\,\mathrm{Im}\left\{\frac{(k_3 s+k_4)}{\Delta(s)}e^{-jb\hat{t}}\right\}\Bigg|_{s=-jb} \qquad \text{(A-32)}$$

Clearly, the only singularity that can take place in Equation (A-32) occurs when $\Delta(-jb) = 0$. Since the characteristic equation appears in the denominator of both terms in Equation (A-32), as well as in the expression for $\lim_{t\to\infty}\beta(\hat{t})$, it is necessary to investigate conditions only for which $\Delta(-jb) = 0$.

The characteristic equation is difficult to factor generally; however, by ignoring damping, i.e., let $\bar{K}_1 = \bar{K}_3 = 0$, the characteristic equation becomes,

$$\Delta(s)\Big|_{s=-jb} = \left| s^4 + \bar{K}_2 s^2 + \bar{K}_4 \right|_{s=-jb} = (-jb)^4 + \bar{K}_2(-jb)^2 + \bar{K}_4 \qquad \text{(A-33)}$$

where

$$\bar{K}_2 = \omega_\alpha^2 + \omega_\beta^2 + \hat{p}^2(2 - 2\hat{\tau} + \hat{\tau}^2)$$

$$\bar{K}_4 = [\omega_\alpha^2 - \hat{p}^2(1-\hat{\tau})][\omega_\beta^2 - \hat{p}^2(1-\hat{\tau})] \qquad \text{(A-34)}$$

Equation (A-33) can now be factored to give:

$$[(\hat{p}-\hat{P})^2 - \omega_{n_1}^2][(\hat{p}-\hat{P})^2 - \omega_{n_2}^2] = 0 \qquad \text{(A-35)}$$

where b has been replaced by $(\hat{p} - \hat{P})$. Using Equation (A-34) and ignoring forebody spin rate, i.e, $\hat{P} = 0$, the factors of Equation (A-33) may be written as

$$\omega_{n_1}^2 = \frac{1}{2}\left[\omega_\alpha^2 + \omega_\beta^2 + \hat{p}^2(2-2\tau+\tau^2) + \sqrt{\omega_\alpha^4 + \omega_\beta^4 - 2\omega_\alpha^2\omega_\beta^2 + 8\hat{p}^2(1-\tau)(\omega_\alpha^2+\omega_\beta^2)}\right] \tag{A-36a}$$

and

$$\omega_{n_2}^2 = \frac{1}{2}\left[\omega_\alpha^2 + \omega_\beta^2 + \hat{p}^2(2-2\tau+\tau^2) - \sqrt{\omega_\alpha^4 + \omega_\beta^4 - 2\omega_\alpha^2\omega_\beta^2 + 8\hat{p}^2(1-\tau)(\omega_\alpha^2+\omega_\beta^2)}\right] \tag{A-36b}$$

From Equation (A-35) modal frequencies ω_{n_1} and ω_{n_2} may be replaced by spin rate, $\hat{p}$. Thus, Equations (A-36) may be rewritten, after dividing through by ω_α^2, as:

$$2\left(\frac{\hat{p}}{\omega_\alpha}\right)^2 = \left[1 + \left(\frac{\omega_\beta}{\omega_\alpha}\right)^2 + \left(\frac{\hat{p}}{\omega_\alpha}\right)^2(2-2\tau+\tau^2) \pm \sqrt{\left[1-\left(\frac{\omega_\beta}{\omega_\alpha}\right)^2\right]^2 + 8\left(\frac{\hat{p}}{\omega_\alpha}\right)^2\left(1-\frac{\tau}{2}\right)^2\left[1+\left(\frac{\omega_\beta}{\omega_\alpha}\right)^2+\left(\frac{\hat{p}}{\omega_\alpha}\right)^2\frac{\tau^2}{2}\right]}\right] \tag{A-37}$$

while the above expression appears quite complicated it is easily solved to give:

$$\left(\frac{\omega_\beta}{\omega_\alpha}\right)^2 = \frac{\left(\frac{\hat{p}}{\omega_\alpha}\right)^2(2-\tau)}{\left[1-\left(\frac{\hat{p}}{\omega_\alpha}\right)^2(2-\tau)\right]} \tag{A-38}$$

The above equation has been plotted in Figure A-6. Figure A-6 presents the locus of variables $(\hat{p}/\omega_\alpha)^2$ and $(\omega_\beta/\omega_\alpha)^2$ for which the amplification of forebody asymmetries is a maximum.

Since the cruciform is the most common fin arrangement, it might be of interest to calculate the value of $(\hat{p}/\omega_\alpha)^2$ for which maximum amplification occurs. Setting $(\omega_\beta/\omega_\alpha)^2$ equal to unity in Equation (A-38) it is easy to show that

$$\left(\frac{\hat{p}}{\omega_\alpha}\right) = \frac{1}{2\left(1-\frac{\tau}{2}\right)^{1/2}} \cong \frac{\left(1+\tau/4\right)}{2} \cong \frac{1}{2} \tag{A-39}$$

or that the forebody asymmetries result in maximum amplification when the spin rate is one half the pitch frequency for negligibly small value of τ.

Returning to Figure A-6, it will be noted that for $(\omega_\beta/\omega_\alpha)^2 > -1$ the forebody asymmetries do not cause maximum amplification provided $(\hat{p}/\omega_\alpha)^2 > 5$. This conclusion follows from Equation (A-38) since

$$\lim_{\left(\frac{\hat{p}}{\omega_\alpha}\right)\to\infty} \left(\frac{\omega_\beta}{\omega_\alpha}\right)^2 = -1 \qquad \text{(A-40)}$$

The above conclusion is true regardless of the value of the inertia ratio, τ.

This section has presented an outline of the analysis of the static- and dynamic-stability characteristics of weapons employing freely spinning stabilizers and the effect that forebody and stabilizer asymmetries have on the amplification of the rolling trim angle. Certain conclusions that might be drawn from this appendix can be summarized as follows:

1. An undamped bistable configuration with no asymmetries is stable provided

$$\left(\frac{\omega_\alpha}{\hat{p}}\right)^2 > (1 - \tau) \quad \text{and} \quad \left(\frac{\omega_\beta}{\hat{p}}\right)^2 > (1 - \tau)$$

or

$$\left(\frac{\omega_\alpha}{\hat{p}}\right)^2 < (1 - \tau) \quad \text{and} \quad \left(\frac{\omega_\beta}{\hat{p}}\right)^2 < (1 - \tau)$$

2. An undamped cruciform configuration ($(\omega_\beta/\omega_\alpha)^2 = 1$) is unstable at the point $(\omega_\alpha/\hat{p})^2 = (1 - \tau)$; otherwise it is stable.

3. A corridor of static stability opens with increasing system damping.

4. A corridor of static stability, independent of τ (mass distriuution) exists for $\lambda = \mu = 0.1$, provided $2/3 \leq (\omega_\beta/\omega_\alpha)^2 \leq 3/2$.

5. If $(\hat{p}/\omega_\alpha)^2 > 1/(1 - \tau)$ and $-4/3 \leq (\omega_\beta/\omega_\alpha)^2 \leq (1 - \tau)(\hat{p}/\omega_\alpha)^2$, a bistable configuration will be statically and dynamically stable, and if $-4/3 \leq (\omega_\beta/\omega_\alpha)^2$, a bistable configuration will be dynamically stable.

6. In the presence of stabilizer-associated asymmetries, a cruciform configuration has a single resonance point at

$$(\hat{p}/\omega_\alpha)^2 = 1/(1 - \tau)$$

and a bistable configuation with a positive value of $(\omega_\beta/\omega_\alpha)^2$ has two resonance points at

$$(\hat{p}/\omega_\alpha)^2 = \frac{1}{1 - \tau}$$

and at

$$\left(\frac{\hat{p}}{\omega_\beta}\right)^2 = \frac{1}{1 - \tau}$$

7. Asymmetries in the forebody can cause large amplification of trim angles with maximum amplification occurring when

$$\left(\frac{\hat{p}}{\omega_\alpha}\right)^2 = \frac{(\omega_\beta/\omega_\alpha)^2}{\left[1 + \left(\frac{\omega_\beta}{\omega_\alpha}\right)^2\right](2 - \tau)}$$

8. In the presence of forebody asymmetries, a cruciform configuration has a single resonance point at

$$\left(\frac{\hat{p}}{\omega_\alpha}\right) = 0.5$$

or when the spin rate equals one half of the pitch frequency.

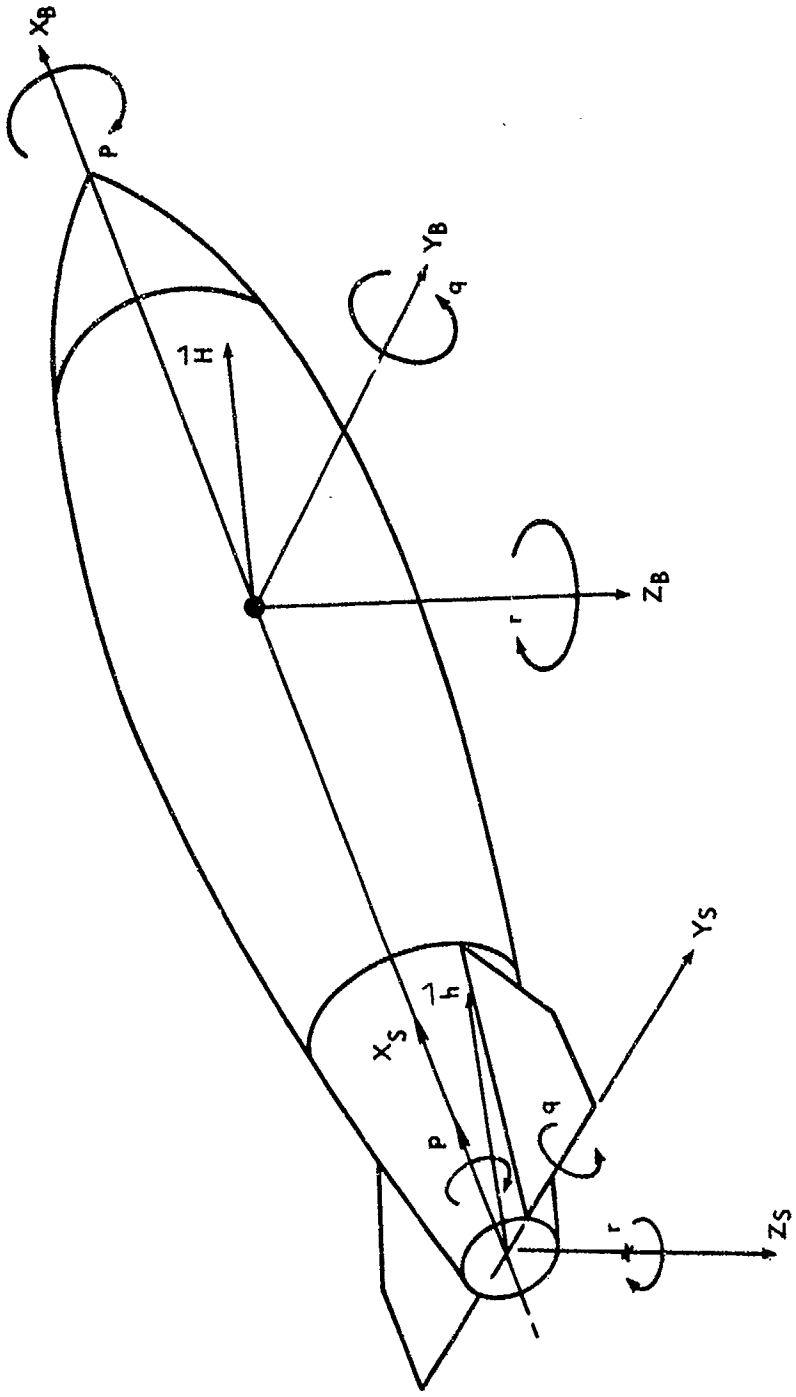

FIG. A-1 BODY AND STABILIZER AXIS SYSTEMS

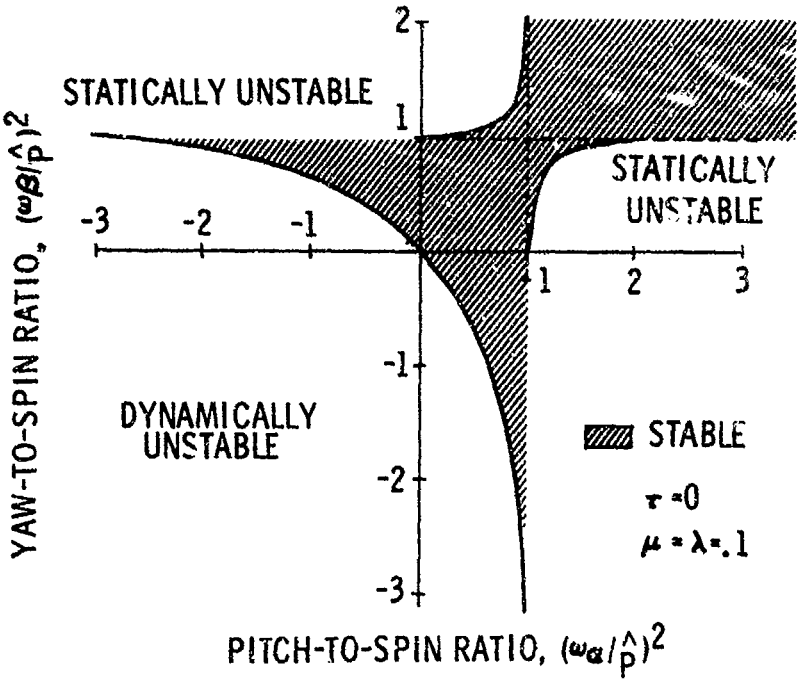

FIG. A-2 YAW-TO-SPIN RATIO VERSUS PITCH-TO-SPIN RATIO

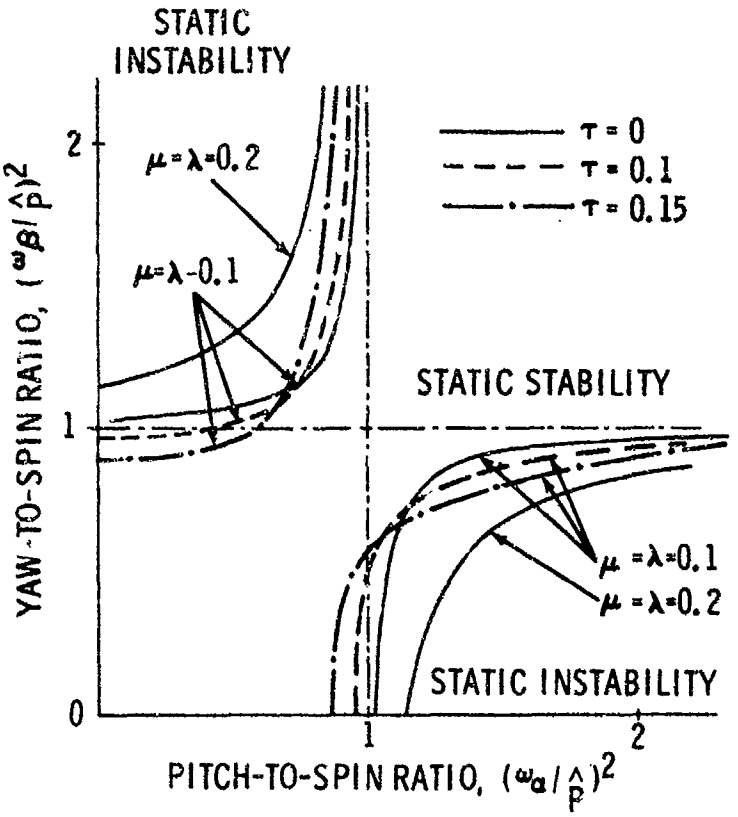

FIG. A-3 YAW-TO-SPIN RATIO VERSUS PITCH-TO-SPIN RATIO

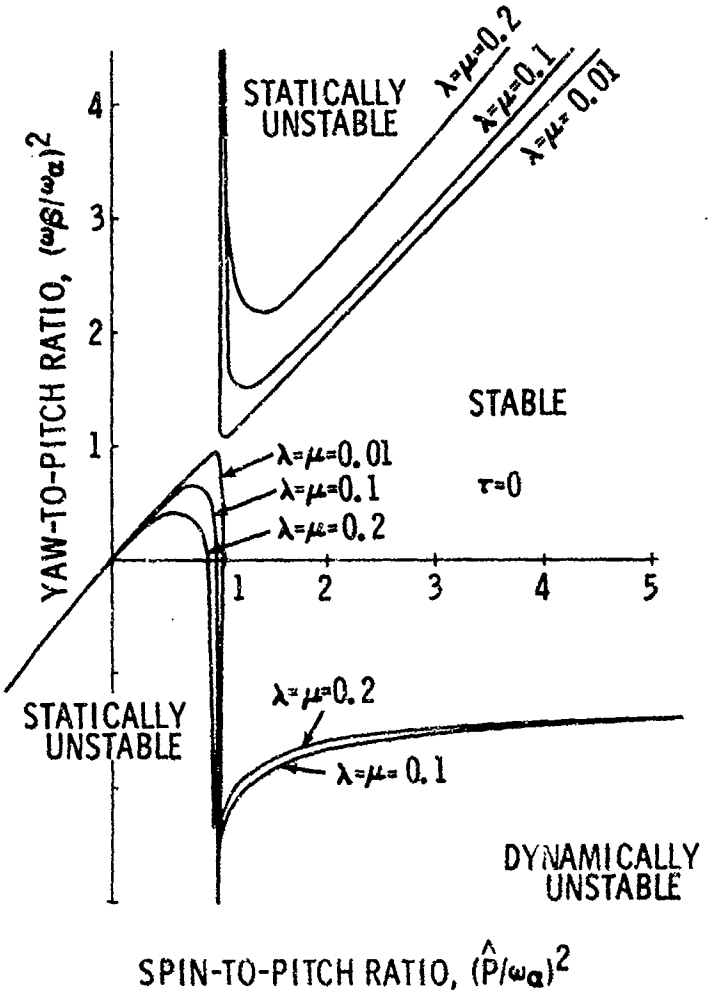

FIG. A-4 YAW-TO-PITCH RATIO VERSUS SPIN-TO-PITCH RATIO

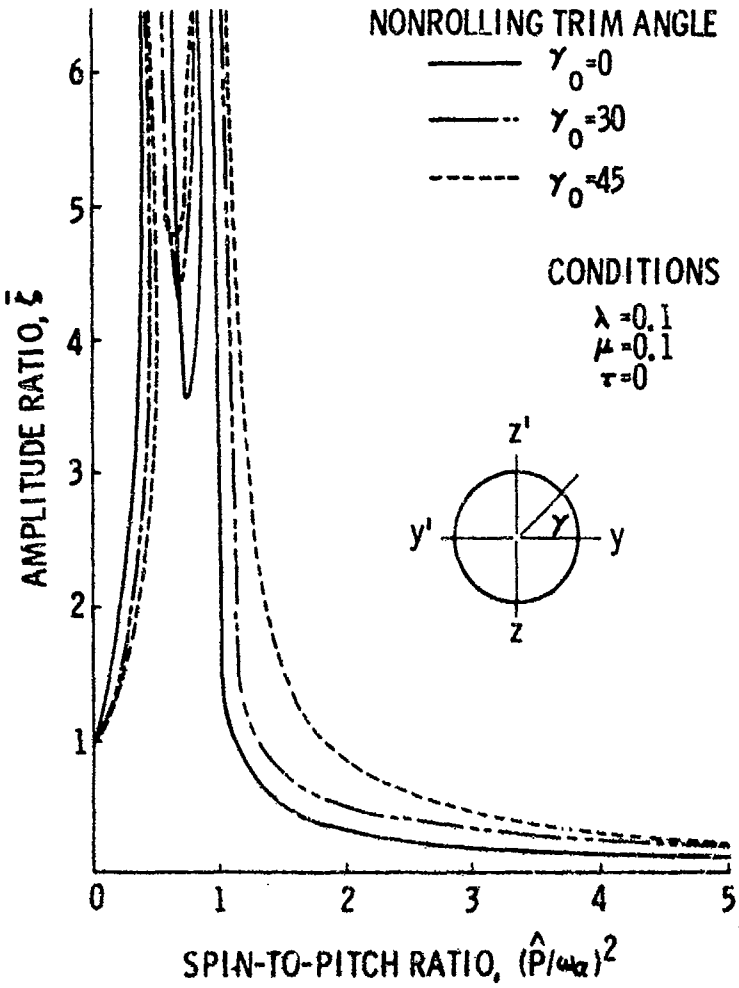

FIG. A-5 AMPLITUDE RATIO VERSUS SPIN-TO-PITCH RATIO FOR A YAW-TO-PITCH RATIO OF 0.5

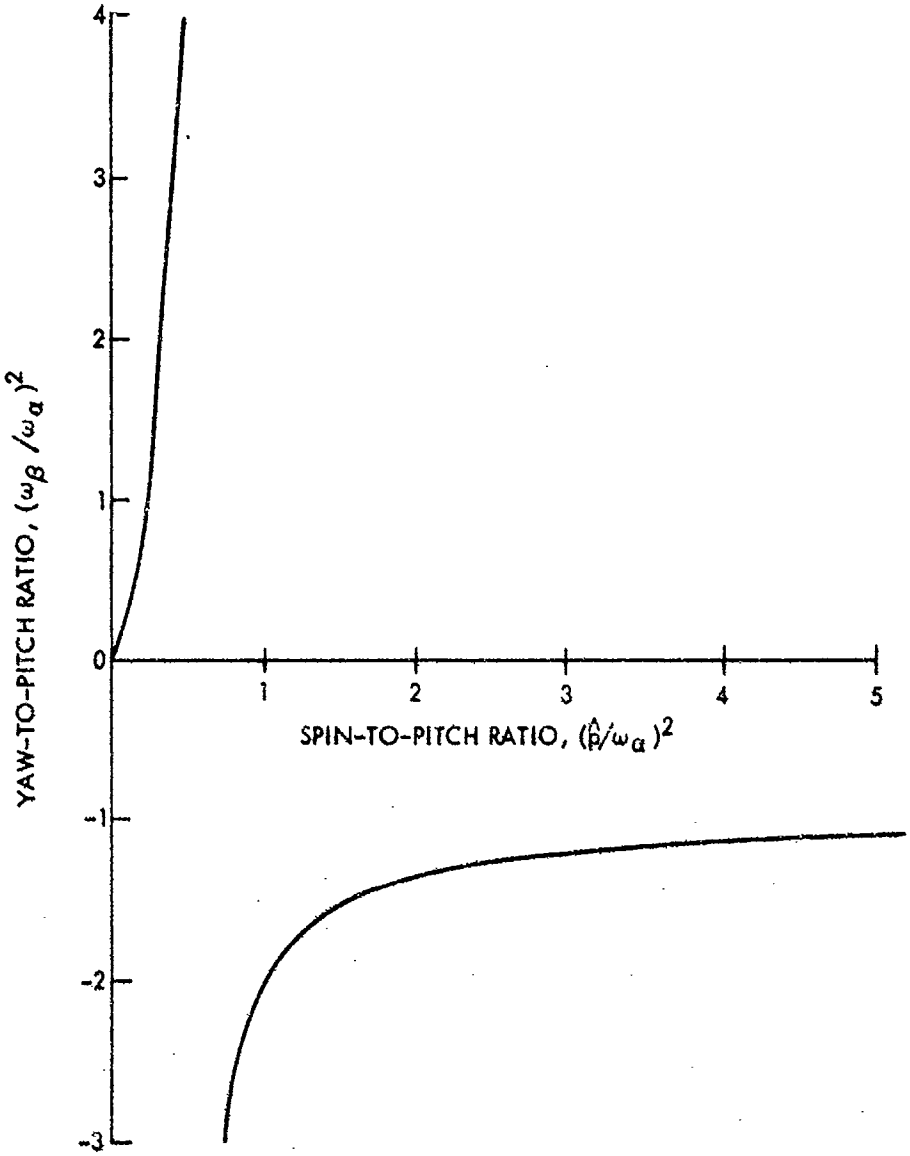

FIG. A-6 YAW-TO-PITCH RATIO VERSUS SPIN-TO-PITCH RATIO FOR MAXIMUM AMPLIFICATION OF FOREBODY ASYMMETRIES